Intranasal virus-particle mimicking vaccine enhances SARS-CoV-2 clearance in the Syrian hamster model

Patel DR[1,4], Minns AM[2,4,6], Sim DG[3,4], Field CJ[1,2], Kerr AE[1,4], Heinly T[1,4], Luley EH[1,5], Rossi, R.M. [4], Bator, C.[4], Mostafa, I.M.[2], Hafenstein SL[2,4,7], Lindner SE[2,4,6*], Sutton TC[1,4*]

[1] Department of Veterinary and Biomedical Sciences, Pennsylvania State University

[2] Department of Biochemistry and Molecular Biology, Pennsylvania State University

[3] Department of Biology, Pennsylvania State University

[4] The Huck Institutes of Life Sciences, Pennsylvania State University

[5] Animal Diagnostic Laboratory, Pennsylvania State University

[6] The Huck Center for Malaria Research

[7] Department of Medicine, Pennsylvania State University

* Co-corresponding Authors:

Corresponding Authors:

Scott E. Lindner, Ph.D.

W230B Millennium Science Complex

University Park, PA 16802

P: +1.814.867.4062

E: Scott.Lindner@psu.edu

ORCID: 0000-0003-1799-3726

Troy C Sutton, Ph.D.

W229A Millennium Science Complex

University Park, PA 16802

P: +1.814.863.0693

E: tcs38@psu.edu

ORCID: 0000-0002-7880-4784

ABSTRACT

Severe acute respiratory syndrome coronavirus-2 (SARS-CoV-2) has caused a pandemic and multiple vaccines have been developed and authorized for human use. While these vaccines reduce disease severity, they do not prevent infection allowing SARS-CoV-2 to continue to spread and evolve. To confer protection against infection and limit transmission, vaccines must be developed that induce mucosal immunity in the respiratory tract. Therefore, we performed proof-of-principle pre-clinical vaccine and challenge studies with a virus-particle mimicking intranasal vaccine against SARS-CoV-2. The vaccine candidate consisted of the self-assembling 60-subunit I3-01 protein scaffold covalently decorated with the SARS-CoV-2 receptor binding domain (RBD) using the SpyCatcher-SpyTag system. We verified the intended antigen display features by reconstructing the I3-01 scaffold to 3.4A using cryo-EM, and established RBD decoration through both SDS-PAGE and negative stain TEM. Using this RBD grafted SpyCage scaffold (RBD+SpyCage), we performed two vaccination studies in Syrian hamsters using an intranasal prime and boost vaccine regiment followed by SARS-CoV-2 challenge. The initial study focused on assessing the immunogenicity of RBD+SpyCage, which indicated that vaccination of hamsters induced a non-neutralizing antibody response that enhanced viral clearance but did not prevent infection. In an expanded study, we demonstrated that covalent bonding of RBD to the scaffold was required to induce an antibody response. Consistent with the initial study, animals vaccinated with RBD+SpyCage more rapidly cleared SARS-CoV-2 from both the upper and lower respiratory tract, whereas admixtures of SpyCage and RBD, or either components alone did not. These findings demonstrate the intranasal SpyCage vaccine platform can induce protection against SARS-CoV-2 and, with additional modifications to improve immunogenicity, is a versatile and adaptable system for the development of intranasal vaccines targeting respiratory pathogens.

INTRODUCTION

Severe acute respiratory syndrome coronavirus- 2 (SARS-CoV-2) is the etiological agent of coronavirus disease 2019 (COVID-19)[1]. In March 2020, COVID-19 was declared a pandemic [1,2], and as of August 2022, SARS-CoV-2 has caused more than 557 million infections resulting in more than 6.3 million deaths worldwide[3]. SARS-CoV-2 is an enveloped betacoronavirus with a non-segmented positive-sense single-stranded RNA genome. The genome encodes 4 structural proteins: spike (S), membrane (M), envelope (E), and nucleocapsid (N) as well as multiple non-structural proteins[4]. The S protein is the major surface protein and mediates viral entry and fusion within a host cell. The receptor-binding domain (RBD) of the S protein binds the host receptor angiotensin-converting enzyme 2 (ACE2) leading to endocytosis of the virion and infection of the host[4,5]. Importantly, the antibody responses against SARS-CoV-2 in humans and experimentally infected animals are predominantly directed towards the S protein. Moreover, titers of RBD-binding antibodies correlate with neutralizing activity, and RBD is considered the immunodominant region of the S protein [6,7]. Therefore, RBD represents a suitable immunogen for vaccine development and blocking this domain has the potential to prevent infection.

Prior to the SARS-CoV-2 pandemic, vaccines targeting coronaviruses in humans had not been advanced through late-stage clinical trials and licensed. Development of multiple SARS-CoV-2 vaccine candidates was enabled by rapid sequencing of the viral genome as well as pre-existing knowledge about vaccination against severe acute respiratory syndrome coronavirus (SARS-CoV) and Middle Eastern respiratory syndrome coronavirus (MERS-CoV) [2]. Currently, there are at least 12 vaccines approved for human use [8,9]. Licensed vaccines such as CoronaVac and QazCovid-in contain inactivated virus [10-14], while vaccines developed by Pfizer/BioNTech and Moderna consist of mRNA encoding the pre-fusion S protein enclosed in a lipid nanoparticle[15]. The Novavax vaccine contains recombinant S protein, and vaccines from Johnson & Johnson, and AstraZeneca use viral vectors to deliver DNA encoding the S protein [16]. Importantly, all

licensed vaccines are delivered by intramuscular (*i.m.*) injection and these vaccines have been shown to reduce the severity of SARS-CoV-2 infection[12,17,18]; however, these vaccines do not prevent infection, and vaccinated individuals can develop symptomatic infections and transmit the virus onwards.

Intramuscular vaccination induces a systemic immune response with high titers of IgG antibodies that enter the lungs limiting viral replication and reducing disease severity[2,19]. However, the delivery of vaccines via the *i.m.* route does not induce a strong mucosal immune response[2], and a mucosal response is required to prevent infection of the upper respiratory tract and transmission. In contrast to *i.m.* administered vaccines, an efficacious intranasal vaccine has the potential to protect mucosal surfaces via the induction of secretory IgA antibodies and mucosal T cells. Moreover, these vaccines can also induce a serum IgG response that can impart similar disease reductions as observed for existing vaccines (reviewed in [20]). On-going analysis of licensed SARS-CoV-2 vaccine efficacy has shown that vaccine-induced immunity wanes over time resulting in breakthrough infections [21-23]. As a result, there is a growing need to develop a second generation of SARS-CoV-2 vaccines that can be administered through intranasal routes to induce mucosal immunity, which can limit infection and viral transmission[24,25].

To date a limited number of intranasal vaccine candidates have been developed against SARS-CoV-2. Most of these candidates are viral vectors or live-attenuated vaccines; however, there have been safety concerns with viral vectored SARS-CoV-2 vaccines and their administration is limited to individuals older than 18 years of age[26,27]. Moreover, due to safety concerns and poor immunogenicity in older individuals, the only licensed live-attenuated intranasal vaccine is against influenza, and its use is restricted to individuals less than 50 years of age without pre-existing health conditions[28]. Therefore, there is a need to develop intranasal vaccines that would be suitable for individuals of all ages.

To address this gap, we adapted the I3-01 self-assembling protein into a nanoparticle bearing a flexible SpyCatcher domain (SpyCage) to display SARS-CoV-2 RBD/SpyTag (RBD+SpyCage) for intranasal vaccination studies in hamsters. The I3-01-based platform has been shown to be an excellent immunization scaffold to present a variety of antigens from viral (SARS-CoV-2, influenza, EBV, CSFV) and parasitic (*Plasmodium*) pathogens that reproducibly boosts immune responses as compared to the unscaffolded antigen[29-36]. However, these trials have been restricted to *i.m.* injections with immune responses as endpoint readouts, with a few notable studies proceeding through challenges with live pathogens[35,37].

Here we tested the impact of displaying RBD on the SpyCage scaffold (RBD+SpyCage) as an intranasal vaccine in Syrian Golden hamsters, which are highly permissive to SARS-CoV-2 infection and support contact and airborne transmission[38-40]. We performed two separate efficacy studies in which hamsters were given a prime and boost vaccination and challenged with SARS-CoV-2. We demonstrated covalent grafting of RBD to SpyCage was required to induce an IgG antibody response in vaccinated animals. Upon SARS-CoV-2 challenge, regardless of vaccination status all hamsters became infected and exhibited weight loss; however, animals vaccinated with RBD+SpyCage more rapidly cleared virus from both the upper and lower respiratory tract and had reduced lung pathology. Collectively, these studies demonstrate the potential for SpyCage as the basis of an intranasal vaccine platform for SARS-CoV-2 and possibly other respiratory pathogens.

MATERIALS AND METHODS

Production and Purification of Apo Cage and SpyCage

The Apo Cage scaffold is based upon the 6xHis/I3-01 protein described previously by Hsia and colleagues[41,42]. The SpyCage scaffold consists of a genetic fusion of a 6xHis tag, the SpyCatcher domain, a flexible linker, and the I3-01 protein[41,43]. These proteins were expressed in the *E. coli* BL21 (DE3) CodonPlus strain bearing either plasmid pSL1013 (Apo Cage) or pSL1040 (SpyCage) using a modified pET28 vector. Cultures were grown in LB media at 37C to an OD600 of ~0.5, at which point protein expression was induced by the addition of 0.5mM (final concentration) for 2.5 hours. Cell pellets were suspended in 50mL of resuspension buffer (50 mM Tris-Cl pH8.0@RT, 500 mM NaCl) per 1L of culture, and cells were lysed by sonication using a disruptor horn attachment, using 3 pulses of 30 seconds each at 70% amplitude and 50% duty cycle (model 450 Branson Digital Sonifier). The crude extract was spun 15500 *xg* for 20 minutes at 4C, and the soluble fraction was then incubated in batch with 2 ml of equilibrated Ni-NTA resin for 1 hour at 4C. The resin was applied to a gravity flow column and washed with 50mL of resuspension buffer followed by 50mL of Mid-Imidazole buffer (25 mM Tris-Cl pH7.5@RT, 500 mM NaCl, 50 mM Imidazole, 250 mM dextrose, 10% v/v glycerol). Apo cage and SpyCage protein were eluted using elution buffer (50 mM Tris-Cl pH8.0@RT, 500 mM NaCl, 300 mM imidazole), and then were exhaustively dialyzed into 50 mM Tris-Cl pH8.0@RT, 500 mM NaCl, 1 mM DTT, 10% v/v glycerol. The dialyzed material was then concentrated to ~2.0 mg/ml using Amicon Ultra Centrifugal Filters (Fisher Scientific Cat#: UFC9-003-08) and snap frozen in liquid nitrogen for long-term storage at -80C. Complete plasmid sequences are provided in Supp File 1.

Production and Purification of SARS-CoV-2 Spike RBD

The Receptor-Binding Domain (RBD) of SARS-CoV2-2 Spike protein was produced with and without a C-terminal SpyTag for covalent attachment to SpyCage using plasmid pSL1515 and

pSL1510 respectively[43]. Plasmid DNA was purified (Qiagen HiSpeed Maxiprep Kit) precipitated with ethanol and resuspended in water before transfection using the Expi293 Expression System (ThermoFisher, Expi293F cells, Expi293 Media, and the ExpiFectamine 293 Transfection Kit) by the Penn State Sartorius Cell Culture Facility as per manufacturer instructions. Briefly, cells maintained in log phase growth at 37C and 8% CO2 in baffled flasks shaking at 120-130 rpm were transfected at a concentration of 5E6/ml, and were supplemented by addition of ExpiFectamine 293 Transfection Enhancer 1 & 2 approximately 20 hours post transfection. Culture supernatant was harvested by centrifugation (273.5 *xg*, 5 minutes, room temperature) on day three, and was incubated in batch with Ni-NTA (ThermoSci HisPur) resin pre-equilibrated in 1xPBS at 4C for 1 hour on a nutator. The resin was then applied to a gravity flow column and was washed four times with 10 column volumes of wash buffer (57 mM NaH2PO4 pH 6.3@RT, 30 mM NaCl, 20mM imidazole). Protein was eluted with 4 column volumes of elution buffer (57 mM NaH2PO4 pH 7.9@RT, 30 mM NaCl, 235 mM imidazole). Eluted protein was dialyzed to completion in 1xPBS and snap frozen in liquid nitrogen for long-term storage at -80C. Complete plasmid sequences are provided in Supp File 1.

Covalent Bonding of SARS-CoV-2 Spike RBD to SpyCage

Purified SpyCage was dialyzed into 1xPBS with 1mM DTT, and then mixed with purified SARS-CoV-2 Spike RBD either with (RBD+SpyTag) or without (RBD only) at a 1.2:1 molar ratio of RBD to SpyCage monomer in a buffer consisting of 1xPBS and 1mM DTT. The binding reaction was allowed to go to completion by incubation for 3 hours at room temperature. The extent of SpyCage saturation was assessed by SDS-PAGE as previously described[43]. The binding reaction was then dialyzed into 1xPBS and stored at -80C until use in immunization efforts.

Cryo-EM specimen preparation and data collection

Purified apo cage protein complex based upon I3-01[41,42] and RBD+SpyCage were first assessed by negative staining to check sample quality and concentration before preparing TEM grids for data collection. Briefly, a 3.5 ul aliquot was applied to a glow-discharged Cu-grid coated with a thin film of continuous carbon, washed, stained with 0.75% w/v uranyl formate for 15 sec, blotted, air-dried and loaded on EFI Tecnai G2 Spirit BioTwin microscope (120 kV) for imaging.

TEM grids (QUANTAFOIL R2/1; QUANTAFOIL, Germany) were plasma cleaned using a PELCO Glow Discharge System (Ted Pella, Redding CA). Aliquots of 3.5 ul of the apo cage sample at approximately 0.1 mg/ml were applied to the grids, blotted for 2 sec, and then plunge-frozen in liquid ethane using a vitrification robot (Vitrobot, Thermo Fisher). Grids were stored in liquid nitrogen until the date of screening and data collection. Data was acquired on a Thermo Fisher Titan Krios electron microscope (300 kV) equipped with Falcon 3EC direct detection camera. EPU software (V 2.13.0.3175REL) was used to setup data acquisition at a nominal magnification of x59,000 and physical pixel size of 1.11 Å/pixel. A total of 1,220 micrographs were recorded as movies (stacks of 39 frames) at an exposure rate of 1.15 e/Å^2/frame and a total exposure time of 69.8 s. The nominal defocus range of -1.2 to -3.0 µm was applied during data collection.

Cryo-EM Image processing

Image analysis was performed using cryoSPARC software package (v3.3.2)[44]. Aligned movie stacks were generated from raw micrographs after correcting for stage drift and anisotropic motion using patch motion correction. Parameters of the contrast transfer function (CTF) were estimated for each aligned movie in patch mode. Manually selected 283 particles from 11 micrographs were used to train a Topaz model for particle picking; a box of 420x420 pixel size was used for particle extraction[45]. The trained model was applied to pick 129,792 particles from 1,202 micrographs. Further cleaning of the data using 2D-classification resulted in 63,430

particles for subsequent data processing. A map from an *ab initio* model (generated using 10,000 particles) along with the selected clean particles were subjected to homogenous refinement in cryoSPARC. Local motion correction[46] of the refined particles followed by homogenous refinement with higher-order CTF terms enabled (including beam-tilt, spherical aberration, trefoil and tetrafoil) and icosahedral symmetry (I1) enforced resulted in a final map at 3.4 Å resolution.

Cryo-EM Model building

The initial model of the apo cage monomer was extracted from the published I3-01 model[41,42]. The monomer model was manually fitted into the 3.4 Å map in ChimeraX[47]; a full icosahedral model of apo cage was generated from the asymmetric unit. PHENIX real-space refinement was used to refine the model against the sharpened map with non-crystallographic symmetry parameters applied[48]. The refined model was visually inspected in Coot and validated by MolProbity[49,50]. All figures of the protein structure and cryo-EM map were created using ChimeraX.

Culture of SARS-CoV-2

The SARS-CoV-2/USA/WA1/2020 isolate was received from The World Reference Center for Emerging Viruses and Arboviruses (WRCEVA), University of Texas Medical Branch at Galveston (UTMB). The virus was obtained at passage 4 and was sub-cultured once on Vero E6/TMPRSS2 cells (Japanese Collection of Research Bioresources Cell Bank). All titrations of virus stocks and tissue homogenates were performed on Vero E6 cells (ATCC) cultured in Dulbecco's modified Eagle Medium (Cytiva) supplemented with 10% FBS, 4 mM L-glutamine, 1 mM sodium pyruvate (Corning), 1X non-essential amino acids and 1X antibiotic and antimycotic (Corning) at 37º C with 5% CO_2. For culture of the VeroE6/TMPRSS2 cells 1 mg/mL geneticin was added to the media and the FBS was reduced to 5%. To determine the titer of viral stocks,

the tissue culture infectious dose 50% (TCID50) was determined by inoculating cells grown in 24-well plates with serial dilutions of the virus. The plates were incubated at 37º C with 5% CO_2 and scored for cytopathic effect at 96 hours post-infection. The $TCID_{50}$ was then calculated using the method of Reed and Muench [51].

Vaccination and Challenge Experiments

Equal numbers of male and female, six to eight-week-old Syrian hamsters (HsdHan:AURA, Envigo, Haslett, MI) were used for all studies. After acclimatization, animals were implanted with a subcutaneous transponder chip (Bio Medic Data Systems) and a pre-vaccination blood sample was collected. For intranasal vaccination and virus inoculation, animals were sedated and intranasally inoculated with vaccine (70 ul in 1xPBS) or SARS-CoV-2 (100 ul in DMEM). For all experimental procedures hamsters were sedated with 150 mg/kg ketamine, 7.5 mg/kg xylazine, and 0.015 mg/kg atropine via intraperitoneal injection. After completion of the procedure, hamsters were given 1 mg/kg atipamezole subcutaneously. For tissue collection and at the end of each study, hamsters were humanely euthanized via CO_2 asphyxiation.

Trial 1: Evaluation of immunogenicity and efficacy of the SpyCage-RBD vaccine candidate

To evaluate the immunogenicity and efficacy of the SpyCage RBD vaccine, groups of hamsters (n=14/group) were vaccinated with PBS (mock), SpyCage (15 ug), SARS-CoV-2 RBD (10 ug), or SARS-CoV-2 RBD (10 ug) bound to SpyCage (15 ug, “RBD+SpyCage”). Animals received a primary (1º) vaccination and a secondary (2º) vaccination 28 days later. Blood samples were collected via gingival vein from 6 animals (3 males and 3 females) per group on days 14, 26, 42, and 55 post- 1º vaccination. Blood samples were centrifuged at 1000 *xg* for 10 minutes at room temperature, and serum was collected and stored at -20º C. On day 56 post-1º vaccination, all animals were intranasally inoculated with 10^5 $TCID_{50}$ SARS-CoV-2/USA/WA1/2020. On days 3 and 6 post-infection (day 59 and 62 post-1º vaccination), lung and nasal turbinate tissues were

collected (n=4/group, 2 males and 2 females) and stored at -80C. The remaining 6 hamsters were monitored for weight-loss until day 14 (day 70 post-primary vaccination).

Trial 2: Assessment of the requirement for grafting of RBD to SpyCage

Groups of hamsters (n=18/group) were intranasally vaccinated with PBS (mock), SpyCage (15 ug), SARS-CoV-2 RBD (10 ug), SARS-CoV-2 RBD without SpyTag (10 ug) mixed with SpyCage (15 ug) (*i.e.,* RBD could not covalently bond to SpyCage, "RBD|SpyCage"), and SARS-CoV-2 RBD (10 ug) grafted to SpyCage (15 ug, "RBD+SpyCage"). The vaccination and blood collection protocol were the same as in the initial study, and on day 56 post-1º vaccination animals were challenged with 1000 TCID50 of SARS-CoV-2. On days 3, 5, and 7 post-challenge (days 59, 61, and 63 post-primary vaccination), lung and nasal turbinates were collected (n=4/group (2 males and 2 females)). One lung lobe was fixed with 10% v/v normal buffered formalin and the remaining lung lobes and nasal turbinates were stored at -80ºC. The remaining 6 hamsters/group were monitored for weight-loss until day 14 post-SARS-CoV-2 challenge (day 70 post-primary vaccination). All animals were euthanized on day 15 post-SARS-CoV-2 challenge.

Viral titration of tissue samples

Collected lungs and nasal turbinates were homogenized in 2% FBS-DMEM containing 2X antibiotic and antimycotic using an Omni tissue homogenizer. The homogenates were centrifuged at 1000 *x g* for 10 minutes at 4C and the supernatant was titrated to determine the tissue culture infectious dose 50% (TCID50) on Vero E6 cells as previously described[52].

Microneutralization Assay

To determine titers of neutralizing antibodies, microneutralization assays were performed on Vero E6 cells as previously described[52].

ELISA

To assess the levels of RBD-binding IgG and IgA antibodies, ELISA assays were performed according to a protocol generously provided by Dr. Sabra Klein, Johns Hopkins, School of Public Health[53,54].

Histopathology

Formalin-fixed lung samples were processed and stained with haematoxylin and eosin as previously described[54]. Slides were scored by a board-certified veterinary pathologist using established methods[55]. Each animal was scored for extent of lesions (0-4), alveolar damage (0-3), bronchial damage (0-3), blood vessel damage (0-3), hemorrhage (0-2), and type II pneumocyte hyperplasia (0-2). For each animal a total pathology score was obtained by calculating the sum of scores.

Biocontainment and Animal Care and Use

All experiments using SARS-CoV-2 were conducted in an animal biosafety level 3 enhanced laboratory. This facility is approved by the US Department of Agriculture and the Centers for Disease Control and Prevention. All animal studies were conducted in compliance with the Institutional Animal Care and Use Committee under protocol number 202001440 to TCS.

Statistical Analysis

Prism GraphPad (v9.0) was used to perform all statistical analysis with $p<0.05$ considered significant. Weight loss and viral titers at each time point were evaluated for normality by D'Agostino & Pearson test. For data sets that passed the normality test, one-way ANOVA with post-hoc Tukey's test was performed. When data sets did not pass the normality test, Kruskal-Wallis tests with a post-hoc Dunn's multiple comparison test were performed. Histopathological

303 scores were also compared using non-parametric Kruskal-Wallis tests with a post-hoc Dunn's

304 multiple comparison.

RESULTS

Cryo-EM reconstruction and refinement of an atomic model of the apo cage scaffold

To establish a robust, multimeric, spherical protein-based scaffold for intranasal immunizations that would mimic the size of a viral particle, we selected a wireframe dodecahedron based upon the previously described I3-01 protein, which was designed to self-assemble from 60 monomers[41,42]. To validate this scaffold structurally, we assessed a purified sample of this apo cage complex by electron microscopy. Samples were first quality controlled by negative staining with uranyl formate to assess particle integrity and concentration, and were then vitrified on gold grids for cryo-EM data collection on our home-source Titan Krios electron microscope equipped with a Falcon 3EC direct detection camera. Data processing and all aspects of the cryo-EM workflow were conducted in cryoSPARC software (v.3.3.2)[44].

To create an experimentally determined high resolution model, we collected a cryo-EM dataset with 1,220 recorded movies to yield 1,202 processed micrographs with good quality ice. These were used to auto-pick and extract 129,792 particles using a box size of 420x420 pixels (calibrated pixel size = 1.11 Å) (**Fig. 1A**, **Supplemental Table 1**). Then 2D-classification was used to clean up the data by removing junk particles (**Fig. 1B**) to produce a total of 63,430 particles for cryo-EM map reconstruction and refinement while imposing icosahedral symmetry. The refinement produced a cryo-EM map at an average resolution of 3.4 Å and estimated local resolution in the range of 3.0 Å to 5.0 Å (**Fig. 1C**). Map resolution was determined based on the gold-standard criterion that applies a Fourier Shell Correlation (FSC) cutoff value of 0.143 (**Fig. 1D**)[56]. The 3.4 Å resolution map showed the typical features of the designed apo cage with an average diameter of 25 nm and the trimeric protein units occupying the vertices of the pentameric faces of the dodecahedron. The I3-01 design PDB of this protein structure was modified and used to initiate model building[41,42]. The map density was clear enough to build the atomic structure using the published model of I3-01 to provide the starting coordinates. Real-

space refinement of the icosahedral model in PHENIX resulted in a 3.4 Å resolution model (**Fig. 1E**) with cross-correlation value for model vs. map of 0.77 (CC masked, **Supplemental Table 1**). The geometrical parameters of the refined model checked by MolProbity revealed a good quality model with a MolProbity score of 1.5, with approximately 98% of residues in the favored region and no residues in the disallowed region of the Ramachandran plot. Quality-check parameters of the model and map-model agreement are listed in **Supplemental Table 1**. The 3.4 Å resolution map showed clear density of most sidechains of the amino acids constituting the apo cage protein (aa 22-222) (**Fig. 1F)**. However, as expected for structures solved in the range of 3.0 to 4.0 Å resolution[57], directionality of some carbonyl groups could not be resolved unambiguously.

Comparing the solved cryo-EM structure and that from the computationally designed I3-01 model[41,42] showed that the two structures are almost identical [r.m.s. values of 0.57 Å for 200 Cα atoms and 1.29 Å for all non-hydrogen atoms], but that the sidechain atoms of surface residues had minor differences between our experimental and the computationally designed structures.

Covalent Bonding of SARS-CoV-2 Spike RBD to SpyCage

As the wireframe cage scaffold was robust, spherical, symmetrical, and could outwardly present up to 60 fused proteins-of-interest, we selected it for further modification for antigen display. Because genetic fusion of antigens directly to protein-based scaffolds can influence expression levels, solubility, and purification conditions needed, we leveraged the SpyTag/SpyCatcher system to covalently link antigens-of-interest to the scaffold following its purification[43]. This approach enables substantial versatility to load different proteins and their variants without modifying the scaffold itself and has been used for a variety of viral and parasitic pathogens to enhance immune responses[29-31,34-36,58]. To this end, we appended a SpyCatcher domain with a flexible linker to the N-terminus of I3-01 (schematic in **Fig. 2A**) and observed it displayed

357 excellent solubility and stability profiles when expressed in *E. coli* (**Fig. 2B**). A comparable
358 arrangement has been described for the mi3 variant of I3-01, which also exhibited favorable
359 display properties[30]. This scaffold, which we have termed SpyCage, was advanced for all
360 immunization studies presented here.
361 The use of SpyTag/SpyCatcher elements permits the versatile loading of antigens that are
362 independently expressed in an ideal expression system for that protein, thus ensuring that
363 proper post-translational modifications and processing events occur. Here, we produced the
364 receptor-binding domain (RBD) of SARS-CoV-2 Spike protein in 293F suspension cells with a
365 C-terminal 6xHis tag, and either with or without an additional C-terminal SpyTag. Secreted
366 protein was purified from the culture supernatant to >99% purity via Ni-NTA affinity
367 chromatography (**Fig. 2B**). Mixing of SpyCage with RBD (1 to 1.2 molar ratio) in 1xPBS led to
368 the formation of a covalent bond that could be detected by a mobility shift by SDS-PAGE with
369 >95% saturation of the scaffold with RBD (**Fig. 2B**). This covalent bond therefore permits
370 permanent grafting of RBD to SpyCage ("RBD+SpyCage"). In contrast, mixing of SpyCage with
371 RBD lacking a SpyTag produced no covalent linkage, as intended (**Fig. 2B**). This second
372 combination creates an admixture ("RBD|SpyCage") that permits testing of the effect that
373 covalent bonding of the antigen to the scaffold has upon efficacy. Further evidence of the
374 covalent grafting of RBD to SpyCage was provided by negative stain transmission electron
375 microscopy of RBD-loaded scaffolds, which revealed additional, nonuniform density along the
376 wireframe bars of the scaffold consistent with the size of RBD that was not seen in unloaded
377 scaffolds (**Fig. 2C**). From this we concluded that SpyCage is a stable and saturable antigen
378 display platform capable of presenting antigens-of-interest in a versatile mix-and-go format. As
379 SpyCage has similar structural properties as a virus particle and displays 5 copies of an antigen
380 on a single face of the scaffold (up to a total of 60 antigens per particle), we hypothesized
381 SpyCage grafted with RBD would be a greatly improved vaccine candidate. As there is an

urgent need for the development of vaccines inducing mucosal immunity, we proceeded to evaluate SpyCage as an intranasal vaccine candidate.

RBD grafting to SpyCage is required to induce an antibody response.

To assess the immunogenicity of RBD+SpyCage as an intranasal vaccine candidate (*i.e.,* Trial 1), hamsters were given a 1º and 2º intranasal vaccine consisting of PBS (mock), SpyCage, RBD, or RBD+SpyCage. The two vaccine doses were administered 28 days apart and serum samples were collected prior to each vaccination and viral challenge. To assess the antibody response, levels of RBD-binding IgG antibodies in the serum were quantified by ELISA and neutralizing antibodies were assayed by a microneutralization assay. We found that only the RBD+SpyCage-vaccinated animals developed an IgG antibody response (**Fig. S1A**). On day 28, one animal had IgG antibodies against RBD, while on day 55, 4/6 animals given RBD+SpyCage developed an antibody response (**Fig. S1A)**; however, while these antibodies were able to bind RBD, they did not exhibit neutralizing activity (**Fig. S1B**).

Subsequently, we conducted an expanded vaccine study (designated Trial 2) to determine if grafting of RBD directly to SpyCage through covalent bonding was required to induce an antibody response. Animals were vaccinated according to the same regimen; however, an additional group in which RBD without SpyTag was mixed with SpyCage (RBD|SpyCage) was included. Therefore, the experimental groups consisted of animals given the following vaccines: 1) Mock (PBS), 2) RBD, 3) SpyCage, 4) RBD mixed with SpyCage (RBD|SpyCage), and 5) RBD grafted to SpyCage (RBD+SpyCage). In both vaccination studies, animals were monitored for 7 days post-1º and 2º vaccination for adverse effects and none of the animals exhibited weight loss or clinical signs, indicating the vaccine was well-tolerated (data not shown).

Evaluation of the antibody response by ELISA and microneutralization assay (**Fig. 3**) showed that none of the mock, SpyCage, RBD alone, or RBD|SpyCage immunized animals developed

RBD-directed antibodies on day 28 or 55. In contrast, animals vaccinated with RBD+SpyCage developed IgG antibodies against RBD on day 28 post-1º vaccination (2/6 animals positive) and on day 55 (5/6 animals positive) (**Fig. 3A**). While most animals in the RBD+SpyCage group developed IgG antibodies, only 1 animal developed an IgA antibody response (**Fig. 3B**). This was one of the two animals that developed IgG antibodies early (day 28) and was the animal with the highest IgG antibody titer on day 55 (1: 12800) (**Fig. 3A**). In addition, the serum from this animal exhibited neutralizing activity (**Fig. 3C**), while none of the other animals developed a neutralizing antibody response. Thus, while we did not observe 100% seroconversion, the RBD+SpyCage vaccine candidate was reproducibly capable of inducing IgG antibodies. As one animal developed both a neutralizing antibody response and IgA antibodies indicative of mucosal immunity, our findings indicate that, with additional modifications to enhance immunogenicity, intranasal vaccination with RBD+SpyCage could induce protective mucosal immunity. Furthermore, these findings demonstrate the RBD+SpyCage vaccine provides a substantial boost in antibody responses compared to RBD alone or an RBD|SpyCage admixture where the covalent bond needed for grafting cannot form.

To address the immunogenicity of SpyCage itself, we also evaluated the antibody response to SpyCage by ELISA (**Fig. 3D)**. All animals given a vaccine containing SpyCage developed IgG antibodies directed towards the scaffold. While there were no statistically significant differences between different vaccine groups that received the SpyCage, the RBD|SpyCage admixture increased the antibody response 2-fold compared to animals given SpyCage alone, and RBD+SpyCage further increased the response by 2-fold (*i.e.,* 4-fold relative to SpyCage alone). These findings indicate the SpyCage scaffold is immunogenic and our collective findings indicate that grafting the antigen to SpyCage enhances the antibody response to both the scaffold and the antigen.

Intranasal vaccination with RBD+SpyCage enhances clearance of SARS-CoV-2 from the respiratory tract

To assess the efficacy of the RBD+SpyCage vaccine, in both trials of this study we assessed whether RBD+SpyCage enhanced viral clearance and reduced clinical illness. In the second trial, we also evaluated the effect of vaccination on reducing lung pathology. In Trial 1, vaccinated hamsters were challenged with 10^5 TCID50 SARS-CoV-2 on day 56 post-1º vaccination (day 28 post-2º vaccination). After viral challenge, animals were monitored for weight loss for 14 days, and on days 3 and 5 post-infection (p.i.), lung and nasal turbinate samples were collected from a subset of animals (n=4/group/timepoint) (**Fig. S2**). After viral challenge, animals in all experimental groups lost weight (**Fig. S2A**) and there were no statistically significant differences between the groups; however, the animals that received RBD+SpyCage had reduced weight loss, and by the end of the study these animals exceeded their pre-challenge weight. When we evaluated viral titers in the lungs and nasal turbinates, on day 3 p.i. all experimental groups had high titers of replicating virus in these tissues with no significant differences between groups. On day 6 p.i., viral titers in both tissues were reduced for all groups; however, while the mock and SpyCage-vaccinated animals had replicating virus in the nose and lungs, no replicating virus was recovered from the RBD only and RBD+SpyCage vaccinated animals (**Fig. S2 B,C**). These findings suggested vaccination with RBD or RBD+SpyCage facilitated viral clearance.

While vaccination with either RBD only or RBD+SpyCage reduced viral load on day 6, only the RBD+SpyCage vaccinated animals developed an IgG antibody response. We therefore performed a second, expanded vaccination study (i.e., Trial 2) to evaluate if grafting of RBD to SpyCage via covalent bonding was required for protection. Here we repeated the vaccination study with an additional group of animals that were vaccinated with an admixture of RBD and SpyCage where the covalent bond needed for grafting could not form (RBD|SpyCage). As the 10^5 $TCID_{50}$ challenge dose used in the initial study is 2-3 orders of magnitude higher than the

estimated infectious dose for humans (*i.e.,* 100-1000 infectious units)[59,60], we reduced the challenge dose to 1000 TCID50 of SARS-CoV-2. This challenge dose was previously shown to induce weight loss in hamsters[61], which we also verified with our virus stock (**Fig. S3)**. Finally, to more comprehensively evaluate the dynamics of viral clearance, we also modified the time points of tissue collection such that tissues were collected on days 3, 5, and 7 p.i.

After viral challenge, the animals in all experimental groups lost weight with peak weight-loss at day 6 or 7. However, while there were no statistically significant differences in weight loss between experimental groups (**Fig. 4A**), consistent with our first study, we also observed that animals vaccinated with RBD+SpyCage trended toward reduced weight loss compared to the other groups (**Fig. 4A**). We next evaluated viral replication in the nasal turbinates and lungs. On day 3 p.i., mean viral load in the nasal turbinates and lungs for all groups were comparable, with titers greater than 10^5 and 10^6 TCID50/gm in each tissue, respectively (**Fig. 4 B,C**). However, on day 5 p.i. the mean viral titer in the nasal turbinates for the RBD+SpyCage group was significantly lower (25 TCID50/gm) compared to the other experimental groups (titer range: 881 – 3955 TCID50/gm) (**Fig. 4B**). Similarly, in the lungs, RBD+SpyCage vaccinated animals also had significantly lower titers (1183 TCID50/gm) (titer range for other experimental groups:11,988 – 59,356 TCID50/gm) (**Fig. 4C**). On day 7 p.i., replicating virus was not detected in the nasal turbinates or lungs from any of the experimental groups (**Fig. 4 B,C**). Therefore, while viral titers on days 3 and 7 in the nasal turbinates and lungs were comparable for all groups, on day 5 viral titers in the RBD+SpyCage vaccinated animals were more than 10-fold lower, indicating that the RBD+SpyCage vaccinated animals more rapidly cleared SARS-CoV-2 from both the upper and lower respiratory tract.

Last, we performed a histopathology analysis to determine if the RBD+SpyCage vaccinated animals had reduced lung inflammation and damage. Lung tissue sections were blinded and scored for extent of lesions, alveolar, bronchial, and blood vessel damage, as well as hemorrhage and type II pneumocyte hyperplasia. These scores were then combined to give a

total pathology score. Representative images of lung pathology and inflammation from each group are shown in **Fig. 5A.** The largest differences in pathology scores were observed in the total pathology score and the extent of lesions (**Fig. 5 B,C)**, with additional scores reported in **Fig. S4**. On day 3, all groups exhibited similar pathology. For the mock vaccinated animals, the total pathology score and extent of lesions peaked on day 5 and then declined on day 7. The RBD+SpyCage vaccinated animals exhibited the lowest scores compared to all other groups on both days 5 and 7. Animals receiving SpyCage, RBD, or the SpyCage|RBD admixture had intermediate scores between the mock and SpyCage+RBD groups on day 5, and had pathology scores comparable to mock infected animals on day 7. While the pathology scoring shows a trend towards reduced pathology and clearance with the SpyCage+RBD group, this difference was not statistically significant due to the limited number of animals used at each time point. Future studies can leverage these observed effect sizes to establish expanded group sizes to determine if these promising trends are maintained.

DISCUSSION

Effective vaccines are required to limit the spread and reduce the disease burden of SARS-CoV-2. Currently licensed vaccines reduce disease severity, but do not prevent infection. As a result, SARS-CoV-2 has continued to evolve to generate new variants[62]. The development of intranasal vaccines has the potential to prevent infection and reduce transmission as they could induce immunity at the mucosal surfaces of the upper respiratory tract[62]. To date several pre-clinical intranasal vaccine candidates have been developed against SARS-CoV-2[63]. Most of these candidates are live-attenuated or viral vector vaccines. Due to safety concerns, the administration of these vaccines is often limited to healthy adults (18-55 years old) and/or older children. In contrast, recombinant protein or inactivated vaccines are widely used in individuals of all ages. Therefore, we sought to develop a recombinant protein-based intranasal vaccine.

Because immune responses can be substantially enhanced when antigens-of-interest are displayed on a scaffold that mimics the structure of a pathogen, we evaluated multiple protein-based scaffold options for the generation of an intranasal vaccine candidate. These included bacteriophage, VLPs, and engineered proteins. We established design criteria that prioritized 1) rigid bodies, 2) spherical shapes of ~20-30 nm in diameter, and 3) genetically accessible N- and/or C-termini presented in an outward facing manner. Among these, I3-01 met all of these design criteria and was selected as the strongest candidate.

To date, only a lower resolution cryo-EM reconstruction and a computational model of I3-01 have previously been published[41]. Therefore, we used both negative stain TEM and cryo-EM to structurally evaluate an I3-01-based scaffold (apo cage). We resolved the structure to a 3.4A average resolution and validated that the experimentally derived atomic model closely matched the computationally designed protein (**Fig. 1**). We therefore proceeded with using I3-01 to create SpyCage by further modifying I3-01 to bear an N-terminal SpyCatcher domain with a 12 amino acid flexible linker to reduce steric hindrance and permit greater saturation of antigens.

As anticipated, the SpyTag/SpyCatcher system enabled rapid, covalent linkage of RBD to SpyCage (RBD+SpyCage) to near saturation as seen by a mobility shift by SDS-PAGE and by negative stain TEM (**Fig. 2**). Importantly, the RBD+SpyCage preparation remained highly soluble and stable over time, which further supports its feasibility as a vaccine candidate.

Subsequently, we assessed the immunogenicity of the RBD+SpyCage vaccine in the hamsters (*i.e.,* Trial 1). Animals were given a prime-boost intranasal vaccination, and then challenged with SARS-CoV-2. On day 26 post-primary vaccination, 1 of 6 RBD+SpyCage vaccinated hamsters developed serum IgG antibodies, and by day 55, most animals (4/6) had a measurable IgG response. None of the animals developed neutralizing antibodies (**Fig. S1**). Following viral challenge, all animals, regardless of vaccination status, lost weight, although there was a trend towards reduced weight loss and earlier recovery in the RBD+SpyCage vaccinated animals (**Fig. S2**). Based on these outcomes, we next sought to determine the properties of the vaccine that enhanced immunogenicity. Studies on intramuscular vaccination have shown that presenting viral antigens on the surface of particles enhances the immune presentation and protective efficacy of vaccines[64]. As there is limited evidence on whether this phenomenon also holds for intranasal vaccination, we expanded upon our initial study and compared RBD+SpyCage (in which RBD is covalently bound to the scaffold) to an RBD|SpyCage admixture lacking this covalent attachment. Covalent grafting was shown to be a requirement for immunogenicity, as 2/6 and 5/6 animals given RBD+SpyCage developed an IgG response on days 28 and 55, respectively against RBD (**Fig 3**). Importantly, the one animal that exhibited the highest IgG titers on day 28 and day 55, also developed an IgA response, and these antibodies exhibited neutralizing activity. In contrast, animals vaccinated with admixed RBD|SpyCage did not develop an antibody response to RBD. Further studies are warranted to explore strategies to enhance the immunogenicity of RBD+SpyCage to match the neutralizing IgG and IgA response we observed in this one animal. As a final component of our antibody

548 analyses, we evaluated the response generated against the SpyCage scaffold. All animals that
549 received SpyCage as a component of the vaccine developed antibodies directed towards the
550 scaffold. While our results do not suggest this immunity interfered with the immunogenicity of
551 the vaccine, as boost vaccination increased the response to RBD, if immunity against the
552 scaffold interferes with immunogenicity for other vaccine antigens, future studies can explore
553 the use of alternative scaffolds[65].

554 Consistent with the requirement that RBD be covalently grafted to SpyCage to induce an
555 antibody response, covalent grafting to SpyCage was also a requirement for vaccine efficacy.
556 Upon SARS-CoV-2 challenge in Trial 2, all animals lost weight; however, compared to the other
557 groups, RBD+SpyCage vaccinated animals had a trend towards reduced weight loss and
558 reduced lung pathology. This was associated with significantly reduced levels of replicating virus
559 in the respiratory tract on day 5 indicating rapid viral clearance in the RBD+SpyCage group
560 relative to the RBD|SpyCage group **(Fig 4)**. Collectively, the induction of a non-neutralizing
561 antibody response associated with accelerated viral clearance and trends towards reduced
562 disease severity and pathology is consistent with an induced non-neutralizing antibody
563 response.
564 To our knowledge, this is the first report of a scaffolded antigen being used as an intranasal
565 protein-based vaccine. Other groups have used the I3-01 scaffold successfully as a vaccine
566 platform to display antigens for influenza, SARS-CoV-2, and *Plasmodium*, but have only
567 explored intramuscular administration[30,37,58,66-69]. To generate SARS-CoV-2 vaccines, several
568 groups have expressed either the RBD or S-protein on I3-01 and evaluated the immunogenicity
569 of these vaccines in several animal models[37,58,66-68]. In these studies, intramuscular vaccines
570 were administered with an adjuvant (*e.g.,* Addavax, Alum, CpG) and potent neutralizing
571 antibody responses were induced in mice, hamsters, pigs, or non-human primates[37,58,66-68].
572 Given both the route of administration and the inclusion of adjuvants, this is the expected

antibody response. In comparison, we administered the RBD+SpyCage vaccine via the intranasal route without an adjuvant which induced a non-neutralizing IgG antibody response. Prior studies have evaluated the protective efficacy of intramuscular vaccination with RBD grafted to I3-01 against SARS-CoV-2 challenge[37,58]. When hamsters were intramuscularly vaccinated and challenged with SARS-CoV-2, consistent with our results, all animals lost weight and the RBD-I3-01 vaccinated animals (designated “RBD-VLP” in that study) had reduced weight loss relative to animals vaccinated with RBD alone[37]. Unfortunately, in this study, viral titers were not evaluated in lung or nasal turbinate samples after viral infection, precluding a comparison with our findings. In another study, when transgenic K18-hACE2 mice were vaccinated with a similar construct, SARS-CoV-2 Beta RBD-mi3, and challenged, all vaccinated mice survived a lethal challenge while only 20% of control animals survived. In parallel, with enhanced survival, no replicating virus was detected in the lungs of the RBD-mi3 vaccinated animals[58]. Similarly, when Rhesus macaques were vaccinated with the same construct and challenged with SARS-CoV-2, at both day 2 and 4 p.i. significantly lower titers of virus were detected in nasal swabs compared to unimmunized controls. Moreover, in RBD-mi3 vaccinated animals, replicating virus was not recovered from bronchioloalveolar lavage fluids (BAL) (i.e., 0/4), while 3/4 unimmunized controls had between 10^3 - 10^6 TCID50/mL of SARS-CoV-2 in the BAL[58]. In addition to I3-01, the bipartite I53-50 icosahedral scaffold consisting of 120-subunit proteins has also been decorated with either the RBD or S-protein and utilized as an intramuscular vaccine[29,70]. Consistent with intramuscular vaccination with I3-01, intramuscular vaccination with RBD or S-protein grafted to I53-50 combined with an adjuvant induced a neutralizing antibody response in mice, rabbits, or macaques [29,70]. In these studies, only macaques vaccinated with S-protein on I53-50 nanoparticles were challenged with SARS-CoV-2. Following viral challenge, relative to unimmunized controls, vaccinated animals had reduced clinical manifestations associated with significantly reduced viral titers in the upper airways and BAL from day 1 until resolution on day 7 p.i.[29]. In contrast to these studies, when we challenged

the RBD+SpyCage vaccinated animals, we did not observe an initial reduction in SARS-CoV-2 replication as all animals had similar titers on day 3 p.i.; however, the RBD+SpyCage vaccinated animals had reduced titers on day 5 indicating accelerated viral clearance. We also observed trends towards reduced weight loss and reduced pathology; however, these were not statistically significant. The reduced efficacy observed in our studies relative to intramuscular vaccination is most likely due to a lack of a neutralizing antibody response following intranasal vaccination. In our studies, we purposefully did not include an adjuvant as there are no licensed intranasal adjuvants for human use; however, future development of the intranasal RBD+SpyCage vaccine warrants the inclusion of intranasal adjuvants to enhance the quality of the antibody response and vaccine efficacy.

Collectively, we demonstrate intranasal vaccination with RBD grafted to SpyCage induced a serum IgG response in hamsters. Upon viral challenge, this response was associated with accelerated viral clearance from both the upper and lower respiratory tract. RBD+SpyCage vaccinated animals also exhibited non-significant reductions in weight loss and lung pathology consistent with a non-neutralizing antibody response. We further show the immunogenicity and efficacy of the RBD+SpyCage vaccine required that RBD was covalently linked to the SpyCage scaffold. These studies demonstrate the potential for intranasal delivery of SpyCage scaffolded antigens as a vaccine platform, and additional vaccine development is warranted with the inclusion of intranasal adjuvants to enhance immunogenicity. Moreover, given the relative ease with which vaccine antigens can be grafted to the scaffold and the potential to induce mucosal immunity, SpyCage derived intranasal vaccines can be developed to target other respiratory viruses, and if successful, this platform could also be used as a rapid response vaccine platform to target novel or pandemic pathogens.

DATA AVAILABILITY

The icosahedral map of the solved apo cage structure is deposited in EM data bank under accession code EMD-27812. The apo cage atomic model is deposited in the PDB data bank under ID 8E01. A validation report is provided as Supp File 2 for peer review purposes.

ACKNOWLEDGMENTS

SH, SEL, and TCS planned all experiments with assistance from DRP and AM. AM and SEL designed and purified recombinant proteins and vaccine candidates. RMR expressed the RBD protein. All cryo-EM studies were conducted by CB, IMM, and SH. Vaccination and challenge studies were conducted by DRP with assistance from DGS, CJF, AK, and TH. EHL performed histopathology and analysis of lung samples. DRP, SH, SEL and TCS prepared the final manuscript.

The molecular graphics and analyses were performed with UCSF ChimeraX, developed by the Resource for Biocomputing, Visualization, and Informatics at the University of California, San Francisco, with support from National Institutes of Health R01-GM129325 and the Office of Cyber Infrastructure and Computational Biology, National Institute of Allergy and Infectious Diseases. We would like to acknowledge Dr. David Baker from the University of Washington for providing I3-01_HisR4 plasmid, Dr. Florian Krammer from Mount Sinai School of Medicine, for providing the pCAGGS plasmid for SARS-CoV-2 Spike RBD expression, and Dr. Sabra Klein, Johns Hopkins, School of Public Health for generously providing the IgG and IgA ELISA protocols. We also acknowledge Bob Ashley at Penn State College of Medicine for pilot electron microscopy efforts. Lastly, we would also like to acknowledge the Sartorius Huck Cell Culture Facility for early access and production of SARS-CoV-2 Spike RBD protein.

FUNDING

The design and expression of the SpyCage scaffold was conducted by SEL and SH under NIGMS R01GM125907. Seed Grant funding to SEL and TCS from the Pennsylvania State University Huck Institutes of Life Sciences supported the vaccination and challenge studies. Funding for TCS was also provided by the USDA National Institute of Food and Agriculture, Hatch project 4771.

DISCLOSURES

We wish to disclose the following intellectual property claims related to this study:

Lindner, S.E. & **Hafenstein, S.** US Patent Application 16/494,502 “Versatile Display for Proteins”

Lindner, S.E., **Hafenstein, S.**, & Butler, N. PCT/US2020/033785 “Specific Selection of Immune Cells Using Versatile Display Scaffolds”

Lindner, S.E., **Sutton, T.C.**, **Hafenstein, S.**, & Butler, N. US Trademark Application 9063755 “SPYCAGE”

660 **REFERENCES**

661

662 1 Zhu, N. *et al.* A Novel Coronavirus from Patients with Pneumonia in China, 2019. *New*
663 *England Journal of Medicine* **382**, 727-733, doi:10.1056/nejmoa2001017 (2020).
664 2 Krammer, F. SARS-CoV-2 vaccines in development. *Nature* **586**, 516-527,
665 doi:10.1038/s41586-020-2798-3 (2020).
666 3 @JohnsHopkins. *COVID-19 Map - Johns Hopkins Coronavirus Resource Center*,
667 <https://coronavirus.jhu.edu/map.html> (2022).
668 4 Kadam, S. B., Sukhramani, G. S., Bishnoi, P., Pable, A. A. & Barvkar, V. T. SARS-CoV-
669 2, the pandemic coronavirus: Molecular and structural insights. *Journal of Basic*
670 *Microbiology* **61**, 180-202, doi:10.1002/jobm.202000537 (2021).
671 5 Fehr, A. R. & Perlman, S. in *Coronaviruses* 1-23 (Springer New York, 2015).
672 6 Premkumar, L. *et al.* The receptor-binding domain of the viral spike protein is an
673 immunodominant and highly specific target of antibodies in SARS-CoV-2 patients.
674 doi:10.1126/sciimmunol.abc8413 (2020).
675 7 Piccoli, L. *et al.* Mapping Neutralizing and Immunodominant Sites on the SARS-CoV-2
676 Spike Receptor-Binding Domain by Structure-Guided High-Resolution Serology. *Cell*
677 **183**, 1024-1042.e1021, doi:10.1016/j.cell.2020.09.037 (2020).
678 8 Organization, W. H. *COVID-19 vaccine tracker and landscape*, <COVID-19 vaccine
679 tracker and landscape (who.int)> (
680 9 *COVID-19 Vaccines: The full list*, <https://covidvax.org> (2022).
681 10 Z, W. *et al.* Safety, tolerability, and immunogenicity of an inactivated SARS-CoV-2
682 vaccine (CoronaVac) in healthy adults aged 60 years and older: a randomised, double-
683 blind, placebo-controlled, phase 1/2 clinical trial. *The Lancet. Infectious diseases* **21**,
684 doi:10.1016/S1473-3099(20)30987-7 (2021).

11 Y, Z. *et al.* Safety, tolerability, and immunogenicity of an inactivated SARS-CoV-2 vaccine in healthy adults aged 18-59 years: a randomised, double-blind, placebo-controlled, phase 1/2 clinical trial. *The Lancet. Infectious diseases* **21**, doi:10.1016/S1473-3099(20)30843-4 (2021).

12 K, Z. *et al.* Safety and immunogenicity of a QazCovid-in® inactivated whole-virion vaccine against COVID-19 in healthy adults: A single-centre, randomised, single-blind, placebo-controlled phase 1 and an open-label phase 2 clinical trials with a 6 months follow-up in Kazakhstan. *EClinicalMedicine* **39**, doi:10.1016/j.eclinm.2021.101078 (2021).

13 S, X. *et al.* Effect of an Inactivated Vaccine Against SARS-CoV-2 on Safety and Immunogenicity Outcomes: Interim Analysis of 2 Randomized Clinical Trials. *JAMA* **324**, doi:10.1001/jama.2020.15543 (2020).

14 N, A. K. *et al.* Effect of 2 Inactivated SARS-CoV-2 Vaccines on Symptomatic COVID-19 Infection in Adults: A Randomized Clinical Trial. *JAMA* **326**, doi:10.1001/jama.2021.8565 (2021).

15 Xia, X. Detailed Dissection and Critical Evaluation of the Pfizer/BioNTech and Moderna mRNA Vaccines. *Vaccines* **9**, 734, doi:10.3390/vaccines9070734 (2021).

16 Creech, C. B., Walker, S. C. & Samuels, R. J. SARS-CoV-2 Vaccines. *JAMA* **325**, 1318, doi:10.1001/jama.2021.3199 (2021).

17 Machhi, J. *et al.* Nanocarrier vaccines for SARS-CoV-2. *Advanced Drug Delivery Reviews* **171**, 215-239, doi:10.1016/j.addr.2021.01.002 (2021).

18 Study of the Safety, Reactogenicity and Immunogenicity of "EpiVacCorona" Vaccine for the Prevention of COVID-19 - Full Text View - ClinicalTrials.gov. (2022).

19 VP, C., LK, V., AK, P. & VB, P. Intranasal vaccines for SARS-CoV-2: From challenges to potential in COVID-19 management. *Drug discovery today* **26**, doi:10.1016/j.drudis.2021.07.021 (2021).

20 Yusuf, H. & Kett, V. Current prospects and future challenges for nasal vaccine delivery. *Hum Vaccin Immunother* **13**, 34-45, doi:10.1080/21645515.2016.1239668 (2017).

21 Chemaitelly, H. *et al.* Waning of BNT162b2 Vaccine Protection against SARS-CoV-2 Infection in Qatar. *New England Journal of Medicine* **385**, e83, doi:10.1056/nejmoa2114114 (2021).

22 Keehner, J. *et al.* Resurgence of SARS-CoV-2 Infection in a Highly Vaccinated Health System Workforce. *New England Journal of Medicine* **385**, 1330-1332, doi:10.1056/nejmc2112981 (2021).

23 RWY, C. *et al.* The Mucosal and Serological Immune Responses to the Novel Coronavirus (SARS-CoV-2) Vaccines. *Frontiers in immunology* **12**, doi:10.3389/fimmu.2021.744887 (2021).

24 Lund, F. E. & Randall, T. D. Scent of a vaccine. *Science* **373**, 397-399, doi:10.1126/science.abg9857 (2021).

25 Topol, E. J. & Iwasaki, A. Operation Nasal Vaccine-Lightning speed to counter COVID-19. *Sci Immunol*, eadd9947, doi:10.1126/sciimmunol.add9947 (2022).

26 WHO, W. H. O. *The Oxford/AstraZeneca (ChAdOx1-S [recombinant] vaccine) COVID-19 vaccine: what you need to know*, <https://www.who.int/news-room/feature-stories/detail/the-oxford-astrazeneca-covid-19-vaccine-what-you-need-to-know> (2022).

27 FDA, U. F. a. D. A. *Coronavirus (COVID-19) Update: FDA Limits Use of Janssen COVID-19 Vaccine to Certain Individuals*, <https://www.fda.gov/news-events/press-announcements/coronavirus-covid-19-update-fda-limits-use-janssen-covid-19-vaccine-certain-individuals> (2022).

28 Sridhar, S., Brokstad, K. A. & Cox, R. J. Influenza Vaccination Strategies: Comparing Inactivated and Live Attenuated Influenza Vaccines. *Vaccines (Basel)* **3**, 373-389, doi:10.3390/vaccines3020373 (2015).

29 Brouwer, P. J. M. *et al.* Two-component spike nanoparticle vaccine protects macaques from SARS-CoV-2 infection. *Cell* **184**, 1188-1200 e1119, doi:10.1016/j.cell.2021.01.035 (2021).

30 Bruun, T. U. J., Andersson, A. C., Draper, S. J. & Howarth, M. Engineering a Rugged Nanoscaffold To Enhance Plug-and-Display Vaccination. *ACS Nano* **12**, 8855-8866, doi:10.1021/acsnano.8b02805 (2018).

31 Caradonna, T. M. & Schmidt, A. G. Protein engineering strategies for rational immunogen design. *NPJ Vaccines* **6**, 154, doi:10.1038/s41541-021-00417-1 (2021).

32 Cohen, A. A. *et al.* Mosaic nanoparticles elicit cross-reactive immune responses to zoonotic coronaviruses in mice. *Science* **371**, 735-741, doi:10.1126/science.abf6840 (2021).

33 Hsieh, C. L. & McLellan, J. S. Protein engineering responses to the COVID-19 pandemic. *Curr Opin Struct Biol* **74**, 102385, doi:10.1016/j.sbi.2022.102385 (2022).

34 Liu, Z. H. *et al.* Self-Assembling Nanovaccine Enhances Protective Efficacy Against CSFV in Pigs. *Front Immunol* **12**, 689187, doi:10.3389/fimmu.2021.689187 (2021).

35 Malhi, H. *et al.* Immunization with a self-assembling nanoparticle vaccine displaying EBV gH/gL protects humanized mice against lethal viral challenge. *Cell Rep Med* **3**, 100658, doi:10.1016/j.xcrm.2022.100658 (2022).

36 Nguyen, B. & Tolia, N. H. Protein-based antigen presentation platforms for nanoparticle vaccines. *NPJ Vaccines* **6**, 70, doi:10.1038/s41541-021-00330-7 (2021).

37 Dalvie, N. C. *et al.* Engineered SARS-CoV-2 receptor binding domain improves manufacturability in yeast and immunogenicity in mice. *Proc Natl Acad Sci U S A* **118**, doi:10.1073/pnas.2106845118 (2021).

38 Chan, J. F. *et al.* Simulation of the Clinical and Pathological Manifestations of Coronavirus Disease 2019 (COVID-19) in a Golden Syrian Hamster Model: Implications

for Disease Pathogenesis and Transmissibility. *Clin Infect Dis* **71**, 2428-2446, doi:10.1093/cid/ciaa325 (2020).

39 Imai, M. *et al.* Syrian hamsters as a small animal model for SARS-CoV-2 infection and countermeasure development. *Proc Natl Acad Sci U S A* **117**, 16587-16595, doi:10.1073/pnas.2009799117 (2020).

40 Rosenke, K. *et al.* Defining the Syrian hamster as a highly susceptible preclinical model for SARS-CoV-2 infection. *Emerg Microbes Infect* **9**, 2673-2684, doi:10.1080/22221751.2020.1858177 (2020).

41 Hsia, Y. *et al.* Design of a hyperstable 60-subunit protein dodecahedron. [corrected]. *Nature* **535**, 136-139, doi:10.1038/nature18010 (2016).

42 Hsia, Y. *et al.* Corrigendum: Design of a hyperstable 60-subunit protein icosahedron. *Nature* **540**, 150, doi:10.1038/nature20108 (2016).

43 Zakeri, B. *et al.* Peptide tag forming a rapid covalent bond to a protein, through engineering a bacterial adhesin. *Proc Natl Acad Sci U S A* **109**, E690-697, doi:10.1073/pnas.1115485109 (2012).

44 Punjani, A., Rubinstein, J. L., Fleet, D. J. & Brubaker, M. A. cryoSPARC: algorithms for rapid unsupervised cryo-EM structure determination. *Nat Methods* **14**, 290-296, doi:10.1038/nmeth.4169 (2017).

45 Bepler, T. *et al.* Positive-unlabeled convolutional neural networks for particle picking in cryo-electron micrographs. *Nat Methods* **16**, 1153-1160, doi:10.1038/s41592-019-0575-8 (2019).

46 Rubinstein, J. L. & Brubaker, M. A. Alignment of cryo-EM movies of individual particles by optimization of image translations. *J Struct Biol* **192**, 188-195, doi:10.1016/j.jsb.2015.08.007 (2015).

47 Pettersen, E. F. *et al.* UCSF ChimeraX: Structure visualization for researchers, educators, and developers. *Protein Sci* **30**, 70-82, doi:10.1002/pro.3943 (2021).

787 48 Liebschner, D. *et al.* Macromolecular structure determination using X-rays, neutrons and
788 electrons: recent developments in Phenix. *Acta Crystallogr D Struct Biol* **75**, 861-877,
789 doi:10.1107/S2059798319011471 (2019).
790 49 Emsley, P., Lohkamp, B., Scott, W. G. & Cowtan, K. Features and development of Coot.
791 *Acta Crystallogr D Biol Crystallogr* **66**, 486-501, doi:10.1107/S0907444910007493
792 (2010).
793 50 Williams, C. J. *et al.* MolProbity: More and better reference data for improved all-atom
794 structure validation. *Protein Sci* **27**, 293-315, doi:10.1002/pro.3330 (2018).
795 51 Reed, L. J. & Muench, H. A SIMPLE METHOD OF ESTIMATING FIFTY PER CENT
796 ENDPOINTS12. *American Journal of Epidemiology* **27**, 493-497,
797 doi:10.1093/oxfordjournals.aje.a118408 (1938).
798 52 Patel, D. R. *et al.* Transmission and Protection against Reinfection in the Ferret Model
799 with the SARS-CoV-2 USA-WA1/2020 Reference Isolate. doi:10.1128/jvi.02232-20
800 (2021).
801 53 Dhakal, S. *et al.* Sex Differences in Lung Imaging and SARS-CoV-2 Antibody
802 Responses in a COVID-19 Golden Syrian Hamster Model. *mBio* **12**, e0097421,
803 doi:10.1128/mBio.00974-21 (2021).
804 54 Field, C. J. *et al.* Immune durability and protection against SARS-CoV-2 re-infection in
805 Syrian hamsters. *Emerg Microbes Infect* **11**, 1103-1114,
806 doi:10.1080/22221751.2022.2058419 (2022).
807 55 Gerhards, N. M. *et al.* Predictive Value of Precision-Cut Lung Slices for the Susceptibility
808 of Three Animal Species for SARS-CoV-2 and Validation in a Refined Hamster Model.
809 *Pathogens* **10**, doi:10.3390/pathogens10070824 (2021).
810 56 Rosenthal, P. B. & Henderson, R. Optimal determination of particle orientation, absolute
811 hand, and contrast loss in single-particle electron cryomicroscopy. *J Mol Biol* **333**, 721-
812 745, doi:10.1016/j.jmb.2003.07.013 (2003).

57 Prisant, M. G., Williams, C. J., Chen, V. B., Richardson, J. S. & Richardson, D. C. New tools in MolProbity validation: CaBLAM for CryoEM backbone, UnDowser to rethink "waters," and NGL Viewer to recapture online 3D graphics. *Protein Sci* **29**, 315-329, doi:10.1002/pro.3786 (2020).

58 Cohen, A. A. *et al.* Mosaic RBD nanoparticles protect against challenge by diverse sarbecoviruses in animal models. *Science* **377**, eabq0839, doi:10.1126/science.abq0839 (2022).

59 Karimzadeh, S., Bhopal, R. & Nguyen Tien, H. Review of infective dose, routes of transmission and outcome of COVID-19 caused by the SARS-COV-2: comparison with other respiratory viruses. *Epidemiol Infect* **149**, e96, doi:10.1017/S0950268821000790 (2021).

60 Prentiss, M., Chu, A. & Berggren, K. K. Finding the infectious dose for COVID-19 by applying an airborne-transmission model to superspreader events. *PLoS One* **17**, e0265816, doi:10.1371/journal.pone.0265816 (2022).

61 Rosenke, K. *et al.* Defining the Syrian hamster as a highly susceptible preclinical model for SARS-CoV-2 infection. *https://doi.org/10.1080/22221751.2020.1858177*, doi:Temi-2020-1569.R1 (2020).

62 Focosi, D., Maggi, F. & Casadevall, A. Mucosal Vaccines, Sterilizing Immunity, and the Future of SARS-CoV-2 Virulence. *Viruses* **14**, 187, doi:10.3390/v14020187 (2022).

63 Chavda, V. P., Vora, L. K., Pandya, A. K. & Patravale, V. B. Intranasal vaccines for SARS-CoV-2: From challenges to potential in COVID-19 management. *Drug Discov Today* **26**, 2619-2636, doi:10.1016/j.drudis.2021.07.021 (2021).

64 Bachmann, M. F. & Jennings, G. T. Vaccine delivery: a matter of size, geometry, kinetics and molecular patterns. *Nature Reviews Immunology* **10**, 787-796, doi:doi:10.1038/nri2868 (2010).

838 65 Ueda, G. *et al.* Tailored design of protein nanoparticle scaffolds for multivalent
839 presentation of viral glycoprotein antigens. *Elife* **9**, doi:10.7554/eLife.57659 (2020).
840 66 He, L. *et al.* Single-component, self-assembling, protein nanoparticles presenting the
841 receptor binding domain and stabilized spike as SARS-CoV-2 vaccine candidates. *Sci*
842 *Adv* **7**, doi:10.1126/sciadv.abf1591 (2021).
843 67 Kang, Y. F. *et al.* Rapid Development of SARS-CoV-2 Spike Protein Receptor-Binding
844 Domain Self-Assembled Nanoparticle Vaccine Candidates. *ACS Nano* **15**, 2738-2752,
845 doi:10.1021/acsnano.0c08379 (2021).
846 68 Tan, T. K. *et al.* A COVID-19 vaccine candidate using SpyCatcher multimerization of the
847 SARS-CoV-2 spike protein receptor-binding domain induces potent neutralising antibody
848 responses. *Nature Communications* **12**, doi:10.1038/s41467-020-20654-7 (2021).
849 69 Cohen, A. A. *et al.* Construction, characterization, and immunization of nanoparticles
850 that display a diverse array of influenza HA trimers. *PLoS One* **16**, e0247963,
851 doi:10.1371/journal.pone.0247963 (2021).
852 70 Walls, A. C. *et al.* Elicitation of Potent Neutralizing Antibody Responses by Designed
853 Protein Nanoparticle Vaccines for SARS-CoV-2. *Cell* **183**, 1367-1382 e1317,
854 doi:10.1016/j.cell.2020.10.043 (2020).

855

FIGURE LEGENDS

Figure 1. Single-particle analysis and Cryo-EM reconstruction of the apo cage used for immunizations. (A) A representative cryo-EM micrograph of apo cage particles (scale bar, 25 nm) is provided. (B) Examples of representative class averages from a 2D classification of the particles extracted from cryo-EM micrographs are provided. (C) A reconstructed icosahedral map of the apo cage structure is colored according to the estimated local resolution; color key is shown to the left of the map. Red numbers in gray boxes on the structural model indicate the two-, three- and five-fold symmetry axes of the dodecahedron. Apo cage particles have an approximate diameter of 25 nm. (D) A fourier shell correlation (FSC) curve of the reconstructed map using gold-standard refinement in cryoSPARC is presented. An approximate map resolution of 3.4 Å based on 0.143 FSC cutoff is indicated. (E) An atomic model of the apo cage was built by applying icosahedral symmetry in ChimeraX to an asymmetric unit fitted to the density of the map shown in (C). (F) Left: A portion of the map covering a single I3-01 monomer is rendered as a transparent surface, with the fitted model (aa 22-222) shown as a light blue cartoon with side chains represented as sticks. Right: A close-up view of residues Val183, Cys184 and the C-terminal helix (aa 205-222) showing clear density of the assigned sidechains is shown with the map contoured at level 0.9 in ChimeraX. The quality of density is sufficient to observe the disulfide bond between Cys184 and the C-terminal Cys222.

Figure 2. Display of RBD via the SpyCage scaffold. (A) A schematic of the SpyCage scaffold illustrates 6xHis purification tags, the SpyCatcher capture domain, a flexible linker, and a C-terminal I3-01 variant used to create the self-assembling protein wireframe platform. (B) The covalent bonding (“grafting”) of RBD to SpyCage is evident when RBD bears a SpyTag, but not in its absence as per a mobility shift seen by SDS-PAGE. SpyCage approaches saturation with RBD at a 1-to-1.2 molar ratio of SpyCage-to-RBD. (C) Differences in appearance of unloaded

881 and RBD-loaded SpyCage by negative stain transmission electron microscopy (TEM) further
882 indicates the grafting of RBD has occurred.
883
884 **Figure 3. Binding and neutralizing antibody responses to intranasal vaccination with**
885 **RBD+SpyCage.** Antibody titers were measured in serum samples on days 0, 28, and 56, prior
886 to primary vaccination, boost vaccination, and viral challenge, respectively. Plotted are (A) anti-
887 RBD IgG, (B) IgA titers, (C) neutralizing antibody titers against SARS-CoV-2, and (D) IgG
888 antibody titers against the SpyCage scaffold. * significantly different from all other groups by
889 Kruskal-Wallis with Dunn's multiple comparison. † significantly different from mock and RBD
890 groups.
891
892 **Figure 4. Weight loss and viral titers in the nasal turbinates and lungs after SARS-CoV-2**
893 **challenge of vaccinated hamsters.** After viral challenge, hamsters were monitored for (A)
894 weight loss, and viral titers were evaluated in (B) nasal turbinates and (C) lung tissues on days
895 3, 5 and 7 post-infection. *significantly different from RBD and RBD|Spycage. **significantly
896 different from RBD|SpyCage. Non-parametric Kruskal-Wallis test with Dunn's multiple
897 comparisons were used to determine significant differences.
898
899 **Figure 5. SARS-CoV-2 induced lung pathology in vaccinated hamsters.** On days 3, 5, and
900 7, post-infection, lung tissues were processed for H&E staining and scored by a veterinary
901 pathologist. Panel (A) displays representative images from each group of hamsters on days 5
902 and 7 post-infection. This panel also includes images of uninfected hamster lung tissues (far
903 right panels). Panels (B) and (C) display total pathology scores and the extent of lesions
904 scoring, respectively.

SUPPLEMENTAL FIGURES, TABLES, AND FILES

Supplemental Figure 1. Evaluation of the immunogenicity of RBD+SpyCage determined by serum IgG and neutralizing antibody titers. Shown are the antibody titers from Trial 1 that evaluated immunogenicity of the RBD+SpyCage vaccine in hamsters. Plotted are (A) IgG antibody titers in serum samples collected on days 0, 26, and 55, and (B) neutralizing antibody titers against SARS-CoV-2 on day 0 and 55. * significantly different from all other groups, ($p<0.03$) determined by Kruskal-Wallis test with Dunn's multiple comparison correction.

Supplemental Figure 2. Weight loss and viral titers in the nasal turbinates and lungs after SARS-CoV-2 challenge of vaccinated hamsters. After viral challenge, hamsters in Trial 1 (immunogenicity study) hamsters were monitored for (A) weight loss, and viral titers were evaluated in (B) nasal turbinates and (C) lung tissues on days 3 and 6 post-infection.

Supplemental Figure 3. Weight loss in unvaccinated hamsters after challenge with 10^5, 10^4, and 10^3 TCID50 of SARS-CoV-2. To determine if lower challenge doses of SARS-CoV-2 would induce weight loss, equal numbers of male and female hamsters (n=3/sex, n=6/group) were intranasally inoculated with 10^5, 10^4, and 10^3 TCID50 of SARS-CoV-2/USA/WA1/2020. Weight loss was then monitored for 14 days until the animals recovered.

Supplemental Figure 4. Lung histopathology scoring for multiple parameters in vaccinated hamsters challenged with SARS-CoV-2. On days 3, 5, and 7 post-infection, lung tissues were processed for H&E staining and scored by a veterinary pathologist. Panels display scoring for (A) Type II Pneumocyte Hyperplasia, (B) Alveoli Pathology, (C) Hemorrhage, (D) Blood Vessels Pathology, and (E) Bronchi Pathology. Black horizontal lines indicate median score with the distribution of scores displayed as violin plots.

Supplementary Table 1: Cryo-EM data collection, processing, and model refinement statistics.

Supplemental File 1. Sequences of plasmids used in this study.

Supplemental File 2. A validation report for the cryo-EM reconstruction of the apo scaffold based on I3-01 is provided for peer review purposes.

Patel *et al*. Figure 1

A.

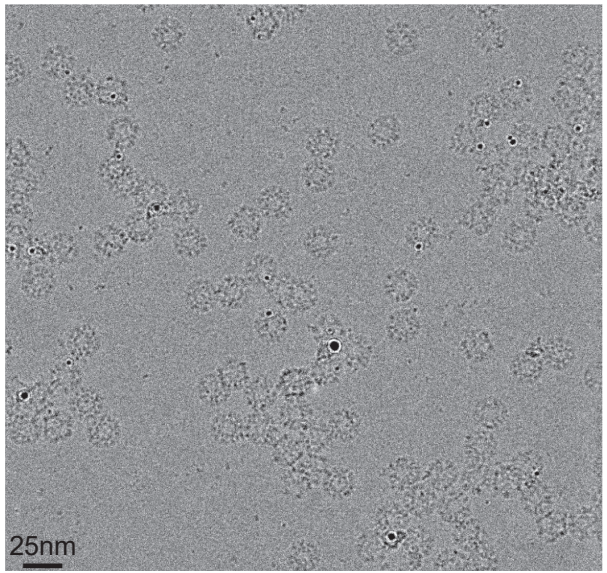

B.

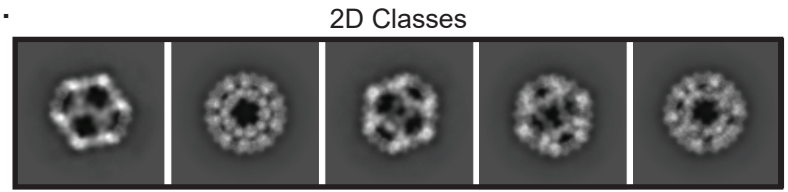

C.

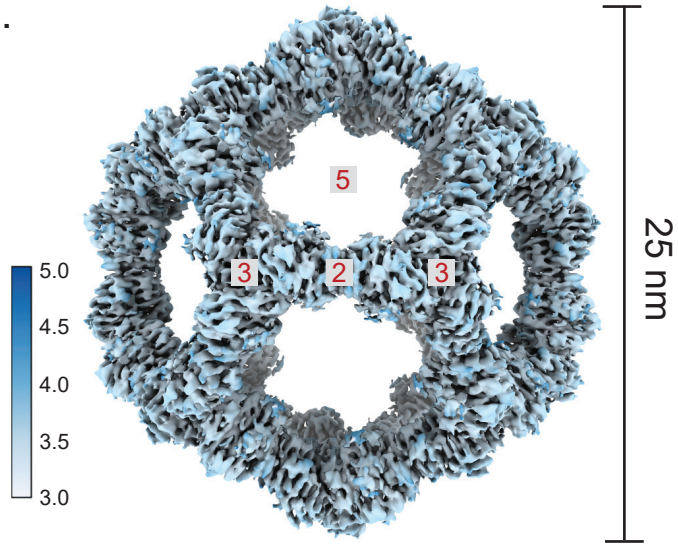

D.

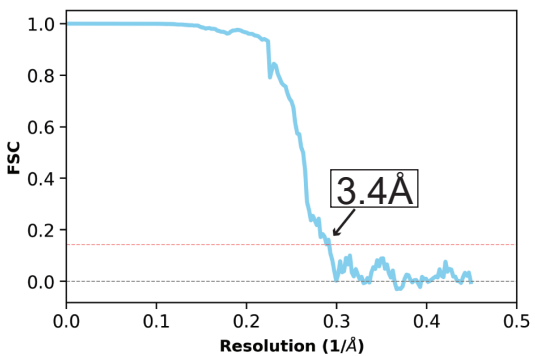

E.

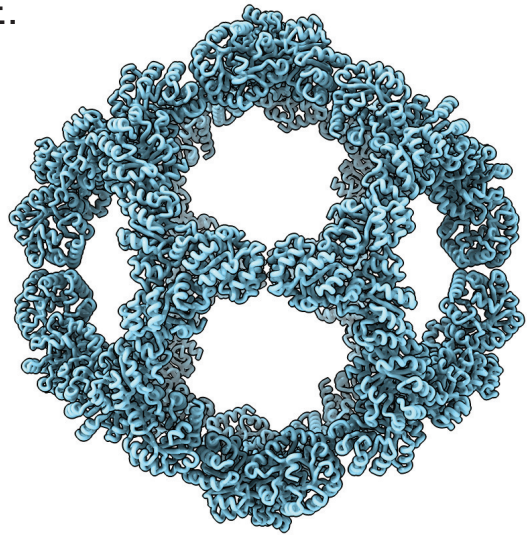

F.

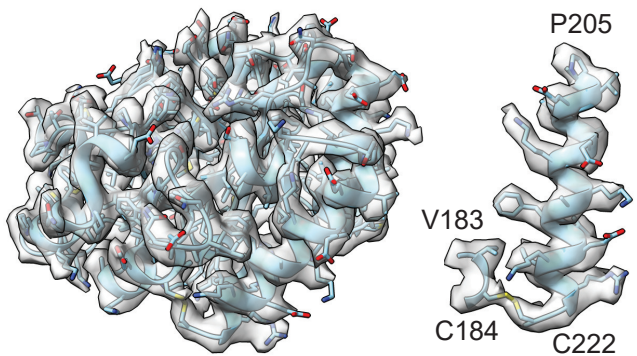

Patel *et al*. Figure 2

A.

SpyCage-Flexible

6xHis/SpyCatcher/6xHis/4x(GGS)/I3-01

B.

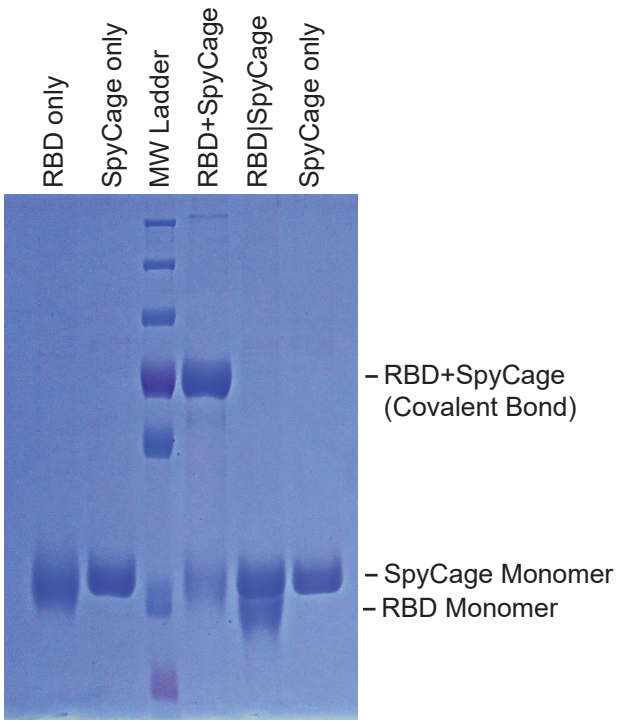

C.

Unloaded SpyCage

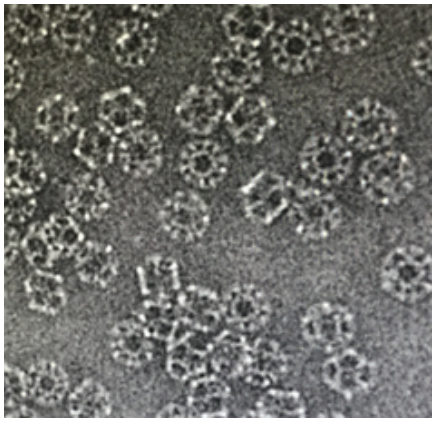

RBD-Loaded SpyCage

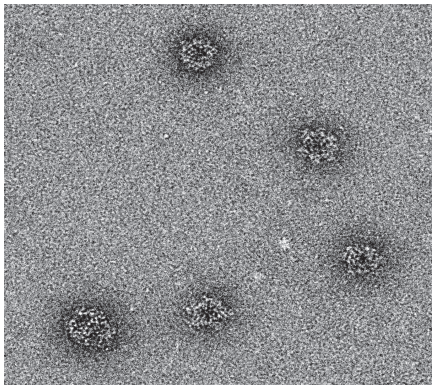

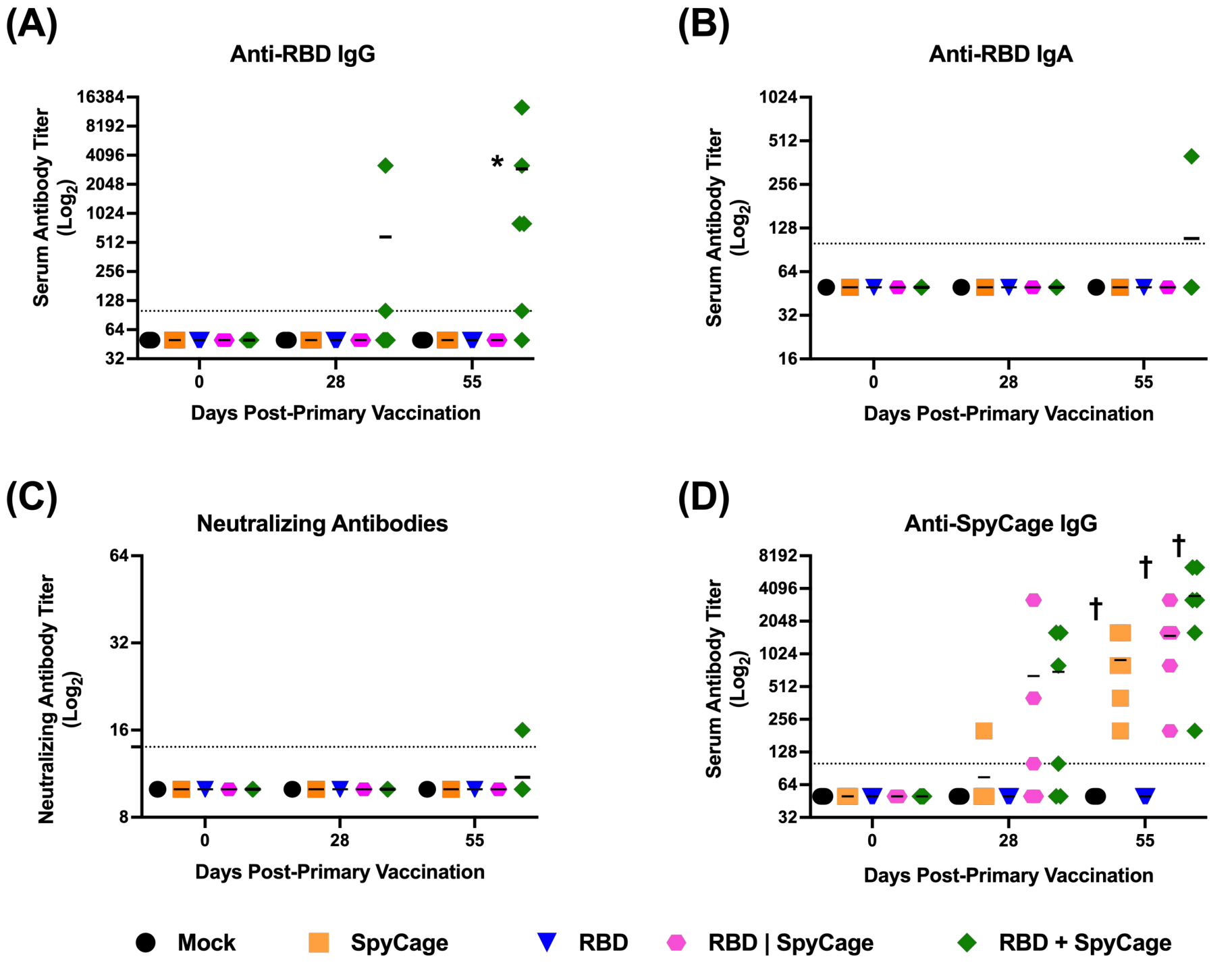
(A)
Anti-RBD IgG
Serum Antibody Titer (Log2)
16384
8192
4096
2048
1024
512
256
128
64
32
0
28
55
Days Post-Primary Vaccination
*
(B)
Anti-RBD IgA
Serum Antibody Titer (Log2)
1024
512
256
128
64
32
16
0
28
55
Days Post-Primary Vaccination
(C)
Neutralizing Antibodies
Neutralizing Antibody Titer (Log2)
64
32
16
8
0
28
55
Days Post-Primary Vaccination
(D)
Anti-SpyCage IgG
Serum Antibody Titer (Log2)
8192
4096
2048
1024
512
256
128
64
32
0
28
55
Days Post-Primary Vaccination
†
Mock
SpyCage
RBD
RBD | SpyCage
RBD + SpyCage

Figure 3

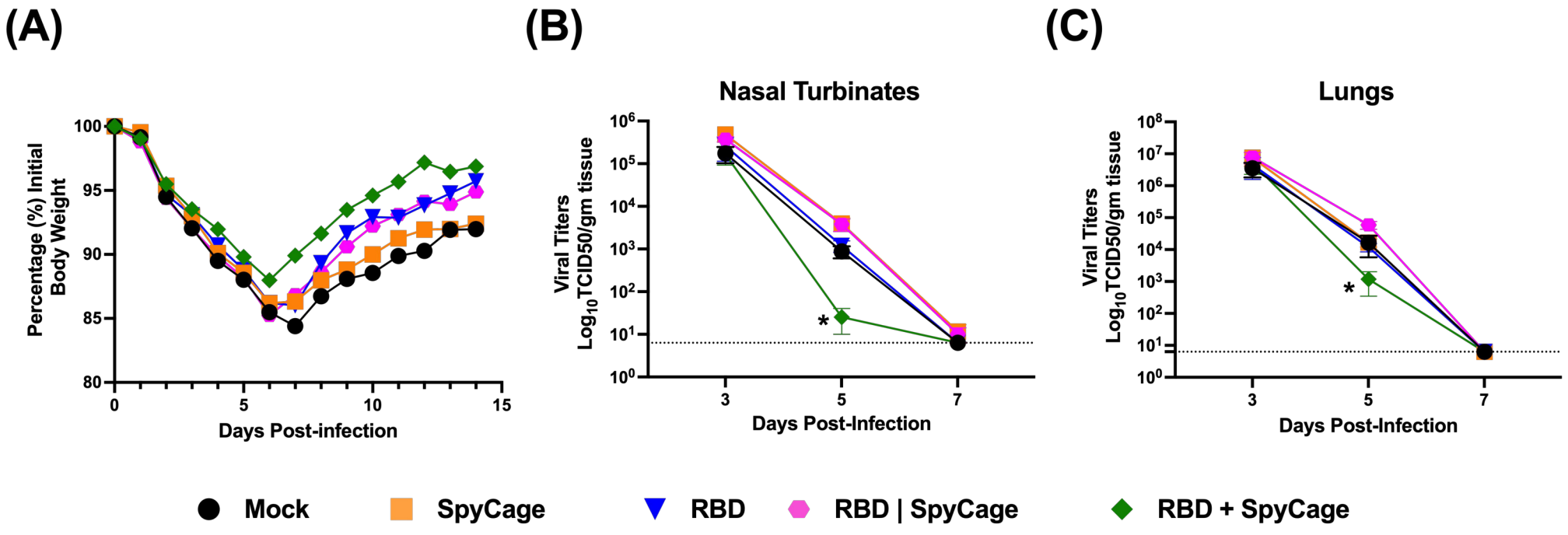
(A)
Percentage (%) Initial Body Weight
100
95
90
85
80
0
5
10
15
Days Post-infection
(B)
Nasal Turbinates
Viral Titers Log10TCID50/gm tissue
10^6
10^5
10^4
10^3
10^2
10^1
10^0
*
3
5
7
Days Post-Infection
(C)
Lungs
Viral Titers Log10TCID50/gm tissue
10^8
10^7
10^6
10^5
10^4
10^3
10^2
10^1
10^0
*
3
5
7
Days Post-Infection
Mock
SpyCage
RBD
RBD | SpyCage
RBD + SpyCage

Figure 4

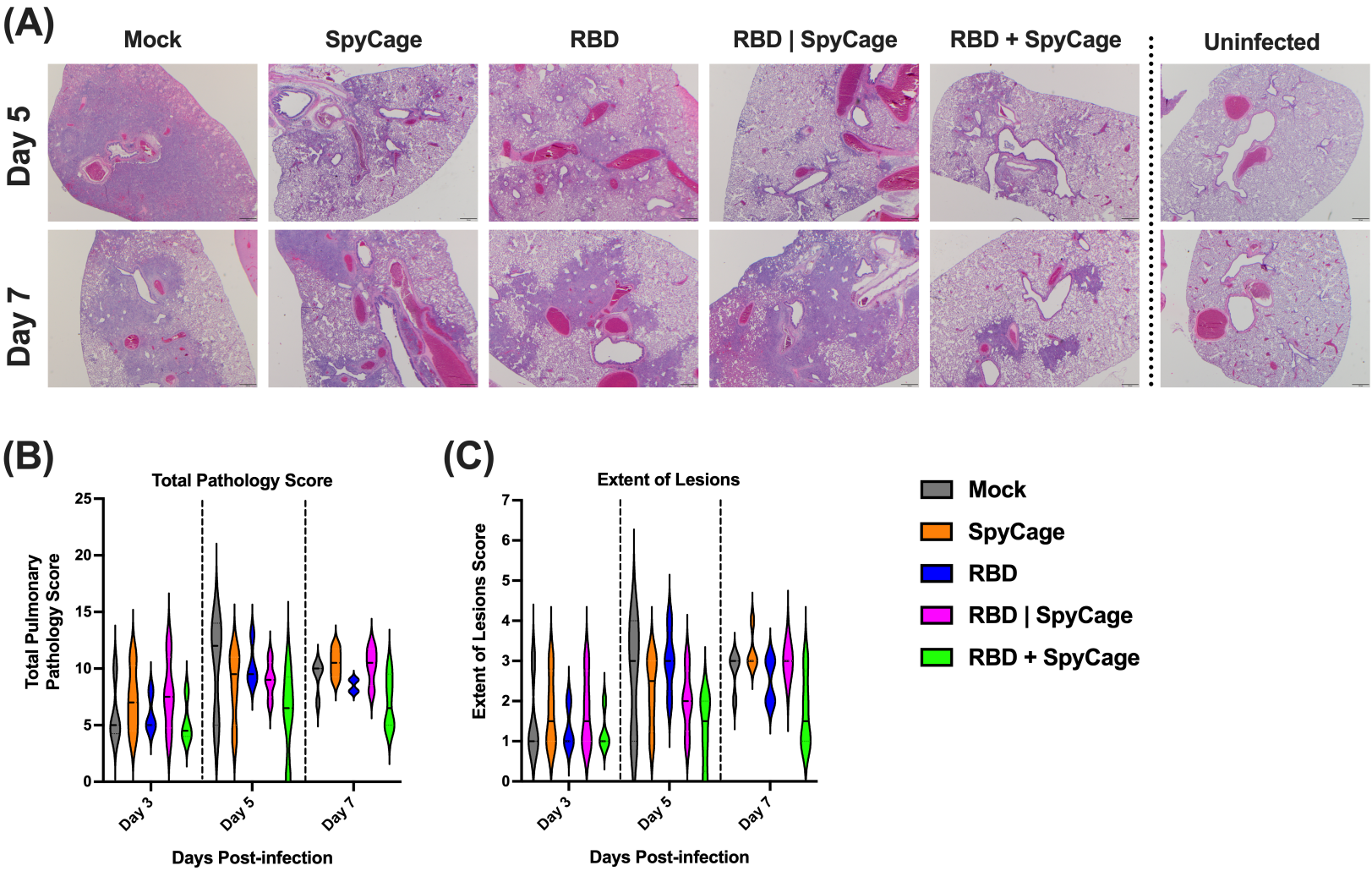

Figure 5

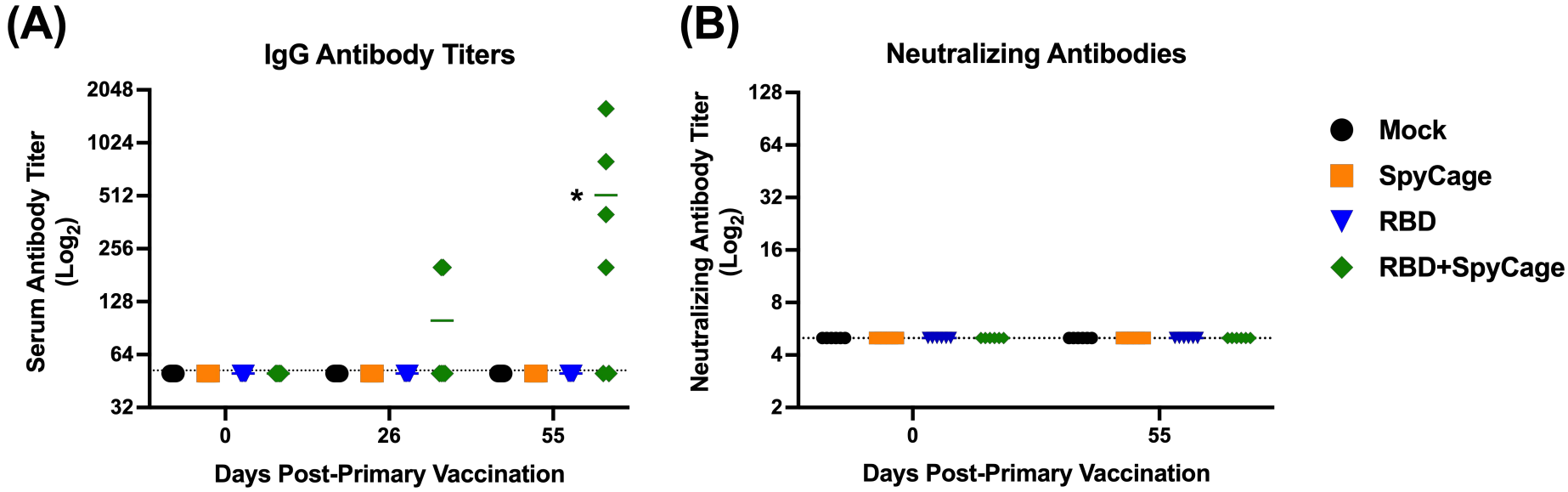
(A)
IgG Antibody Titers
Serum Antibody Titer (Log2)
2048
1024
512
256
128
64
32
*
0
26
55
Days Post-Primary Vaccination
(B)
Neutralizing Antibodies
Neutralizing Antibody Titer (Log2)
128
64
32
16
8
4
2
0
55
Days Post-Primary Vaccination
Mock
SpyCage
RBD
RBD+SpyCage

Figure S1

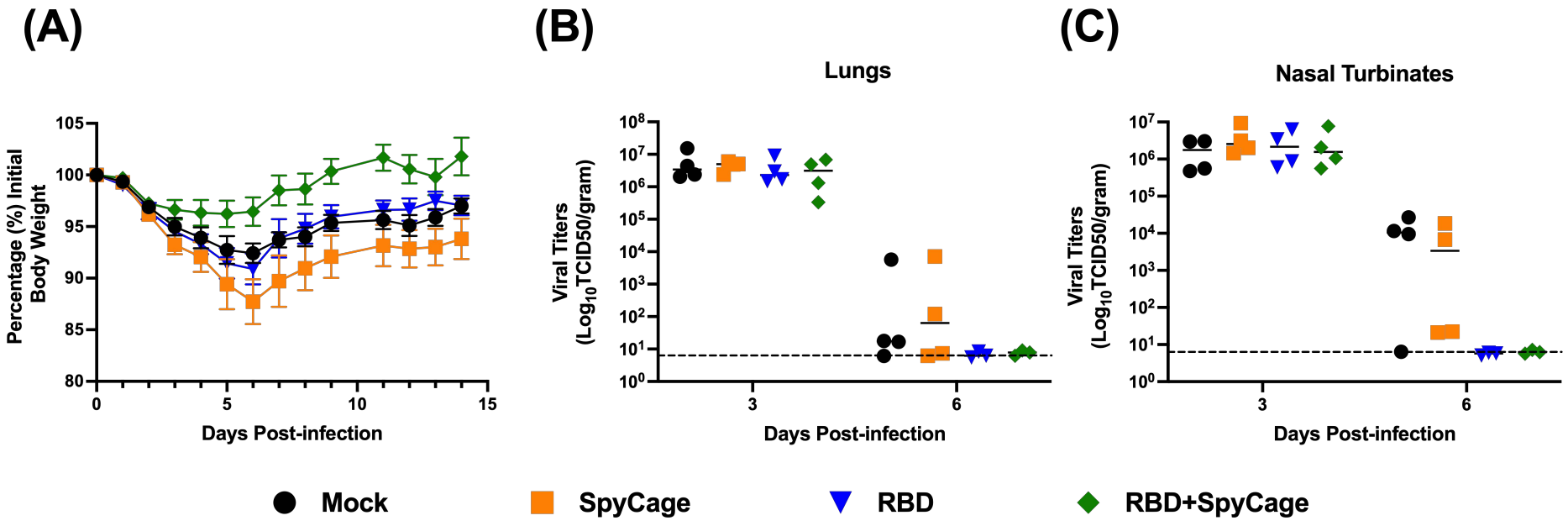
(A)
Percentage (%) Initial Body Weight
105
100
95
90
85
80
0
5
10
15
Days Post-infection
(B)
Lungs
Viral Titers (Log10TCID50/gram)
10^8
10^7
10^6
10^5
10^4
10^3
10^2
10^1
10^0
3
6
Days Post-infection
(C)
Nasal Turbinates
Viral Titers (Log10TCID50/gram)
10^7
10^6
10^5
10^4
10^3
10^2
10^1
10^0
3
6
Days Post-infection
Mock
SpyCage
RBD
RBD+SpyCage

Figure S2

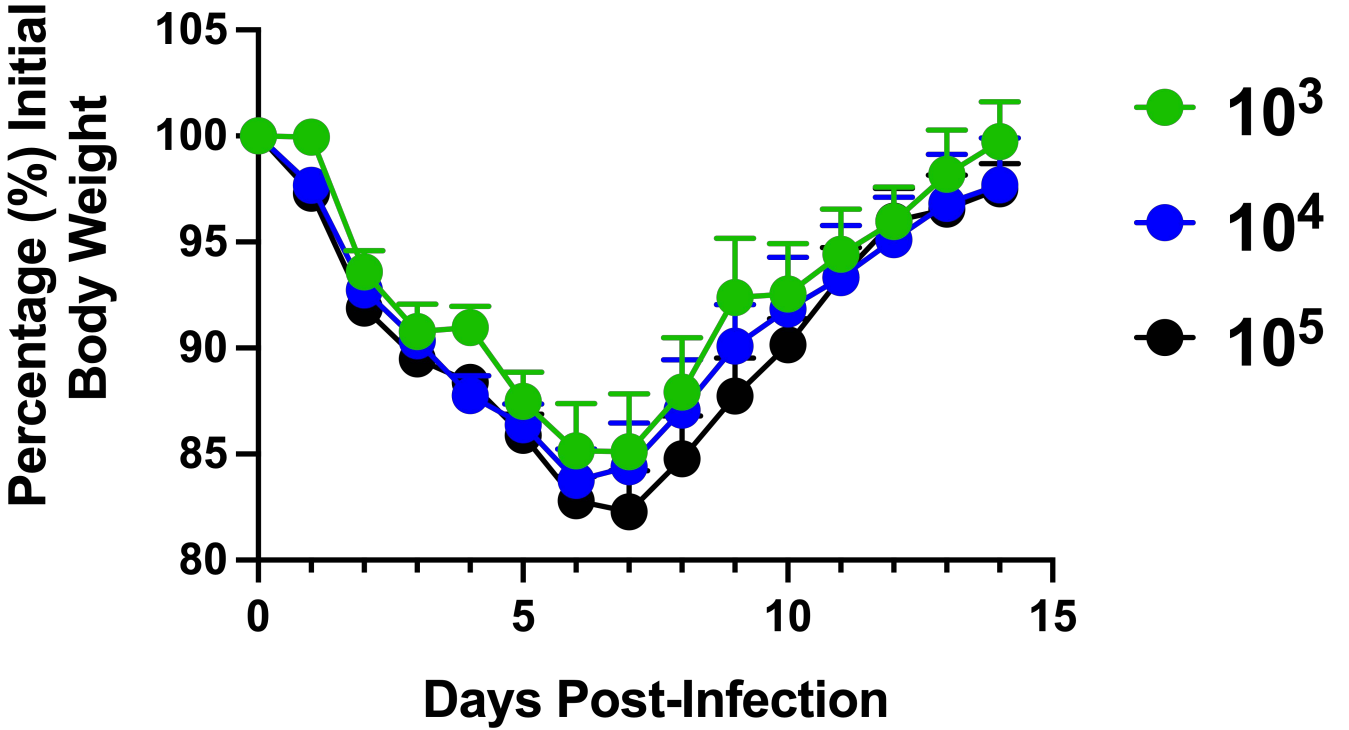
Percentage (%) Initial Body Weight
105
100
95
90
85
80
0
5
10
15
Days Post-Infection
10^3
10^4
10^5

Figure S3

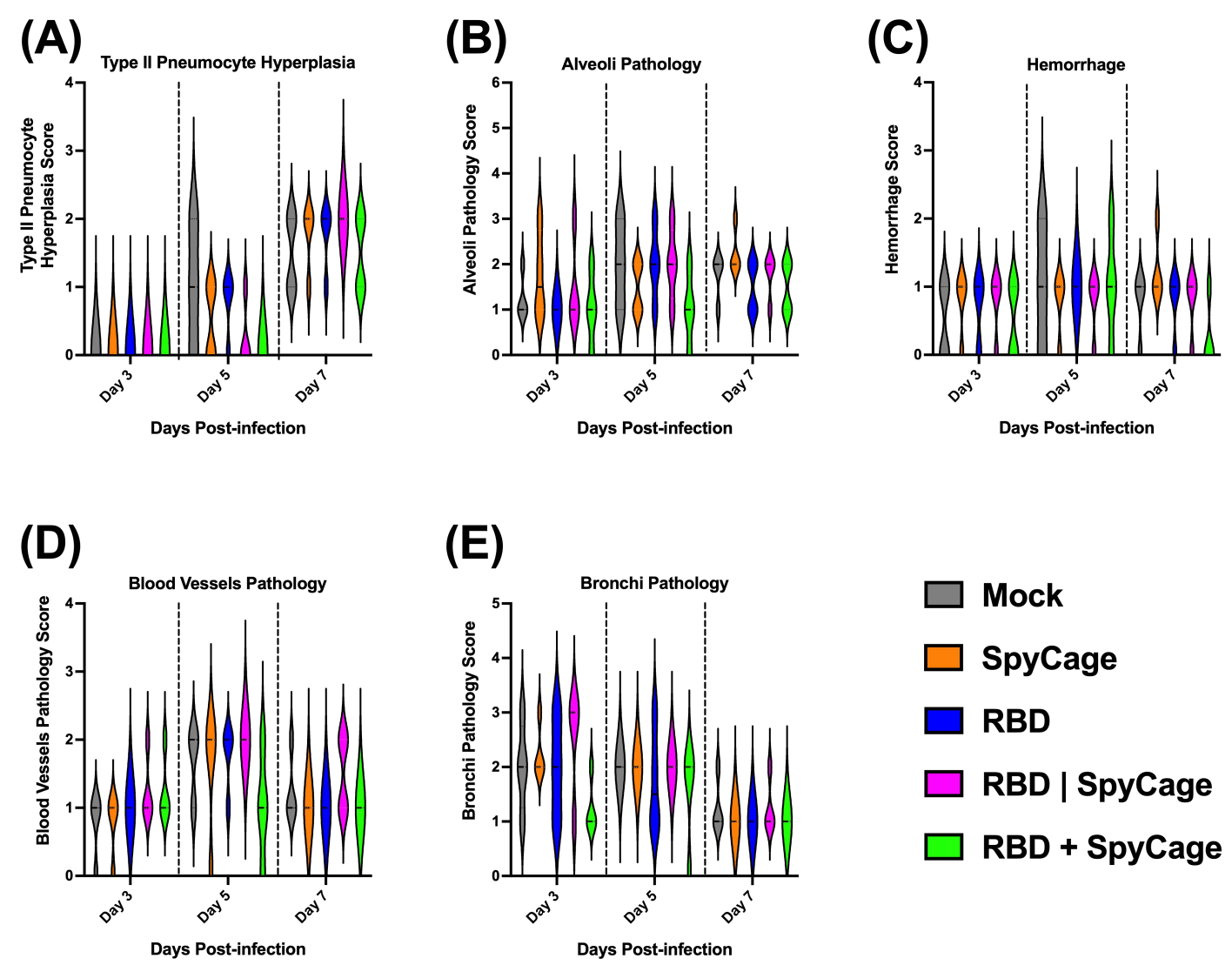
(A)
Type II Pneumocyte Hyperplasia
Type II Pneumocyte Hyperplasia Score
0
1
2
3
4
Day 3
Day 5
Day 7
Days Post-infection
(B)
Alveoli Pathology
Alveoli Pathology Score
0
1
2
3
4
5
6
Day 3
Day 5
Day 7
Days Post-infection
(C)
Hemorrhage
Hemorrhage Score
0
1
2
3
4
Day 3
Day 5
Day 7
Days Post-infection
(D)
Blood Vessels Pathology
Blood Vessels Pathology Score
0
1
2
3
4
Day 3
Day 5
Day 7
Days Post-infection
(E)
Bronchi Pathology
Bronchi Pathology Score
0
1
2
3
4
5
Day 3
Day 5
Day 7
Days Post-infection
Mock
SpyCage
RBD
RBD | SpyCage
RBD + SpyCage

Figure S4

Supplementary Table 1: Cryo-EM data collection, processing, and model refinement statistics

Data collection and processing	
Microscope	Titan Krios
Detector	Falcon 3EC
Voltage (kV)	300
Recording mode	Counting
Nominal magnification	x59,000
Electron exposure ($e^-/Å^2$)	45
No. of frames	39
Defocus range (μm)	-1.2 to -3.0
Pixel size (Å)	1.11
Symmetry	Icosahedral
Initial particles (no.)	129,792
Final particles (no.)	63,430
Map resolution (Å)	3.4
FSC Threshold	0.143
Map sharpening B-factor ($Å^2$)	-196.1
Model refinement	
Initial model used	I3-01
FSC model vs. map at FSC=0.5	3.77
CC model vs. map (masked)	0.77
Average B-factor ($Å^2$)	69.1
Bond length rmsd (Å)	0.002
Bond angle rmsd (^{o})	0.562
Model composition	
No. of chains	60
Non-hydrogen atoms/chain	1,519
protein residues/chain	201 (aa 22-222)
Validation	
Molprobity score	1.5
Clashscore	9.4
Poor rotamers (%)	none
Ramachandran plot	
Favored (%)	97.99
Allowed (%)	2.01
Disallowed (%)	none

Supplemental File 1: Sequences of plasmids used in this study.

```
>pSL1013_Apo_Cage_Expression_Plasmid
LOCUS       pSL1013              5916 bp    DNA       circular     20-JUL-2022
DEFINITION  .
ACCESSION
VERSION
SOURCE      .
  ORGANISM  .
COMMENT     pET29b(+) from 1 to 5370
COMMENT     pET29b(+)
COMMENT     ApEinfo:methylated:0
FEATURES             Location/Qualifiers
     misc_feature    5076..5750
                     /locus_tag="6xHis_4xGGS_I3-01"
                     /label="6xHis_4xGGS_I3-01"
                     /ApEinfo_label="6xHis_4xGGS_I3-01"
                     /ApEinfo_fwdcolor="cyan"
                     /ApEinfo_revcolor="green"
                     /ApEinfo_graphicformat="arrow_data {{0 1 2 0 0 -1} {} 0}
                     width 5 offset 0"
     rep_origin      1421..2103
                     /locus_tag="ColE1 origin"
                     /label="ColE1 origin"
                     /ApEinfo_label="ColE1 origin"
                     /ApEinfo_fwdcolor="gray50"
                     /ApEinfo_revcolor="gray50"
                     /ApEinfo_graphicformat="arrow_data {{0 1 2 0 0 -1} {} 0}
                     width 5 offset 0"
     rep_origin      29..335
                     /locus_tag="F1 ori"
                     /label="F1 ori"
                     /ApEinfo_label="F1 ori"
                     /ApEinfo_fwdcolor="gray50"
                     /ApEinfo_revcolor="gray50"
                     /ApEinfo_graphicformat="arrow_data {{0 1 2 0 0 -1} {} 0}
                     width 5 offset 0"
     rep_origin      12..467
                     /locus_tag="M13 origin"
                     /label="M13 origin"
                     /ApEinfo_label="M13 origin"
                     /ApEinfo_fwdcolor="gray50"
                     /ApEinfo_revcolor="gray50"
                     /ApEinfo_graphicformat="arrow_data {{0 1 2 0 0 -1} {} 0}
                     width 5 offset 0"
     misc_binding    5007..5029
                     /locus_tag="LacO"
                     /label="LacO"
                     /ApEinfo_label="LacO"
                     /ApEinfo_fwdcolor="#6495ed"
                     /ApEinfo_revcolor="#6495ed"
                     /ApEinfo_graphicformat="arrow_data {{0 1 2 0 0 -1} {} 0}
                     width 5 offset 0"
     CDS             complement(3518..4474)
                     /locus_tag="LacI"
                     /label="LacI"
                     /ApEinfo_label="LacI"
                     /ApEinfo_fwdcolor="gray50"
                     /ApEinfo_revcolor="gray50"
```

```
                     /ApEinfo_graphicformat="arrow_data {{0 1 2 0 0 -1} {} 0}
                     width 5 offset 0"
     CDS             complement(563..1375)
                     /locus_tag="KanR"
                     /label="KanR"
                     /ApEinfo_label="KanR"
                     /ApEinfo_fwdcolor="yellow"
                     /ApEinfo_revcolor="yellow"
                     /ApEinfo_graphicformat="arrow_data {{0 1 2 0 0 -1} {} 0}
                     width 5 offset 0"
     misc_feature    5788..5916
                     /locus_tag="T7 Terminator"
                     /label="T7 Terminator"
                     /ApEinfo_label="T7 Terminator"
                     /ApEinfo_fwdcolor="#8080ff"
                     /ApEinfo_revcolor="#8080ff"
                     /ApEinfo_graphicformat="arrow_data {{0 1 2 0 0 -1} {} 0}
                     width 5 offset 0"
     misc_feature    4988..5006
                     /locus_tag="T7prom"
                     /label="T7prom"
                     /ApEinfo_label="T7prom"
                     /ApEinfo_fwdcolor="#8080ff"
                     /ApEinfo_revcolor="#8080ff"
                     /ApEinfo_graphicformat="arrow_data {{0 1 2 0 0 -1} {} 0}
                     width 5 offset 0"
     misc_feature    5760..5777
                     /locus_tag="6xHis Epitope Tag (not translated)"
                     /label="6xHis Epitope Tag (not translated)"
                     /ApEinfo_label="6xHis Epitope Tag (not translated)"
                     /ApEinfo_fwdcolor="#0080c0"
                     /ApEinfo_revcolor="green"
                     /ApEinfo_graphicformat="arrow_data {{0 1 2 0 0 -1} {} 0}
                     width 5 offset 0"
ORIGIN
        1 tggcgaatgg gacgcgccct gtagcggcgc attaagcgcg gcgggtgtgg tggttacgcg
       61 cagcgtgacc gctacacttg ccagcgccct agcgcccgct cctttcgctt tcttcccttc
      121 ctttctcgcc acgttcgccg gctttccccg tcaagctcta aatcgggggc tcccttagg
      181 gttccgattt agtgctttac ggcacctcga ccccaaaaaa cttgattagg gtgatggttc
      241 acgtagtggg ccatcgccct gatagacggt ttttcgccct ttgacgttgg agtccacgtt
      301 ctttaatagt ggactcttgt tccaaactgg aacaacactc aaccctatct cggtctattc
      361 ttttgattta taagggattt tgccgatttc ggcctattgg ttaaaaaatg agctgattta
      421 acaaaaattt aacgcgaatt ttaacaaaat attaacgttt acaatttcag gtggcacttt
      481 tcggggaaat gtgcgcggaa cccctatttg tttatttttc taaatacatt caaatatgta
      541 tccgctcatg aattaattct tagaaaaact catcgagcat caaatgaaac tgcaatttat
      601 tcatatcagg attatcaata ccatattttt gaaaaagccg tttctgtaat gaaggagaaa
      661 actcaccgag gcagttccat aggatggcaa gatcctggta tcggtctgcg attccgactc
      721 gtccaacatc aatacaacct attaatttcc cctcgtcaaa ataaggtta tcaagtgaga
      781 aatcaccatg agtgacgact gaatccggtg agaatggcaa aagtttatgc atttctttcc
      841 agacttgttc aacaggccag ccattacgct cgtcatcaaa atcactcgca tcaaccaaac
      901 cgttattcat tcgtgattgc gcctgagcga gacgaaatac gcgatcgctg ttaaaaggac
      961 aattacaaac aggaatcgaa tgcaaccggc gcaggaacac tgccagcgca tcaacaatat
     1021 tttcacctga atcaggatat tcttctaata cctggaatgc tgttttcccg gggatcgcag
     1081 tggtgagtaa ccatgcatca tcaggagtac ggataaaatg cttgatggtc ggaagaggca
     1141 taaattccgt cagccagttt agtctgacca tctcatctgt aacatcattg gcaacgctac
     1201 ctttgccatg tttcagaaac aactctggcg catcgggctt cccatacaat cgatagattg
     1261 tcgcacctga ttgcccgaca ttatcgcgag cccatttata cccatataaa tcagcatcca
     1321 tgttggaatt taatcgcggc ctagagcaag acgtttcccg ttgaatatgg ctcataacac
```

1381 cccttgtatt actgtttatg taagcagaca gttttattgt tcatgaccaa aatcccttaa
1441 cgtgagtttt cgttccactg agcgtcagac cccgtagaaa agatcaaagg atcttcttga
1501 gatccttttt ttctgcgcgt aatctgctgc ttgcaaacaa aaaaaccacc gctaccagcg
1561 gtggtttgtt tgccggatca agagctacca actctttttc cgaaggtaac tggcttcagc
1621 agagcgcaga taccaaatac tgtccttcta gtgtagccgt agttaggcca ccacttcaag
1681 aactctgtag caccgcctac atacctcgct ctgctaatcc tgttaccagt ggctgctgcc
1741 agtggcgata agtcgtgtct taccgggttg gactcaagac gatagttacc ggataaggcg
1801 cagcggtcgg gctgaacggg gggttcgtgc acacagccca gcttggagcg aacgacctac
1861 accgaactga gatacctaca gcgtgagcta tgagaaagcg ccacgcttcc cgaagggaga
1921 aaggcggaca ggtatccggt aagcggcagg gtcggaacag gagagcgcac gagggagctt
1981 ccagggggaa acgcctggta tctttatagt cctgtcgggt ttcgccacct ctgacttgag
2041 cgtcgatttt tgtgatgctc gtcaggggggg cggagcctat ggaaaaacgc cagcaacgcg
2101 gccttttttac ggttcctggc cttttgctgg ccttttgctc acatgttctt tcctgcgtta
2161 tcccctgatt ctgtggataa ccgtattacc gcctttgagt gagctgatac cgctcgccgc
2221 agccgaacga ccgagcgcag cgagtcagtg agcgaggaag cggaagagcg cctgatgcgg
2281 tattttctcc ttacgcatct gtgcggtatt tcacaccgca tatatggtgc actctcagta
2341 caatctgctc tgatgccgca tagttaagcc agtatacact ccgctatcgc tacgtgactg
2401 ggtcatggct gcgccccgac acccgccaac acccgctgac gcgccctgac gggcttgtct
2461 gctcccggca tccgcttaca gacaagctgt gaccgtctcc gggagctgca tgtgtcagag
2521 gttttcaccg tcatcaccga aacgcgcgag gcagctgcgg taaagctcat cagcgtggtc
2581 gtgaagcgat tcacagatgt ctgcctgttc atccgcgtcc agctcgttga gtttctccag
2641 aagcgttaat gtctggcttc tgataaagcg ggccatgtta agggcggttt tttcctgttt
2701 ggtcactgat gcctccgtgt aaggggggatt tctgttcatg ggggtaatga taccgatgaa
2761 acgagagagg atgctcacga tacgggttac tgatgatgaa catgcccggt tactggaacg
2821 ttgtgagggt aaacaactgg cggtatggat gcggcgggac cagagaaaaa tcactcaggg
2881 tcaatgccag cgcttcgtta atacagatgt aggtgttcca cagggtagcc agcagcatcc
2941 tgcgatgcag atccggaaca taatggtgca gggcgctgac ttccgcgttt ccagacttta
3001 cgaaacacgg aaaccgaaga ccattcatgt tgttgctcag gtcgcagacg ttttgcagca
3061 gcagtcgctt cacgttcgct cgcgtatcgg tgattcattc tgctaaccag taaggcaacc
3121 ccgccagcct agccgggtcc tcaacgacag gagcacgatc atgcgcaccc gtggggccgc
3181 catgccggcg ataatggcct gcttctcgcc gaaacgtttg gtggcgggac cagtgacgaa
3241 ggcttgagcg agggcgtgca agattccgaa taccgcaagc gacaggccga tcatcgtcgc
3301 gctccagcga aagcggtcct cgccgaaaat gacccagagc gctgccggca cctgtcctac
3361 gagttgcatg ataaagaaga cagtcataag tgcggcgacg atagtcatgc cccgcgccca
3421 ccggaaggag ctgactgggt tgaaggctct caagggcatc ggtcgagatc ccggtgccta
3481 atgagtgagc taacttacat taattgcgtt gcgctcactg cccgctttcc agtcgggaaa
3541 cctgtcgtgc cagctgcatt aatgaatcgg ccaacgcgcg gggagaggcg gtttgcgtat
3601 tgggcgccag ggtggttttt cttttcacca gtgagacggg caacagctga ttgcccttca
3661 ccgcctggcc ctgagagagt tgcagcaagc ggtccacgct ggtttgcccc agcaggcgaa
3721 aatcctgttt gatggtggtt aacggcggga tataacatga gctgtcttcg gtatcgtcgt
3781 atcccactac cgagatgtcc gcaccaacgc gcagcccgga ctcggtaatg gcgcgcattg
3841 cgcccagcgc catctgatcg ttggcaacca gcatcgcagt gggaacgatg ccctcattca
3901 gcatttgcat ggtttgttga aaaccggaca tggcactcca gtcgccttcc cgttccgcta
3961 tcggctgaat ttgattgcga gtgagatatt tatgccagcc agccagacgc agacgcgccg
4021 agacagaact taatgggccc gctaacagcg cgatttgctg gtgacccaat gcgaccagat
4081 gctccacgcc cagtcgcgta ccgtcttcat gggagaaaat aatactgttg atgggtgtct
4141 ggtcagagac atcaagaaat aacgccggaa cattagtgca ggcagcttcc acagcaatgg
4201 catcctggtc atccagcgga tagttaatga tcagcccact gacgcgttgc gcgagaagat
4261 tgtgcaccgc cgctttacag gcttcgacgc cgcttcgttc taccatcgac accaccacgc
4321 tggcacccag ttgatcggcg cgagatttaa tcgccgcgac aatttgcgac ggcgcgtgca
4381 gggccagact ggaggtggca acgccaatca gcaacgactg tttgcccgcc agttgttgtg
4441 ccacgcggtt gggaatgtaa ttcagctccg ccatcgccgc ttccactttt tcccgcgttt
4501 tcgcagaaac gtggctggcc tggttcacca cgcgggaaac ggtctgataa gagacaccgg
4561 catactctgc gacatcgtat aacgttactg gtttcacatt caccaccctg aattgactct
4621 cttccgggcg ctatcatgcc ataccgcgaa aggttttgcg ccattcgatg gtgtccggga
4681 tctcgacgct ctcccttatg cgactcctgc attaggaagc agcccagtag taggttgagg
4741 ccgttgagca ccgccgccgc aaggaatggt gcatgcaagg agatggcgcc caacagtccc
4801 ccggccacgg ggcctgccac catacccacg ccgaaacaag cgctcatgag cccgaagtgg

```
4861 cgagcccgat cttccccatc ggtgatgtcg gcgatatagg cgccagcaac cgcacctgtg
4921 gcgccggtga tgccggccac gatgcgtccg gcgtagagga tcgagatcga tctcgatccc
4981 gcgaaattaa tacgactcac tataggggaa ttgtgagcgg ataacaattc ccctctagaa
5041 ataattttgt ttaactttaa gaaggagata taCATATGCA CCACCACCAC CACCACGGCG
5101 GCAGCGGCGG CAGCGGCGGT AGCGGCGGTA GCATGAAGAT GGAAGAGCTG TTCAAGAAAC
5161 ACAAGATCGT TGCCGTGCTG CGTGCCAATA GTGTGGAAGA AGCGAAAAAG AAAGCGCTGG
5221 CGGTTTTCCT GGGCGGCGTT CATCTGATTG AAATTACCTT TACCGTGCCG GATGCGGATA
5281 CCGTGATTAA GGAACTGAGC TTTCTGAAGG AAATGGGCGC GATTATTGGT GCGGGCACCG
5341 TGACCAGCGT GGAGCAGTGC CGTAAAGCGG TGGAAAGTGG CGCCGAATTC ATTGTGAGTC
5401 CGCACCTGGA CGAGGAAATT AGCCAATTTT GCAAGGAGAA GGGTGTGTTC TATATGCCAG
5461 GCGTTATGAC CCCGACCGAA CTGGTGAAAG CCATGAAACT GGGCCATACC ATCTTAAAAC
5521 TGTTTCCGGG TGAGGTGGTG GGTCCGCAGT TTGTTAAAGC GATGAAAGGT CCGTTTCCGA
5581 ATGTGAAATT TGTGCCAACC GGCGGTGTTA ATCTGGACAA TGTGTGCGAA TGGTTCAAAG
5641 CGGGCGTGCT GGCCGTGGGC GTGGGCAGCG CGTTAGTGAA AGGCACCCCG GTGGAAGTGG
5701 CGGAAAAGGC CAAGGCGTTC GTTGAGAAGA TTCGTGGCTG CACCGAATAA TAGCTCGAGc
5761 accaccacca ccaccactga gatccggctg ctaacaaagc ccgaaaggaa gctgagttgg
5821 ctgctgccac cgctgagcaa taactagcat aacccccttgg ggcctctaaa cgggtcttga
5881 ggggtttttt gctgaaagga ggaactatat ccggat
//
```

```
>pSL1040_SpyCage-Flexible_Expression_Plasmid
LOCUS       pSL1040              6259 bp    DNA       circular     12-MAY-2022
DEFINITION  .
ACCESSION
VERSION
SOURCE      .
  ORGANISM  .
COMMENT     pSL0045+I3-01
COMMENT     ApEinfo:methylated:0
FEATURES             Location/Qualifiers
     CDS             5071..5388
                     /codon_start=1
                     /note="SpyCatcher"
                     /translation="MGSSHHHHHHGSGDSATHIKFSKRDEDGKELAGATMELRDSSGK
                     T
                     ISTWISDGQVKDFYLYPGKYTFVETAAPDGYEVATAITFTVNEQGQVTVNGKATKGDA
                     H
                     IGSGGSGGSGANKPMQPITSTANKIVWSDPTRLSTTFSASLLRQRVKVGIAELNNVSG
                     Q
                     YVSVYKRPAPKPEGCADACVIMPNENQSIRTVISGSAENLATLKAEWETHKRNVDTLF
                     A SGNAGLGFLDPTAAIVSSDTTA"
                     /locus_tag="SpyCatcher"
                     /label="SpyCatcher"
                     /ApEinfo_label="SpyCatcher"
                     /ApEinfo_fwdcolor="pink"
                     /ApEinfo_revcolor="pink"
                     /ApEinfo_graphicformat="arrow_data {{0 1 2 0 0 -1} {} 0}
                     width 5 offset 0"
     primer_bind     4984..5003
                     /locus_tag="T7"
                     /label="T7"
                     /ApEinfo_label="T7"
                     /ApEinfo_fwdcolor="cyan"
                     /ApEinfo_revcolor="green"
                     /ApEinfo_graphicformat="arrow_data {{0 1 2 0 0 -1} {} 0}
                     width 5 offset 0"
     CDS             5071..5073
                     /codon_start=1
                     /note="TIR 10295"
                     /translation="M"
                     /locus_tag="TIR 10295"
                     /label="TIR 10295"
                     /ApEinfo_label="TIR 10295"
                     /ApEinfo_fwdcolor="pink"
                     /ApEinfo_revcolor="pink"
                     /ApEinfo_graphicformat="arrow_data {{0 1 2 0 0 -1} {} 0}
                     width 5 offset 0"
     rep_origin      1421..2103
                     /locus_tag="Origin of DNA Replication"
                     /label="Origin of DNA Replication"
                     /ApEinfo_label="Origin of DNA Replication"
                     /ApEinfo_fwdcolor="gray50"
                     /ApEinfo_revcolor="gray50"
                     /ApEinfo_graphicformat="arrow_data {{0 1 2 0 0 -1} {} 0}
                     width 5 offset 0"
     rep_origin      12..467
                     /locus_tag="M13 origin"
                     /label="M13 origin"
```

/ApEinfo_label="M13 origin"
/ApEinfo_fwdcolor="gray50"
/ApEinfo_revcolor="gray50"
/ApEinfo_graphicformat="arrow_data {{0 1 2 0 0 -1} {} 0}
width 5 offset 0"
misc_feature 4984..5002
/locus_tag="T7prom"
/label="T7prom"
/ApEinfo_label="T7prom"
/ApEinfo_fwdcolor="#8080ff"
/ApEinfo_revcolor="#8080ff"
/ApEinfo_graphicformat="arrow_data {{0 1 2 0 0 -1} {} 0}
width 5 offset 0"
CDS 5083..5100
/codon_start=1
/product="6xHis"
/note="6xHis"
/translation="HHHHHH"
/locus_tag="6xHis"
/label="6xHis"
/ApEinfo_label="6xHis"
/ApEinfo_fwdcolor="pink"
/ApEinfo_revcolor="pink"
/ApEinfo_graphicformat="arrow_data {{0 1 2 0 0 -1} {} 0}
width 5 offset 0"
rep_origin 29..335
/locus_tag="F1 ori"
/label="F1 ori"
/ApEinfo_label="F1 ori"
/ApEinfo_fwdcolor="gray50"
/ApEinfo_revcolor="gray50"
/ApEinfo_graphicformat="arrow_data {{0 1 2 0 0 -1} {} 0}
width 5 offset 0"
CDS 5386..5388
/codon_start=1
/note="3xGSG"
/translation="GSGGSGGSG"
/locus_tag="3xGSG"
/label="3xGSG"
/ApEinfo_label="3xGSG"
/ApEinfo_fwdcolor="pink"
/ApEinfo_revcolor="pink"
/ApEinfo_graphicformat="arrow_data {{0 1 2 0 0 -1} {} 0}
width 5 offset 0"
CDS complement(563..1375)
/locus_tag="KanR"
/label="KanR"
/ApEinfo_label="KanR"
/ApEinfo_fwdcolor="yellow"
/ApEinfo_revcolor="yellow"
/ApEinfo_graphicformat="arrow_data {{0 1 2 0 0 -1} {} 0}
width 5 offset 0"
misc_feature 6079..6096
/locus_tag="TEVc Site"
/label="TEVc Site"
/ApEinfo_label="TEVc Site"
/ApEinfo_fwdcolor="#ff0000"
/ApEinfo_revcolor="green"

```
                     /ApEinfo_graphicformat="arrow_data {{0 1 2 0 0 -1} {} 0}
                     width 5 offset 0"
     misc_feature    5137..5139
                     /note="reactive 255K from CnaB2"
                     /locus_tag="reactive 255K from CnaB2"
                     /label="reactive 255K from CnaB2"
                     /ApEinfo_label="reactive 255K from CnaB2"
                     /ApEinfo_fwdcolor="#0080ff"
                     /ApEinfo_revcolor="#008200"
                     /ApEinfo_graphicformat="arrow_data {{0 1 2 0 0 -1} {} 0}
                     width 5 offset 0"
     misc_binding    5003..5025
                     /locus_tag="LacO"
                     /label="LacO"
                     /ApEinfo_label="LacO"
                     /ApEinfo_fwdcolor="#6495ed"
                     /ApEinfo_revcolor="#6495ed"
                     /ApEinfo_graphicformat="arrow_data {{0 1 2 0 0 -1} {} 0}
                     width 5 offset 0"
     misc_feature    complement(3515..4606)
                     /locus_tag="lacI"
                     /label="lacI"
                     /ApEinfo_label="lacI"
                     /ApEinfo_fwdcolor="#8080c0"
                     /ApEinfo_revcolor="#008200"
                     /ApEinfo_graphicformat="arrow_data {{0 1 2 0 0 -1} {} 0}
                     width 5 offset 0"
     misc_feature    5395..6063
                     /locus_tag="I3-01"
                     /label="I3-01"
                     /ApEinfo_label="I3-01"
                     /ApEinfo_fwdcolor="cyan"
                     /ApEinfo_revcolor="green"
                     /ApEinfo_graphicformat="arrow_data {{0 1 2 0 0 -1} {} 0}
                     width 5 offset 0"
     misc_feature    6131..6259
                     /locus_tag="T7 Terminator"
                     /label="T7 Terminator"
                     /ApEinfo_label="T7 Terminator"
                     /ApEinfo_fwdcolor="#0000a0"
                     /ApEinfo_revcolor="#0000a0"
                     /ApEinfo_graphicformat="arrow_data {{0 1 2 0 0 -1} {} 0}
                     width 5 offset 0"
     misc_feature    6103..6120
                     /locus_tag="6xHis Epitope Tag"
                     /label="6xHis Epitope Tag"
                     /ApEinfo_label="6xHis Epitope Tag"
                     /ApEinfo_fwdcolor="#0080c0"
                     /ApEinfo_revcolor="green"
                     /ApEinfo_graphicformat="arrow_data {{0 1 2 0 0 -1} {} 0}
                     width 5 offset 0"
ORIGIN
        1 tggcgaatgg gacgcgccct gtagcggcgc attaagcgcg gcgggtgtgg tggttacgcg
       61 cagcgtgacc gctacacttg ccagcgccct agcgcccgct cctttcgctt tcttcccttc
      121 ctttctcgcc acgttcgccg gctttccccg tcaagctcta aatcgggggc tccctttagg
      181 gttccgattt agtgctttac ggcacctcga ccccaaaaaa cttgattagg gtgatggttc
      241 acgtagtggg ccatcgccct gatagacggt ttttcgccct ttgacgttgg agtccacgtt
      301 ctttaatagt ggactcttgt tccaaactgg aacaacactc aaccctatct cggtctattc
```

361 ttttgattta taagggattt tgccgatttc ggcctattgg ttaaaaaatg agctgattta
421 acaaaaattt aacgcgaatt ttaacaaaat attaacgttt acaatttcag gtggcacttt
481 tcggggaaat gtgcgcggaa cccctatttg tttatttttc taaatacatt caaatatgta
541 tccgctcatg aattaattct tagaaaaact catcgagcat caaatgaaac tgcaatttat
601 tcatatcagg attatcaata ccatattttt gaaaaagccg tttctgtaat gaaggagaaa
661 actcaccgag gcagttccat aggatggcaa gatcctggta tcggtctgcg attccgactc
721 gtccaacatc aatacaacct attaatttcc cctcgtcaaa aataaggtta tcaagtgaga
781 aatcaccatg agtgacgact gaatccggtg agaatggcaa aagtttatgc atttctttcc
841 agacttgttc aacaggccag ccattacgct cgtcatcaaa atcactcgca tcaaccaaac
901 cgttattcat tcgtgattgc gcctgagcga gacgaaatac gcgatcgctg ttaaaaggac
961 aattacaaac aggaatcgaa tgcaaccggc gcaggaacac tgccagcgca tcaacaatat
1021 tttcacctga atcaggatat tcttctaata cctggaatgc tgttttcccg gggatcgcag
1081 tggtgagtaa ccatgcatca tcaggagtac ggataaaatg cttgatggtc ggaagaggca
1141 taaattccgt cagccagttt agtctgacca tctcatctgt aacatcattg gcaacgctac
1201 ctttgccatg tttcagaaac aactctggcg catcgggctt cccatacaat cgatagattg
1261 tcgcacctga ttgcccgaca ttatcgcgag cccatttata cccatataaa tcagcatcca
1321 tgttggaatt taatcgcggc ctagagcaag acgtttcccg ttgaatatgg ctcataacac
1381 cccttgtatt actgtttatg taagcagaca gttttattgt tcatgaccaa aatcccttaa
1441 cgtgagtttt cgttccactg agcgtcagac cccgtagaaa agatcaaagg atcttcttga
1501 gatccttttt ttctgcgcgt aatctgctgc ttgcaaacaa aaaaaccacc gctaccagcg
1561 gtggtttgtt tgccggatca agagctacca actcttttte cgaaggtaac tggcttcagc
1621 agagcgcaga taccaaatac tgtccttcta gtgtagccgt agttaggcca ccacttcaag
1681 aactctgtag caccgcctac atacctcgct ctgctaatcc tgttaccagt ggctgctgcc
1741 agtggcgata agtcgtgtct taccgggttg gactcaagac gatagttacc ggataaggcg
1801 cagcggtcgg gctgaacggg gggttcgtgc acacagccca gcttggagcg aacgacctac
1861 accgaactga gatacctaca gcgtgagcta tgagaaagcg ccacgcttcc cgaagggaga
1921 aaggcggaca ggtatccggt aagcggcagg gtcggaacag gagagcgcac gagggagctt
1981 ccagggggaa acgcctggta tctttatagt cctgtcgggt ttcgccacct ctgacttgag
2041 cgtcgatttt tgtgatgctc gtcaggggggg cggagcctat ggaaaaacgc cagcaacgcg
2101 gccttttttac ggttcctggc cttttgctgg ccttttgctc acatgttctt tcctgcgtta
2161 tcccctgatt ctgtggataa ccgtattacc gcctttgagt gagctgatac cgctcgccgc
2221 agccgaacga ccgagcgcag cgagtcagtg agcgaggaag cggaagagcg cctgatgcgg
2281 tattttctcc ttacgcatct gtgcggtatt tcacaccgca tatatggtgc actctcagta
2341 caatctgctc tgatgccgca tagttaagcc agtatacact ccgctatcgc tacgtgactg
2401 ggtcatggct gcgccccgac acccgccaac acccgctgac gcgccctgac gggcttgtct
2461 gctcccggca tccgcttaca gacaagctgt gaccgtctcc gggagctgca tgtgtcagag
2521 gttttcaccg tcatcaccga aacgcgcgag gcagctgcgg taaagctcat cagcgtggtc
2581 gtgaagcgat tcacagatgt ctgcctgttc atccgcgtcc agctcgttga gtttctccag
2641 aagcgttaat gtctggcttc tgataaagcg ggccatgtta agggcggttt tttcctgttt
2701 ggtcactgat gcctccgtgt aagggggatt tctgttcatg ggggtaatga taccgatgaa
2761 acgagagagg atgctcacga tacgggttac tgatgatgaa catgcccggt tactggaacg
2821 ttgtgagggt aaacaactgg cggtatggat gcggcgggac cagagaaaaa tcactcaggg
2881 tcaatgccag cgcttcgtta atacagatgt aggtgttcca cagggtagcc agcagcatcc
2941 tgcgatgcag atccggaaca taatggtgca gggcgctgac ttccgcgttt ccagacttta
3001 cgaaacacgg aaaccgaaga ccattcatgt tgttgctcag gtcgcagacg ttttgcagca
3061 gcagtcgctt cacgttcgct cgcgtatcgg tgattcattc tgctaaccag taaggcaacc
3121 ccgccagcct agccgggtcc tcaacgacag gagcacgatc atgcgcaccc gtggggccgc
3181 catgccggcg ataatggcct gcttctcgcc gaaacgtttg gtggcgggac cagtgacgaa
3241 ggcttgagcg agggcgtgca agattccgaa taccgcaagc gacaggccga tcatcgtcgc
3301 gctccagcga aagcggtcct cgccgaaaat gacccagagc gctgccggca cctgtcctac
3361 gagttgcatg ataaagaaga cagtcataag tgcggcgacg atagtcatgc cccgcgccca
3421 ccggaaggag ctgactgggt tgaaggctct caagggcatc ggtcgagatc ccggtgccta
3481 atgagtgagc taacttacat taattgcgtt gcgctcactg cccgctttcc agtcgggaaa
3541 cctgtcgtgc cagctgcatt aatgaatcgg ccaacgcgcg gggagaggcg gtttgcgtat
3601 tgggcgccag ggtggttttt cttttcacca gtgagacggg caacagctga ttgcccttca
3661 ccgcctggcc ctgagagagt tgcagcaagc ggtccacgct ggtttgcccc agcaggcgaa
3721 aatcctgttt gatggtggtt aacggcggga tataacatga gctgtcttcg gtatcgtcgt
3781 atcccactac cgagatatcc gcaccaacgc gcagcccgga ctcggtaatg gcgcgcattg

3841 cgcccagcgc catctgatcg ttggcaacca gcatcgcagt gggaacgatg ccctcattca
3901 gcatttgcat ggtttgttga aaaccggaca tggcactcca gtcgccttcc cgttccgcta
3961 tcggctgaat ttgattgcga gtgagatatt tatgccagcc agccagacgc agacgcgccg
4021 agacagaact taatgggccc gctaacagcg cgatttgctg gtgacccaat gcgaccagat
4081 gctccacgcc cagtcgcgta ccgtcttcat gggagaaaat aatactgttg atgggtgtct
4141 ggtcagagac atcaagaaat aacgccggaa cattagtgca ggcagcttcc acagcaatgg
4201 catcctggtc atccagcgga tagttaatga tcagcccact gacgcgttgc gcgagaagat
4261 tgtgcaccgc cgctttacag gcttcgacgc cgcttcgttc taccatcgac accaccacgc
4321 tggcacccag ttgatcggcg cgagatttaa tcgccgcgac aatttgcgac ggcgcgtgca
4381 gggccagact ggaggtggca acgccaatca gcaacgactg tttgcccgcc agttgttgtg
4441 ccacgcggtt gggaatgtaa ttcagctccg ccatcgccgc ttccactttt tcccgcgttt
4501 tcgcagaaac gtggctggcc tggttcacca cgcgggaaac ggtctgataa gagacaccgg
4561 catactctgc gacatcgtat aacgttactg gtttcacatt caccaccctg aattgactct
4621 cttccgggcg ctatcatgcc ataccgcgaa aggttttgcg ccattcgatg gtgtccggga
4681 tctcgacgct ctcccttatg cgactcctgc attaggaagc agcccagtag taggttgagg
4741 ccgttgagca ccgccgccgc aaggaatggt gcatgcaagg agatggcgcc caacagtccc
4801 ccggccacgg ggcctgccac catacccacg ccgaaacaag cgctcatgag cccgaagtgg
4861 cgagcccgat cttccccatc ggtgatgtcg gcgatatagg cgccagcaac cgcacctgtg
4921 gcgccggtga tgccggccac gatgcgtccg gcgtagagga tcgagatctc gatcccgcga
4981 aattaatacg actcactata ggggaattgt gagcggataa caattcccct ctagaaataa
5041 ttttgtttaa ctttaagaag gagatatacc atggGCAGCA GCCATCATCA TCATCATCAC
5101 GGCAGCGGCG ATAGTGCTAC CCATATTAAA TTCTCAAAAC GTGATGAGGA CGGCAAAGAG
5161 TTAGCTGGTG CAACTATGGA GTTGCGTGAT TCATCTGGTA AAACTATTAG TACATGGATT
5221 TCAGATGGAC AAGTGAAAGA TTTCTACCTG TATCCAGGAA AATATACATT TGTCGAAACC
5281 GCAGCACCAG ACGGTTATGA GGTAGCAACT GCTATTACCT TTACAGTTAA TGAGCAAGGT
5341 CAGGTTACTG TAAACGGCAA AGCAACTAAA GGTGACGCTC ATATTGGCgt cgacCACCAC
5401 CACCACCACC ACGGCGGCAG CGGCGGCAGC GGCGGTAGCG GCGGTAGCAT GAAGATGGAA
5461 GAGCTGTTCA AGAAACACAA GATCGTTGCC GTGCTGCGTG CCAATAGTGT GGAAGAAGCG
5521 AAAAAGAAAG CGCTGGCGGT TTTCCTGGGC GGCGTTCATC TGATTGAAAT TACCTTTACC
5581 GTGCCGGATG CGGATACCGT GATTAAGGAA CTGAGCTTTC TGAAGGAAAT GGGCGCGATT
5641 ATTGGTGCGG GCACCGTGAC CAGCGTGGAG CAGTGCCGTA AAGCGGTGGA AAGTGGCGCC
5701 GAATTCATTG TGAGTCCGCA CCTGGACGAG GAAATTAGCC AATTTTGCAA GGAGAAGGGT
5761 GTGTTCTATA TGCCAGGCGT TATGACCCCG ACCGAACTGG TGAAAGCCAT GAAACTGGGC
5821 CATACCATCT TAAAACTGTT TCCGGGTGAG GTGGTGGGTC CGCAGTTTGT TAAAGCGATG
5881 AAAGGTCCGT TTCCGAATGT GAAATTTGTG CCAACCGGCG GTGTTAATCT GGACAATGTG
5941 TGCGAATGGT TCAAAGCGGG CGTGCTGGCC GTGGGCGTGG GCAGCGCGTT AGTGAAAGGC
6001 ACCCCGGTGG AAGTGGCGGA AAAGGCCAAG GCGTTCGTTG AGAAGATTCG TGGCTGCACC
6061 GAAcatatgt agctcgagAA CCTGTACTTC CAGGGAgtcg agcaccacca ccaccaccac
6121 tgagatccgg ctgctaacaa agcccgaaag gaagctgagt tggctgctgc caccgctgag
6181 caataactag cataacccct tggggcctct aaacgggtct tgaggggttt tttgctgaaa
6241 ggaggaacta tatccggat
//

```
>pSL1510_SARS-CoV-2-Spike-RBD-NoSpyTag_Expression Plasmid
LOCUS       pSL1510       5498 bp    DNA       circular     12-MAY-2022
DEFINITION  .
ACCESSION
VERSION
SOURCE      .
  ORGANISM  .
COMMENT
COMMENT
COMMENT     ApEinfo:methylated:1
FEATURES             Location/Qualifiers
     rep_origin      complement(3730..4412)
                     /locus_tag="ColE1 origin"
                     /label="ColE1 origin"
                     /ApEinfo_label="ColE1 origin"
                     /ApEinfo_fwdcolor="gray50"
                     /ApEinfo_revcolor="gray50"
                     /ApEinfo_graphicformat="arrow_data {{0 1 2 0 0 -1} {} 0}
                     width 5 offset 0"
     misc_binding    complement(3023..3045)
                     /locus_tag="LacO"
                     /label="LacO"
                     /ApEinfo_label="LacO"
                     /ApEinfo_fwdcolor="#6495ed"
                     /ApEinfo_revcolor="#6495ed"
                     /ApEinfo_graphicformat="arrow_data {{0 1 2 0 0 -1} {} 0}
                     width 5 offset 0"
     misc_feature    3375..3505
                     /locus_tag="SV40 early poly-A signal"
                     /label="SV40 early poly-A signal"
                     /ApEinfo_label="SV40 early poly-A signal"
                     /ApEinfo_fwdcolor="#808000"
                     /ApEinfo_revcolor="green"
                     /ApEinfo_graphicformat="arrow_data {{0 1 2 0 0 -1} {} 0}
                     width 5 offset 0"
     misc_feature    complement(4510..5169)
                     /locus_tag="AmpR"
                     /label="AmpR"
                     /ApEinfo_label="AmpR"
                     /ApEinfo_fwdcolor="#ffff00"
                     /ApEinfo_revcolor="#ffff00"
                     /ApEinfo_graphicformat="arrow_data {{0 1 2 0 0 -1} {} 0}
                     width 5 offset 0"
     misc_feature    3185..3364
                     /locus_tag="SV40 Promoter"
                     /label="SV40 Promoter"
                     /ApEinfo_label="SV40 Promoter"
                     /ApEinfo_fwdcolor="#8080c0"
                     /ApEinfo_revcolor="green"
                     /ApEinfo_graphicformat="arrow_data {{0 1 2 0 0 -1} {} 0}
                     width 5 offset 0"
     misc_feature    complement(776..781)
                     /locus_tag="Ribosome Binding Site"
                     /label="Ribosome Binding Site"
                     /ApEinfo_label="Ribosome Binding Site"
                     /ApEinfo_fwdcolor="cyan"
                     /ApEinfo_revcolor="green"
                     /ApEinfo_graphicformat="arrow_data {{0 1 2 0 0 -1} {} 0}
```

```
            width 5 offset 0"
misc_feature    complement(2918..2923)
            /locus_tag="Ribosome Binding Site(1)"
            /label="Ribosome Binding Site(1)"
            /ApEinfo_label="Ribosome Binding Site"
            /ApEinfo_fwdcolor="cyan"
            /ApEinfo_revcolor="green"
            /ApEinfo_graphicformat="arrow_data {{0 1 2 0 0 -1} {} 0}
            width 5 offset 0"
misc_feature    complement(3869..3874)
            /locus_tag="Ribosome Binding Site(2)"
            /label="Ribosome Binding Site(2)"
            /ApEinfo_label="Ribosome Binding Site"
            /ApEinfo_fwdcolor="cyan"
            /ApEinfo_revcolor="green"
            /ApEinfo_graphicformat="arrow_data {{0 1 2 0 0 -1} {} 0}
            width 5 offset 0"
misc_feature    complement(3023..3040)
            /locus_tag="Minimal LacO"
            /label="Minimal LacO"
            /ApEinfo_label="Minimal LacO"
            /ApEinfo_fwdcolor="#ff80c0"
            /ApEinfo_revcolor="green"
            /ApEinfo_graphicformat="arrow_data {{0 1 2 0 0 -1} {} 0}
            width 5 offset 0"
misc_feature    84..371
            /locus_tag="CAG Enhancer / CMV immediate early promoter"
            /label="CAG Enhancer / CMV immediate early promoter"
            /ApEinfo_label="CAG Enhancer / CMV immediate early
            promoter"
            /ApEinfo_fwdcolor="#8080c0"
            /ApEinfo_revcolor="green"
            /ApEinfo_graphicformat="arrow_data {{0 1 2 0 0 -1} {} 0}
            width 5 offset 0"
misc_feature    2517..2955
            /locus_tag="rb glob PA terminator"
            /label="rb glob PA terminator"
            /ApEinfo_label="rb glob PA terminator"
            /ApEinfo_fwdcolor="#800000"
            /ApEinfo_revcolor="green"
            /ApEinfo_graphicformat="arrow_data {{0 1 2 0 0 -1} {} 0}
            width 5 offset 0"
misc_feature    1734..2465
            /locus_tag="SARS-CoV-2 Spike SP+RBD+6xHis"
            /label="SARS-CoV-2 Spike SP+RBD+6xHis"
            /ApEinfo_label="SARS-CoV-2 Spike SP+RBD+6xHis"
            /ApEinfo_fwdcolor="cyan"
            /ApEinfo_revcolor="green"
            /ApEinfo_graphicformat="arrow_data {{0 1 2 0 0 -1} {} 0}
            width 5 offset 0"
misc_feature    385..1630
            /locus_tag="CAG promoter"
            /label="CAG promoter"
            /ApEinfo_label="CAG promoter"
            /ApEinfo_fwdcolor="#0080c0"
            /ApEinfo_revcolor="green"
            /ApEinfo_graphicformat="arrow_data {{0 1 2 0 0 -1} {} 0}
            width 5 offset 0"
```

ORIGIN

```
   1 GTCGACATTG ATTATTGACT AGTTATTAAT AGTAATCAAT TACGGGGTCA TTAGTTCATA
  61 GCCCATATAT GGAGTTCCGC GTTACATAAC TTACGGTAAA TGGCCCGCCT GGCTGACCGC
 121 CCAACGACCC CCGCCCATTG ACGTCAATAA TGACGTATGT TCCCATAGTA ACGCCAATAG
 181 GGACTTTCCA TTGACGTCAA TGGGTGGAGT ATTTACGGTA AACTGCCCAC TTGGCAGTAC
 241 ATCAAGTGTA TCATATGCCA AGTACGCCCC CTATTGACGT CAATGACGGT AAATGGCCCG
 301 CCTGGCATTA TGCCCAGTAC ATGACCTTAT GGGACTTTCC TACTTGGCAG TACATCTACG
 361 TATTAGTCAT CGCTATTACC ATGGTCGAGG TGAGCCCCAC GTTCTGCTTC ACTCTCCCCA
 421 TCTCCCCCCC CTCCCCACCC CCAATTTTGT ATTTATTTAT TTTTTAATTA TTTTGTGCAG
 481 CGATGGGGGC GGGGGGGGGG GGGGCGCGCG CCAGGCGGGG CGGGGCGGGG CGAGGGGCGG
 541 GGCGGGGCGA GGCGGAGAGG TGCGGCGGCA GCCAATCAGA GCGGCGCGCT CCGAAAGTTT
 601 CCTTTTATGG CGAGGCGGCG GCGGCGGCGG CCCTATAAAA AGCGAAGCGC GCGGCGGGCG
 661 GGAGTCGCTG CGCGCGCTGC CTTCGCCCCG TGCCCCGCTC CGCGCCGCCT CGCGCCGCCC
 721 GCCCCGGCTC TGACTGACCG CGTTACTCCC ACAGGTGAGC GGGCGGGACG GCCCTTCTCC
 781 TCCGGGCTGT AATTAGCGCT TGGTTTAATG ACGGCTTGTT TCTTTTCTGT GGCTGCGTGA
 841 AAGCCTTGAG GGGCTCCGGG AGGGCCCTTT GTGCGGGGGG GAGCGGCTCG GGGGGTGCGT
 901 GCGTGTGTGT GTGCGTGGGG AGCGCCGCGT GCGGCTCCGC GCTGCCCGGC GGCTGTGAGC
 961 GCTGCGGGCG CGGCGCGGGG CTTTGTGCGC TCCGCAGTGT GCGCGAGGGG AGCGCGGCCG
1021 GGGGCGGTGC CCCGCGGTGC GGGGGGGGCT GCGAGGGGAA CAAAGGCTGC GTGCGGGGTG
1081 TGTGCGTGGG GGGGTGAGCA GGGGGTGTGG GCGCGTCGGT CGGGCTGCAA CCCCCCCCTG
1141 CACCCCCCTC CCCGAGTTGC TGAGCACGGC CCGGCTTCGG GTGCGGGGCT CCGTACGGGG
1201 CGTGGCGCGG GGCTCGCCGT GCCGGGCGGG GGGTGGCGGC AGGTGGGGGT GCCGGGCGGG
1261 GCGGGGCCGC CTCGGGCCGG GGAGGGCTCG GGGGAGGGGC GCGGCGGCCC CCGGAGCGCC
1321 GGCGGCTGTC GAGGCGCGGC GAGCCGCAGC CATTGCCTTT TATGGTAATC GTGCGAGAGG
1381 GCGCAGGGAC TTCCTTTGTC CCAAATCTGG CGGAGCCGAA ATCTGGGAGG CGCCGCCGCA
1441 CCCCCTCTAG CGGGCGCGGG GCGAAGCGGT GCGGCGCCGG CAGGAAGGAA ATGGGCGGGG
1501 AGGGCCTTCG TGCGTCGCCG CGCCGCCGTC CCCTTCTCCC TCTCCAGCCT CGGGGCTGCC
1561 GCGGGGGGAC GGCTGCCTTC GGGGGGGACG GGGCAGGGCG GGGTTCGGCT TCTGGCGTGT
1621 GACCGGCGGC TCTAGAGCCT CTGCTAACCA TGTTCATGCC TTCTTCTTTT TCCTACAGCT
1681 CCTGGGCAAC GTGCTGGTTA TTGTGCTGTC TCATCATTTT GGCAAAGGCC ACCATGTTCG
1741 TGTTTCTGGT GCTGCTGCCT CTGGTGTCCA GCCAGCGGGT GCAGCCCACC GAATCCATCG
1801 TGCGGTTCCC CAATATCACC AATCTGTGCC CCTTCGGCGA GGTGTTCAAT GCCACCAGAT
1861 TCGCCTCTGT GTACGCCTGG AACCGGAAGC GGATCAGCAA TTGCGTGGCC GACTACTCCG
1921 TGCTGTACAA CTCCGCCAGC TTCAGCACCT TCAAGTGCTA CGGCGTGTCC CCTACCAAGC
1981 TGAACGACCT GTGCTTCACA AACGTGTACG CCGACAGCTT CGTGATCCGG GGAGATGAAG
2041 TGCGGCAGAT TGCCCCTGGA CAGACAGGCA AGATCGCCGA CTACAACTAC AAGCTGCCCG
2101 ACGACTTCAC CGGCTGTGTG ATTGCCTGGA ACAGCAACAA CCTGGACTCC AAAGTCGGCG
2161 GCAACTACAA TTACCTGTAC CGGCTGTTCC GGAAGTCCAA TCTGAAGCCC TTCGAGCGGG
2221 ACATCTCCAC CGAGATCTAT CAGGCCGGCA GCACCCCTTG TAACGGCGTG GAAGGCTTCA
2281 ACTGCTACTT CCCACTGCAG TCCTACGGCT TTCAGCCCAC AAATGGCGTG GGCTATCAGC
2341 CCTACAGAGT GGTGGTGCTG AGCTTCGAAC TGCTGCATGC CCCTGCCACA GTGTGCGGCC
2401 CTAAGAAAAG CACCAATCTC GTGAAGAACA AATGCGTGAA CTTCCACCAT CACCATCACC
2461 ATTGATAAAA TTCGAGCTCG CGGCCGCATC GATCTTAAGT CGCGACTCGA GCTAGCAGAT
2521 CTTTTTCCCT CTGCCAAAAA TTATGGGGAC ATCATGAAGC CCCTTGAGCA TCTGACTTCT
2581 GGCTAATAAA GGAAATTTAT TTTCATTGCA ATAGTGTGTT GGAATTTTTT GTGTCTCTCA
2641 CTCGGAAGGA CATATGGGAG GGCAAATCAT TTAAAACATC AGAATGAGTA TTTGGTTTAG
2701 AGTTTGGCAA CATATGCCCA TATGCTGGCT GCCATGAACA AAGGTTGGCT ATAAAGAGGT
2761 CATCAGTATA TGAAACAGCC CCCTGCTGTC CATTCCTTAT TCCATAGAAA AGCCTTGACT
2821 TGAGGTTAGA TTTTTTTTAT ATTTTGTTTT GTGTTATTTT TTTCTTTAAC ATCCCTAAAA
2881 TTTTCCTTAC ATGTTTTACT AGCCAGATTT TTCCTCCTCT CCTGACTACT CCCAGTCATA
2941 GCTGTCCCTC TTCTCTTATG GAGATCCCTC GACCTGCAGC CCAAGCTTGG CGTAATCATG
3001 GTCATAGCTG TTTCCTGTGT GAAATTGTTA TCCGCTCACA ATTCCACACA ACATACGAGC
3061 CGGAAGCATA AAGTGTAAAG CCTGGGGTGC CTAATGAGTG AGCTAACTCA CATTAATTGC
3121 GTTGCGCTCA CTGCCCGCTT TCCAGTCGGG AAACCTGTCG TGCCAGCGGA TCCGCATCTC
3181 AATTAGTCAG CAACCATAGT CCCGCCCCTA ACTCCGCCCA TCCCGCCCCT AACTCCGCCC
3241 AGTTCCGCCC ATTCTCCGCC CCATGGCTGA CTAATTTTTT TTATTTATGC AGAGGCCGAG
3301 GCCGCCTCGG CCTCTGAGCT ATTCCAGAAG TAGTGAGGAG GCTTTTTTGG AGGCCTAGGC
3361 TTTTGCAAAA AGCTAACTTG TTTATTGCAG CTTATAATGG TTACAAATAA AGCAATAGCA
```

3421 TCACAAATTT CACAAATAAA GCATTTTTTT CACTGCATTC TAGTTGTGGT TTGTCCAAAC
3481 TCATCAATGT ATCTTATCAT GTCTGGATCC GCTGCATTAA TGAATCGGCC AACGCGCGGG
3541 GAGAGGCGGT TTGCGTATTG GGCGCTCTTC CGCTTCCTCG CTCACTGACT CGCTGCGCTC
3601 GGTCGTTCGG CTGCGGCGAG CGGTATCAGC TCACTCAAAG GCGGTAATAC GGTTATCCAC
3661 AGAATCAGGG GATAACGCAG GAAAGAACAT GTGAGCAAAA GGCCAGCAAA AGGCCAGGAA
3721 CCGTAAAAAG GCCGCGTTGC TGGCGTTTTT CCATAGGCTC CGCCCCCCTG ACGAGCATCA
3781 CAAAAATCGA CGCTCAAGTC AGAGGTGGCG AAACCCGACA GGACTATAAA GATACCAGGC
3841 GTTTCCCCCT GGAAGCTCCC TCGTGCGCTC TCCTGTTCCG ACCCTGCCGC TTACCGGATA
3901 CCTGTCCGCC TTTCTCCCTT CGGGAAGCGT GGCGCTTTCT CATAGCTCAC GCTGTAGGTA
3961 TCTCAGTTCG GTGTAGGTCG TTCGCTCCAA GCTGGGCTGT GTGCACGAAC CCCCCGTTCA
4021 GCCCGACCGC TGCGCCTTAT CCGGTAACTA TCGTCTTGAG TCCAACCCGG TAAGACACGA
4081 CTTATCGCCA CTGGCAGCAG CCACTGGTAA CAGGATTAGC AGAGCGAGGT ATGTAGGCGG
4141 TGCTACAGAG TTCTTGAAGT GGTGGCCTAA CTACGGCTAC ACTAGAAGAA CAGTATTTGG
4201 TATCTGCGCT CTGCTGAAGC CAGTTACCTT CGGAAAAAGA GTTGGTAGCT CTTGATCCGG
4261 CAAACAAACC ACCGCTGGTA GCGGTGGTTT TTTTGTTTGC AAGCAGCAGA TTACGCGCAG
4321 AAAAAAAGGA TCTCAAGAAG ATCCTTTGAT CTTTTCTACG GGGTCTGACG CTCAGTGGAA
4381 CGAAAACTCA CGTTAAGGGA TTTTGGTCAT GAGATTATCA AAAAGGATCT TCACCTAGAT
4441 CCTTTTAAAT TAAAAATGAA GTTTTAAATC AATCTAAAGT ATATATGAGT AAACTTGGTC
4501 TGACAGTTAC CAATGCTTAA TCAGTGAGGC ACCTATCTCA GCGATCTGTC TATTTCGTTC
4561 ATCCATAGTT GCCTGACTCC CCGTCGTGTA GATAACTACG ATACGGGAGG GCTTACCATC
4621 TGGCCCCAGT GCTGCAATGA TACCGCGAGA CCCACGCTCA CCGGCTCCAG ATTTATCAGC
4681 AATAAACCAG CCAGCCGGAA GGGCCGAGCG CAGAAGTGGT CCTGCAACTT TATCCGCCTC
4741 CATCCAGTCT ATTAATTGTT GCCGGGAAGC TAGAGTAAGT AGTTCGCCAG TTAATAGTTT
4801 GCGCAACGTT GTTGCCATTG CTACAGGCAT CGTGGTGTCA CGCTCGTCGT TTGGTATGGC
4861 TTCATTCAGC TCCGGTTCCC AACGATCAAG GCGAGTTACA TGATCCCCCA TGTTGTGCAA
4921 AAAAGCGGTT AGCTCCTTCG GTCCTCCGAT CGTTGTCAGA AGTAAGTTGG CCGCAGTGTT
4981 ATCACTCATG GTTATGGCAG CACTGCATAA TTCTCTTACT GTCATGCCAT CCGTAAGATG
5041 CTTTTCTGTG ACTGGTGAGT ACTCAACCAA GTCATTCTGA GAATAGTGTA TGCGGCGACC
5101 GAGTTGCTCT TGCCCGGCGT CAATACGGGA TAATACCGCG CCACATAGCA GAACTTTAAA
5161 AGTGCTCATC ATTGGAAAAC GTTCTTCGGG GCGAAAACTC TCAAGGATCT TACCGCTGTT
5221 GAGATCCAGT TCGATGTAAC CCACTCGTGC ACCCAACTGA TCTTCAGCAT CTTTTACTTT
5281 CACCAGCGTT TCTGGGTGAG CAAAAACAGG AAGGCAAAAT GCCGCAAAAA AGGGAATAAG
5341 GGCGACACGG AAATGTTGAA TACTCATACT CTTCCTTTTT CAATATTATT GAAGCATTTA
5401 TCAGGGTTAT TGTCTCATGA GCGGATACAT ATTTGAATGT ATTTAGAAAA ATAAACAAAT
5461 AGGGGTTCCG CGCACATTTC CCCGAAAAGT GCCACCTG
//

```
>pSL1515_SARS-CoV-2-Spike-RBD-WithSpyTag_Expression Plasmid
LOCUS       pSL1515              5512 bp    DNA       circular     12-MAY-2022
DEFINITION  .
ACCESSION
VERSION
SOURCE      .
  ORGANISM  .
COMMENT
COMMENT     ApEinfo:methylated:1
FEATURES             Location/Qualifiers
     primer_bind     complement(3011..3031)
                     /locus_tag="M13-rev"
                     /label="M13-rev"
                     /ApEinfo_label="M13-rev"
                     /ApEinfo_fwdcolor="cyan"
                     /ApEinfo_revcolor="green"
                     /ApEinfo_graphicformat="arrow_data {{0 1 2 0 0 -1} {} 0}
                     width 5 offset 0"
     misc_feature    1898..2462
                     /locus_tag="SARS-CoV-2 Spike SP+RBD+6xHis"
                     /label="SARS-CoV-2 Spike SP+RBD+6xHis"
                     /ApEinfo_label="SARS-CoV-2 Spike SP+RBD+6xHis"
                     /ApEinfo_fwdcolor="cyan"
                     /ApEinfo_revcolor="green"
                     /ApEinfo_graphicformat="arrow_data {{0 1 2 0 0 -1} {} 0}
                     width 5 offset 0"
     rep_origin      complement(3744..4426)
                     /locus_tag="ColE1 origin"
                     /label="ColE1 origin"
                     /ApEinfo_label="ColE1 origin"
                     /ApEinfo_fwdcolor="gray50"
                     /ApEinfo_revcolor="gray50"
                     /ApEinfo_graphicformat="arrow_data {{0 1 2 0 0 -1} {} 0}
                     width 5 offset 0"
     misc_binding    complement(3037..3059)
                     /locus_tag="LacO"
                     /label="LacO"
                     /ApEinfo_label="LacO"
                     /ApEinfo_fwdcolor="#6495ed"
                     /ApEinfo_revcolor="#6495ed"
                     /ApEinfo_graphicformat="arrow_data {{0 1 2 0 0 -1} {} 0}
                     width 5 offset 0"
     misc_feature    3389..3519
                     /locus_tag="SV40 early poly-A signal"
                     /label="SV40 early poly-A signal"
                     /ApEinfo_label="SV40 early poly-A signal"
                     /ApEinfo_fwdcolor="#808000"
                     /ApEinfo_revcolor="green"
                     /ApEinfo_graphicformat="arrow_data {{0 1 2 0 0 -1} {} 0}
                     width 5 offset 0"
     misc_feature    complement(4524..5183)
                     /locus_tag="AmpR"
                     /label="AmpR"
                     /ApEinfo_label="AmpR"
                     /ApEinfo_fwdcolor="#ffff00"
                     /ApEinfo_revcolor="#ffff00"
                     /ApEinfo_graphicformat="arrow_data {{0 1 2 0 0 -1} {} 0}
                     width 5 offset 0"
```

misc_feature 3199..3378
/locus_tag="SV40 Promoter"
/label="SV40 Promoter"
/ApEinfo_label="SV40 Promoter"
/ApEinfo_fwdcolor="#8080c0"
/ApEinfo_revcolor="green"
/ApEinfo_graphicformat="arrow_data {{0 1 2 0 0 -1} {} 0}
width 5 offset 0"
misc_feature complement(776..781)
/locus_tag="Ribosome Binding Site"
/label="Ribosome Binding Site"
/ApEinfo_label="Ribosome Binding Site"
/ApEinfo_fwdcolor="cyan"
/ApEinfo_revcolor="green"
/ApEinfo_graphicformat="arrow_data {{0 1 2 0 0 -1} {} 0}
width 5 offset 0"
misc_feature complement(2932..2937)
/locus_tag="Ribosome Binding Site(1)"
/label="Ribosome Binding Site(1)"
/ApEinfo_label="Ribosome Binding Site"
/ApEinfo_fwdcolor="cyan"
/ApEinfo_revcolor="green"
/ApEinfo_graphicformat="arrow_data {{0 1 2 0 0 -1} {} 0}
width 5 offset 0"
misc_feature complement(3883..3888)
/locus_tag="Ribosome Binding Site(2)"
/label="Ribosome Binding Site(2)"
/ApEinfo_label="Ribosome Binding Site"
/ApEinfo_fwdcolor="cyan"
/ApEinfo_revcolor="green"
/ApEinfo_graphicformat="arrow_data {{0 1 2 0 0 -1} {} 0}
width 5 offset 0"
misc_feature complement(3037..3054)
/locus_tag="Minimal LacO"
/label="Minimal LacO"
/ApEinfo_label="Minimal LacO"
/ApEinfo_fwdcolor="#ff80c0"
/ApEinfo_revcolor="green"
/ApEinfo_graphicformat="arrow_data {{0 1 2 0 0 -1} {} 0}
width 5 offset 0"
misc_feature 84..371
/locus_tag="CAG Enhancer / CMV immediate early promoter"
/label="CAG Enhancer / CMV immediate early promoter"
/ApEinfo_label="CAG Enhancer / CMV immediate early
promoter"
/ApEinfo_fwdcolor="#8080c0"
/ApEinfo_revcolor="green"
/ApEinfo_graphicformat="arrow_data {{0 1 2 0 0 -1} {} 0}
width 5 offset 0"
misc_feature 2531..2969
/locus_tag="rb glob PA terminator"
/label="rb glob PA terminator"
/ApEinfo_label="rb glob PA terminator"
/ApEinfo_fwdcolor="#800000"
/ApEinfo_revcolor="green"
/ApEinfo_graphicformat="arrow_data {{0 1 2 0 0 -1} {} 0}
width 5 offset 0"
misc_feature 1734..1897

```
                /locus_tag="SARS-CoV-2 Spike SP+RBD+6xHis(1)"
                /label="SARS-CoV-2 Spike SP+RBD+6xHis(1)"
                /ApEinfo_label="SARS-CoV-2 Spike SP+RBD+6xHis"
                /ApEinfo_fwdcolor="cyan"
                /ApEinfo_revcolor="green"
                /ApEinfo_graphicformat="arrow_data {{0 1 2 0 0 -1} {} 0}
                width 5 offset 0"
     misc_feature    385..1630
                /locus_tag="CAG promoter"
                /label="CAG promoter"
                /ApEinfo_label="CAG promoter"
                /ApEinfo_fwdcolor="#0080c0"
                /ApEinfo_revcolor="green"
                /ApEinfo_graphicformat="arrow_data {{0 1 2 0 0 -1} {} 0}
                width 5 offset 0"
ORIGIN
        1 GTCGACATTG ATTATTGACT AGTTATTAAT AGTAATCAAT TACGGGGTCA TTAGTTCATA
       61 GCCCATATAT GGAGTTCCGC GTTACATAAC TTACGGTAAA TGGCCCGCCT GGCTGACCGC
      121 CCAACGACCC CCGCCCATTG ACGTCAATAA TGACGTATGT TCCCATAGTA ACGCCAATAG
      181 GGACTTTCCA TTGACGTCAA TGGGTGGAGT ATTTACGGTA AACTGCCCAC TTGGCAGTAC
      241 ATCAAGTGTA TCATATGCCA AGTACGCCCC CTATTGACGT CAATGACGGT AAATGGCCCG
      301 CCTGGCATTA TGCCCAGTAC ATGACCTTAT GGGACTTTCC TACTTGGCAG TACATCTACG
      361 TATTAGTCAT CGCTATTACC ATGGTCGAGG TGAGCCCCAC GTTCTGCTTC ACTCTCCCCA
      421 TCTCCCCCCC CTCCCCACCC CCAATTTTGT ATTTATTTAT TTTTTAATTA TTTTGTGCAG
      481 CGATGGGGGC GGGGGGGGGG GGGGCGCGCG CCAGGCGGGG CGGGGCGGGG CGAGGGGCGG
      541 GGCGGGGCGA GGCGGAGAGG TGCGGCGGCA GCCAATCAGA GCGGCGCGCT CCGAAAGTTT
      601 CCTTTTATGG CGAGGCGGCG GCGGCGGCGG CCCTATAAAA AGCGAAGCGC GCGGCGGGCG
      661 GGAGTCGCTG CGCGCGCTGC CTTCGCCCCG TGCCCCGCTC CGCGCCGCCT CGCGCCGCCC
      721 GCCCCGGCTC TGACTGACCG CGTTACTCCC ACAGGTGAGC GGGCGGGACG GCCCTTCTCC
      781 TCCGGGCTGT AATTAGCGCT TGGTTTAATG ACGGCTTGTT TCTTTTCTGT GGCTGCGTGA
      841 AAGCCTTGAG GGGCTCCGGG AGGGCCCTTT GTGCGGGGGG GAGCGGCTCG GGGGGTGCGT
      901 GCGTGTGTGT GTGCGTGGGG AGCGCCGCGT GCGGCTCCGC GCTGCCCGGC GGCTGTGAGC
      961 GCTGCGGGCG CGGCGCGGGG CTTTGTGCGC TCCGCAGTGT GCGCGAGGGG AGCGCGGCCG
     1021 GGGGCGGTGC CCCGCGGTGC GGGGGGGGCT GCGAGGGGAA CAAAGGCTGC GTGCGGGGTG
     1081 TGTGCGTGGG GGGGTGAGCA GGGGGTGTGG GCGCGTCGGT CGGGCTGCAA CCCCCCCCTG
     1141 CACCCCCCTC CCCGAGTTGC TGAGCACGGC CCGGCTTCGG GTGCGGGGCT CCGTACGGGG
     1201 CGTGGCGCGG GGCTCGCCGT GCCGGGCGGG GGGTGGCGGC AGGTGGGGGT GCCGGGCGGG
     1261 GCGGGGCCGC CTCGGGCCGG GGAGGGCTCG GGGGAGGGGC GCGGCGGCCC CCGGAGCGCC
     1321 GGCGGCTGTC GAGGCGCGGC GAGCCGCAGC CATTGCCTTT TATGGTAATC GTGCGAGAGG
     1381 GCGCAGGGAC TTCCTTTGTC CCAAATCTGG CGGAGCCGAA ATCTGGGAGG CGCCGCCGCA
     1441 CCCCCTCTAG CGGGCGCGGG GCGAAGCGGT GCGGCGCCGG CAGGAAGGAA ATGGGCGGGG
     1501 AGGGCCTTCG TGCGTCGCCG CGCCGCCGTC CCCTTCTCCC TCTCCAGCCT CGGGGCTGCC
     1561 GCGGGGGGAC GGCTGCCTTC GGGGGGGACG GGGCAGGGCG GGGTTCGGCT TCTGGCGTGT
     1621 GACCGGCGGC TCTAGAGCCT CTGCTAACCA TGTTCATGCC TTCTTCTTTT TCCTACAGCT
     1681 CCTGGGCAAC GTGCTGGTTA TTGTGCTGTC TCATCATTTT GGCAAAGGCC ACCATGTTCG
     1741 TGTTTCTGGT GCTGCTGCCT CTGGTGTCCA GCCAGCGGGT GCAGCCCACC GAATCCATCG
     1801 TGCGGTTCCC CAATATCACC AATCTGTGCC CCTTCGGCGA GGTGTTCAAT GCCACCAGAT
     1861 TCGCCTCTGT GTACGCCTGG AACCGGAAGC GGATCAGCAA TTGCGTGGCC GACTACTCCG
     1921 TGCTGTACAA CTCCGCCAGC TTCAGCACCT TCAAGTGCTA CGGCGTGTCC CCTACCAAGC
     1981 TGAACGACCT GTGCTTCACA AACGTGTACG CCGACAGCTT CGTGATCCGG GGAGATGAAG
     2041 TGCGGCAGAT TGCCCCTGGA CAGACAGGCA AGATCGCCGA CTACAACTAC AAGCTGCCCG
     2101 ACGACTTCAC CGGCTGTGTG ATTGCCTGGA ACAGCAACAA CCTGGACTCC AAAGTCGGCG
     2161 GCAACTACAA TTACCTGTAC CGGCTGTTCC GGAAGTCCAA TCTGAAGCCC TTCGAGCGGG
     2221 ACATCTCCAC CGAGATCTAT CAGGCCGGCA GCACCCCTTG TAACGGCGTG GAAGGCTTCA
     2281 ACTGCTACTT CCCACTGCAG TCCTACGGCT TTCAGCCCAC AAATGGCGTG GGCTATCAGC
     2341 CCTACAGAGT GGTGGTGCTG AGCTTCGAAC TGCTGCATGC CCCTGCCACA GTGTGCGGCC
     2401 CTAAGAAAAG CACCAATCTC GTGAAGAACA AATGCGTGAA CTTCCACCAT CACCATCACC
     2461 ATggttccgg tggagcacat attgtgatgg ttgacgctta caagccaacc aaataatgac
```

2521 tcgagCTAGC AGATCTTTTT CCCTCTGCCA AAAATTATGG GGACATCATG AAGCCCCTTG
2581 AGCATCTGAC TTCTGGCTAA TAAAGGAAAT TTATTTTCAT TGCAATAGTG TGTTGGAATT
2641 TTTTGTGTCT CTCACTCGGA AGGACATATG GGAGGGCAAA TCATTTAAAA CATCAGAATG
2701 AGTATTTGGT TTAGAGTTTG GCAACATATG CCCATATGCT GGCTGCCATG AACAAAGGTT
2761 GGCTATAAAG AGGTCATCAG TATATGAAAC AGCCCCCTGC TGTCCATTCC TTATTCCATA
2821 GAAAAGCCTT GACTTGAGGT TAGATTTTTT TTATATTTTG TTTTGTGTTA TTTTTTTCTT
2881 TAACATCCCT AAAATTTTCC TTACATGTTT TACTAGCCAG ATTTTTCCTC CTCTCCTGAC
2941 TACTCCCAGT CATAGCTGTC CCTCTTCTCT TATGGAGATC CCTCGACCTG CAGCCCAAGC
3001 TTGGCGTAAT CATGGTCATA GCTGTTTCCT GTGTGAAATT GTTATCCGCT CACAATTCCA
3061 CACAACATAC GAGCCGGAAG CATAAAGTGT AAAGCCTGGG GTGCCTAATG AGTGAGCTAA
3121 CTCACATTAA TTGCGTTGCG CTCACTGCCC GCTTTCCAGT CGGGAAACCT GTCGTGCCAG
3181 CGGATCCGCA TCTCAATTAG TCAGCAACCA TAGTCCCGCC CCTAACTCCG CCCATCCCGC
3241 CCCTAACTCC GCCCAGTTCC GCCCATTCTC CGCCCCATGG CTGACTAATT TTTTTTATTT
3301 ATGCAGAGGC CGAGGCCGCC TCGGCCTCTG AGCTATTCCA GAAGTAGTGA GGAGGCTTTT
3361 TTGGAGGCCT AGGCTTTTGC AAAAAGCTAA CTTGTTTATT GCAGCTTATA ATGGTTACAA
3421 ATAAAGCAAT AGCATCACAA ATTTCACAAA TAAAGCATTT TTTTCACTGC ATTCTAGTTG
3481 TGGTTTGTCC AAACTCATCA ATGTATCTTA TCATGTCTGG ATCCGCTGCA TTAATGAATC
3541 GGCCAACGCG CGGGGAGAGG CGGTTTGCGT ATTGGGCGCT CTTCCGCTTC CTCGCTCACT
3601 GACTCGCTGC GCTCGGTCGT TCGGCTGCGG CGAGCGGTAT CAGCTCACTC AAAGGCGGTA
3661 ATACGGTTAT CCACAGAATC AGGGGATAAC GCAGGAAAGA ACATGTGAGC AAAAGGCCAG
3721 CAAAAGGCCA GGAACCGTAA AAAGGCCGCG TTGCTGGCGT TTTTCCATAG GCTCCGCCCC
3781 CCTGACGAGC ATCACAAAAA TCGACGCTCA AGTCAGAGGT GGCGAAACCC GACAGGACTA
3841 TAAAGATACC AGGCGTTTCC CCCTGGAAGC TCCCTCGTGC GCTCTCCTGT TCCGACCCTG
3901 CCGCTTACCG GATACCTGTC CGCCTTTCTC CCTTCGGGAA GCGTGGCGCT TTCTCATAGC
3961 TCACGCTGTA GGTATCTCAG TTCGGTGTAG GTCGTTCGCT CCAAGCTGGG CTGTGTGCAC
4021 GAACCCCCCG TTCAGCCCGA CCGCTGCGCC TTATCCGGTA ACTATCGTCT TGAGTCCAAC
4081 CCGGTAAGAC ACGACTTATC GCCACTGGCA GCAGCCACTG GTAACAGGAT TAGCAGAGCG
4141 AGGTATGTAG GCGGTGCTAC AGAGTTCTTG AAGTGGTGGC CTAACTACGG CTACACTAGA
4201 AGAACAGTAT TTGGTATCTG CGCTCTGCTG AAGCCAGTTA CCTTCGGAAA AAGAGTTGGT
4261 AGCTCTTGAT CCGGCAAACA AACCACCGCT GGTAGCGGTG GTTTTTTTGT TTGCAAGCAG
4321 CAGATTACGC GCAGAAAAAA AGGATCTCAA GAAGATCCTT TGATCTTTTC TACGGGGTCT
4381 GACGCTCAGT GGAACGAAAA CTCACGTTAA GGGATTTTGG TCATGAGATT ATCAAAAAGG
4441 ATCTTCACCT AGATCCTTTT AAATTAAAAA TGAAGTTTTA AATCAATCTA AAGTATATAT
4501 GAGTAAACTT GGTCTGACAG TTACCAATGC TTAATCAGTG AGGCACCTAT CTCAGCGATC
4561 TGTCTATTTC GTTCATCCAT AGTTGCCTGA CTCCCCGTCG TGTAGATAAC TACGATACGG
4621 GAGGGCTTAC CATCTGGCCC CAGTGCTGCA ATGATACCGC GAGACCCACG CTCACCGGCT
4681 CCAGATTTAT CAGCAATAAA CCAGCCAGCC GGAAGGGCCG AGCGCAGAAG TGGTCCTGCA
4741 ACTTTATCCG CCTCCATCCA GTCTATTAAT TGTTGCCGGG AAGCTAGAGT AAGTAGTTCG
4801 CCAGTTAATA GTTTGCGCAA CGTTGTTGCC ATTGCTACAG GCATCGTGGT GTCACGCTCG
4861 TCGTTTGGTA TGGCTTCATT CAGCTCCGGT TCCCAACGAT CAAGGCGAGT TACATGATCC
4921 CCCATGTTGT GCAAAAAAGC GGTTAGCTCC TTCGGTCCTC CGATCGTTGT CAGAAGTAAG
4981 TTGGCCGCAG TGTTATCACT CATGGTTATG GCAGCACTGC ATAATTCTCT TACTGTCATG
5041 CCATCCGTAA GATGCTTTTC TGTGACTGGT GAGTACTCAA CCAAGTCATT CTGAGAATAG
5101 TGTATGCGGC GACCGAGTTG CTCTTGCCCG GCGTCAATAC GGGATAATAC CGCGCCACAT
5161 AGCAGAACTT TAAAAGTGCT CATCATTGGA AAACGTTCTT CGGGGCGAAA ACTCTCAAGG
5221 ATCTTACCGC TGTTGAGATC CAGTTCGATG TAACCCACTC GTGCACCCAA CTGATCTTCA
5281 GCATCTTTTA CTTTCACCAG CGTTTCTGGG TGAGCAAAAA CAGGAAGGCA AAATGCCGCA
5341 AAAAAGGGAA TAAGGGCGAC ACGGAAATGT TGAATACTCA TACTCTTCCT TTTTCAATAT
5401 TATTGAAGCA TTTATCAGGG TTATTGTCTC ATGAGCGGAT ACATATTTGA ATGTATTTAG
5461 AAAAATAAAC AAATAGGGGT TCCGCGCACA TTTCCCCGAA AAGTGCCACC TG
//

Supp File 2 - Cryo-EM Validation Report

WORLDWIDE PDB PROTEIN DATA BANK

Full wwPDB EM Validation Report (i)

Aug 9, 2022 – 12:48 PM EDT

PDB ID	:	8E01
EMDB ID	:	EMD-27812
Title	:	Structure of engineered nano-cage fusion protein
Deposited on	:	2022-08-08
Resolution	:	3.40 Å(reported)

This wwPDB validation report is for manuscript review

This is a Full wwPDB EM Validation Report.

This report is produced by the wwPDB biocuration pipeline after annotation of the structure.

We welcome your comments at *validation@mail.wwpdb.org*
A user guide is available at
https://www.wwpdb.org/validation/2017/EMValidationReportHelp
with specific help available everywhere you see the (i) symbol.

The types of validation reports are described at http://www.wwpdb.org/validation/2017/FAQs#types.

The following versions of software and data (see references (i)) were used in the production of this report:

EMDB validation analysis	:	0.0.1.dev8
MolProbity	:	4.02b-467
Percentile statistics	:	20191225.v01 (using entries in the PDB archive December 25th 2019)
Ideal geometry (proteins)	:	Engh & Huber (2001)
Ideal geometry (DNA, RNA)	:	Parkinson et al. (1996)
Validation Pipeline (wwPDB-VP)	:	2.29

1 Overall quality at a glance

The following experimental techniques were used to determine the structure:
ELECTRON MICROSCOPY

The reported resolution of this entry is 3.40 Å.

Percentile scores (ranging between 0-100) for global validation metrics of the entry are shown in the following graphic. The table shows the number of entries on which the scores are based.

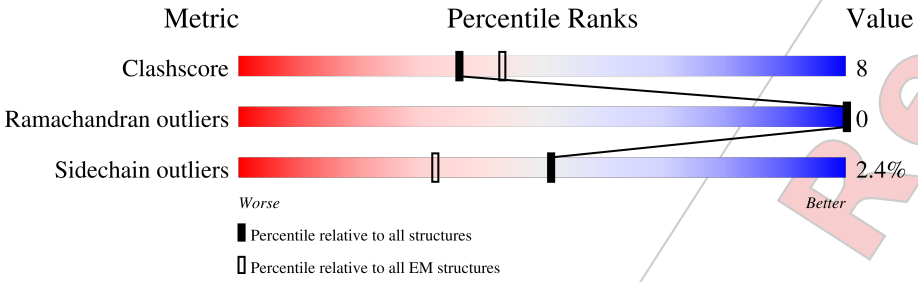

Metric	Whole archive (#Entries)	EM structures (#Entries)
Clashscore	158937	4297
Ramachandran outliers	154571	4023
Sidechain outliers	154315	3826

The table below summarises the geometric issues observed across the polymeric chains and their fit to the map. The red, orange, yellow and green segments of the bar indicate the fraction of residues that contain outliers for >=3, 2, 1 and 0 types of geometric quality criteria respectively. A grey segment represents the fraction of residues that are not modelled. The numeric value for each fraction is indicated below the corresponding segment, with a dot representing fractions <=5% The upper red bar (where present) indicates the fraction of residues that have poor fit to the EM map (all-atom inclusion < 40%). The numeric value is given above the bar.

Mol	Chain	Length	Quality of chain
1	A	224	70% 20% 10%

2 Entry composition

There is only 1 type of molecule in this entry. The entry contains 1518 atoms, of which 0 are hydrogens and 0 are deuteriums.

In the tables below, the AltConf column contains the number of residues with at least one atom in alternate conformation and the Trace column contains the number of residues modelled with at most 2 atoms.

- Molecule 1 is a protein called 2-dehydro-3-deoxyphosphogluconate aldolase/4-hydroxy-2-oxoglutarate aldolase.

Mol	Chain	Residues	Atoms					AltConf	Trace
			Total	C	N	O	S		
1	A	201	1518	988	248	272	10	0	0

There are 24 discrepancies between the modelled and reference sequences:

Chain	Residue	Modelled	Actual	Comment	Reference
A	1	MET	-	initiating methionine	UNP Q9WXS1
A	2	HIS	-	expression tag	UNP Q9WXS1
A	3	HIS	-	expression tag	UNP Q9WXS1
A	4	HIS	-	expression tag	UNP Q9WXS1
A	5	HIS	-	expression tag	UNP Q9WXS1
A	6	HIS	-	expression tag	UNP Q9WXS1
A	7	HIS	-	expression tag	UNP Q9WXS1
A	8	GLY	-	expression tag	UNP Q9WXS1
A	9	GLY	-	expression tag	UNP Q9WXS1
A	10	SER	-	expression tag	UNP Q9WXS1
A	11	GLY	-	expression tag	UNP Q9WXS1
A	12	GLY	-	expression tag	UNP Q9WXS1
A	13	SER	-	expression tag	UNP Q9WXS1
A	14	GLY	-	expression tag	UNP Q9WXS1
A	15	GLY	-	expression tag	UNP Q9WXS1
A	16	SER	-	expression tag	UNP Q9WXS1
A	17	GLY	-	expression tag	UNP Q9WXS1
A	18	GLY	-	expression tag	UNP Q9WXS1
A	19	SER	-	expression tag	UNP Q9WXS1
A	45	LYS	GLU	conflict	UNP Q9WXS1
A	52	LEU	GLU	conflict	UNP Q9WXS1
A	80	MET	LYS	conflict	UNP Q9WXS1
A	206	VAL	ASP	conflict	UNP Q9WXS1
A	209	ALA	ARG	conflict	UNP Q9WXS1

3 Residue-property plots

These plots are drawn for all protein, RNA, DNA and oligosaccharide chains in the entry. The first graphic for a chain summarises the proportions of the various outlier classes displayed in the second graphic. The second graphic shows the sequence view annotated by issues in geometry and atom inclusion in map density. Residues are color-coded according to the number of geometric quality criteria for which they contain at least one outlier: green = 0, yellow = 1, orange = 2 and red = 3 or more. A red diamond above a residue indicates a poor fit to the EM map for this residue (all-atom inclusion < 40%). Stretches of 2 or more consecutive residues without any outlier are shown as a green connector. Residues present in the sample, but not in the model, are shown in grey.

• Molecule 1: 2-dehydro-3-deoxyphosphogluconate aldolase/4-hydroxy-2-oxoglutarate aldolase

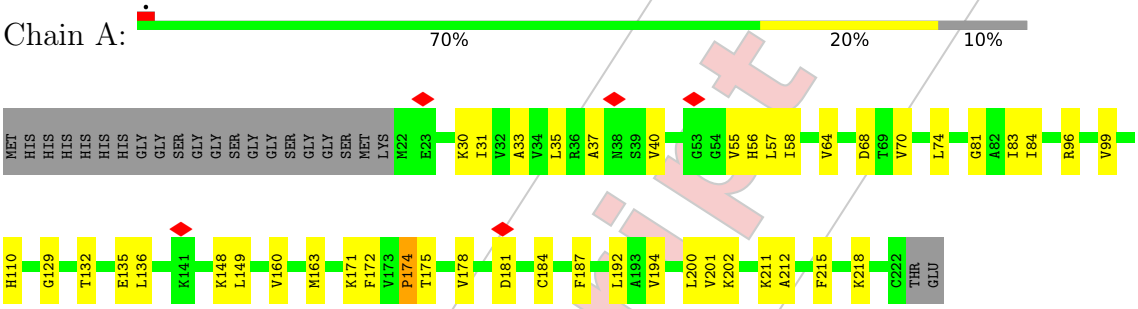

4 Experimental information

Property	Value	Source
EM reconstruction method	SINGLE PARTICLE	Depositor
Imposed symmetry	POINT, I	Depositor
Number of particles used	63430	Depositor
Resolution determination method	FSC 0.143 CUT-OFF	Depositor
CTF correction method	PHASE FLIPPING AND AMPLITUDE CORRECTION	Depositor
Microscope	FEI TITAN KRIOS	Depositor
Voltage (kV)	300	Depositor
Electron dose ($e^-/Å^2$)	44.85	Depositor
Minimum defocus (nm)	1200	Depositor
Maximum defocus (nm)	3000	Depositor
Magnification	59000	Depositor
Image detector	FEI FALCON III (4k x 4k)	Depositor
Maximum map value	6.362	Depositor
Minimum map value	-4.024	Depositor
Average map value	0.007	Depositor
Map value standard deviation	0.216	Depositor
Recommended contour level	0.9	Depositor
Map size (Å)	462.0, 462.0, 462.0	wwPDB
Map dimensions	420, 420, 420	wwPDB
Map angles (°)	90.0, 90.0, 90.0	wwPDB
Pixel spacing (Å)	1.1, 1.1, 1.1	Depositor

5 Model quality

5.1 Standard geometry

The Z score for a bond length (or angle) is the number of standard deviations the observed value is removed from the expected value. A bond length (or angle) with $|Z| > 5$ is considered an outlier worth inspection. RMSZ is the root-mean-square of all Z scores of the bond lengths (or angles).

Mol	Chain	Bond lengths		Bond angles	
		RMSZ	#$\|Z\|>5$	RMSZ	#$\|Z\|>5$
1	A	0.25	0/1547	0.45	0/2086

There are no bond length outliers.

There are no bond angle outliers.

There are no chirality outliers.

There are no planarity outliers.

5.2 Too-close contacts

In the following table, the Non-H and H(model) columns list the number of non-hydrogen atoms and hydrogen atoms in the chain respectively. The H(added) column lists the number of hydrogen atoms added and optimized by MolProbity. The Clashes column lists the number of clashes within the asymmetric unit, whereas Symm-Clashes lists symmetry-related clashes.

Mol	Chain	Non-H	H(model)	H(added)	Clashes	Symm-Clashes
1	A	1518	0	1587	26	0
All	All	1518	0	1587	26	0

The all-atom clashscore is defined as the number of clashes found per 1000 atoms (including hydrogen atoms). The all-atom clashscore for this structure is 8.

All (26) close contacts within the same asymmetric unit are listed below, sorted by their clash magnitude.

Atom-1	Atom-2	Interatomic distance (Å)	Clash overlap (Å)
1:A:202:LYS:O	1:A:211:LYS:NZ	2.31	0.60
1:A:148:LYS:NZ	1:A:175:THR:OG1	2.35	0.59
1:A:171:LYS:HD2	1:A:192:LEU:HD22	1.85	0.58
1:A:136:LEU:HD11	1:A:172:PHE:HZ	1.72	0.55
1:A:178:VAL:HG11	1:A:194:VAL:HG11	1.89	0.55

Continued on next page...

Continued from previous page...

Atom-1	Atom-2	Interatomic distance (Å)	Clash overlap (Å)
1:A:37:ALA:H	1:A:64:VAL:HG22	1.73	0.54
1:A:35:LEU:HA	1:A:201:VAL:HG11	1.96	0.48
1:A:160:VAL:HG12	1:A:172:PHE:CD2	2.48	0.48
1:A:33:ALA:HB2	1:A:55:VAL:HG11	1.94	0.48
1:A:56:HIS:ND1	1:A:81:GLY:O	2.28	0.48
1:A:31:ILE:HG21	1:A:55:VAL:HG22	1.97	0.47
1:A:149:LEU:HB3	1:A:174:PRO:HA	1.98	0.46
1:A:149:LEU:HD23	1:A:174:PRO:HB3	1.98	0.45
1:A:184:CYS:SG	1:A:218:LYS:NZ	2.89	0.45
1:A:132:THR:OG1	1:A:135:GLU:OE2	2.35	0.45
1:A:200:LEU:HD11	1:A:212:ALA:HA	1.98	0.44
1:A:31:ILE:HG22	1:A:55:VAL:HG13	2.00	0.44
1:A:57:LEU:HD23	1:A:83:ILE:HB	2.00	0.44
1:A:68:ASP:OD2	1:A:68:ASP:N	2.51	0.43
1:A:163:MET:O	1:A:163:MET:HG3	2.19	0.43
1:A:40:VAL:HG13	1:A:70:VAL:HG22	2.01	0.42
1:A:129:GLY:HA2	1:A:148:LYS:HB3	2.01	0.42
1:A:30:LYS:HB3	1:A:187:PHE:HZ	1.84	0.42
1:A:58:ILE:O	1:A:84:ILE:HA	2.20	0.42
1:A:74:LEU:O	1:A:74:LEU:HD23	2.21	0.40
1:A:96:ARG:HA	1:A:99:VAL:HG22	2.02	0.40

There are no symmetry-related clashes.

5.3 Torsion angles (i)

5.3.1 Protein backbone (i)

In the following table, the Percentiles column shows the percent Ramachandran outliers of the chain as a percentile score with respect to all PDB entries followed by that with respect to all EM entries.

The Analysed column shows the number of residues for which the backbone conformation was analysed, and the total number of residues.

Mol	Chain	Analysed	Favoured	Allowed	Outliers	Percentiles	
1	A	199/224 (89%)	195 (98%)	4 (2%)	0	100	100

There are no Ramachandran outliers to report.

5.3.2 Protein sidechains (i)

In the following table, the Percentiles column shows the percent sidechain outliers of the chain as a percentile score with respect to all PDB entries followed by that with respect to all EM entries.

The Analysed column shows the number of residues for which the sidechain conformation was analysed, and the total number of residues.

Mol	Chain	Analysed	Rotameric	Outliers	Percentiles
1	A	164/179 (92%)	160 (98%)	4 (2%)	49 74

All (4) residues with a non-rotameric sidechain are listed below:

Mol	Chain	Res	Type
1	A	110	HIS
1	A	174	PRO
1	A	181	ASP
1	A	215	PHE

Sometimes sidechains can be flipped to improve hydrogen bonding and reduce clashes. There are no such sidechains identified.

5.3.3 RNA (i)

There are no RNA molecules in this entry.

5.4 Non-standard residues in protein, DNA, RNA chains (i)

There are no non-standard protein/DNA/RNA residues in this entry.

5.5 Carbohydrates (i)

There are no monosaccharides in this entry.

5.6 Ligand geometry (i)

There are no ligands in this entry.

5.7 Other polymers (i)

There are no such residues in this entry.

5.8 Polymer linkage issues

There are no chain breaks in this entry.

6 Map visualisation

This section contains visualisations of the EMDB entry EMD-27812. These allow visual inspection of the internal detail of the map and identification of artifacts.

Images derived from a raw map, generated by summing the deposited half-maps, are presented below the corresponding image components of the primary map to allow further visual inspection and comparison with those of the primary map.

6.1 Orthogonal projections

6.1.1 Primary map

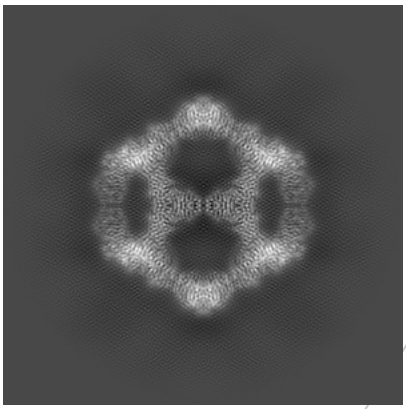

X

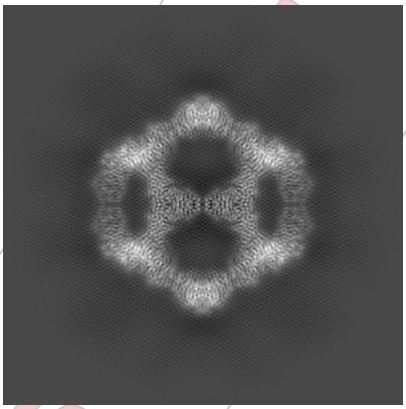

Y

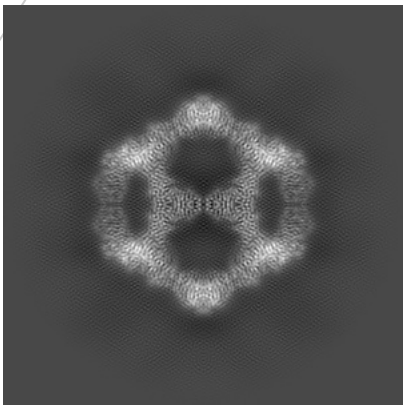

Z

6.1.2 Raw map

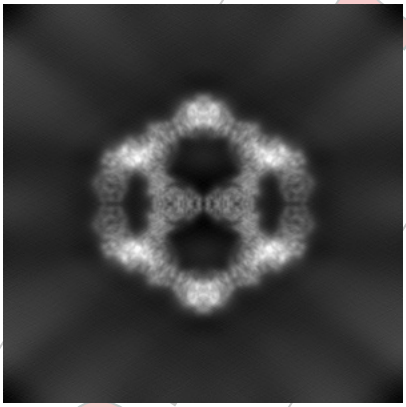

X

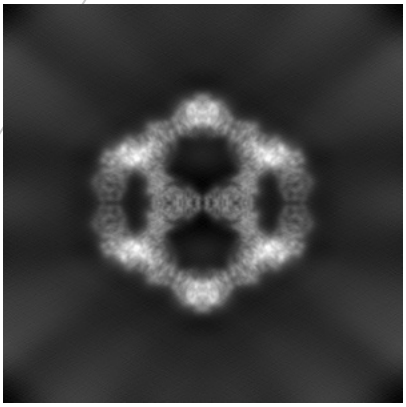

Y

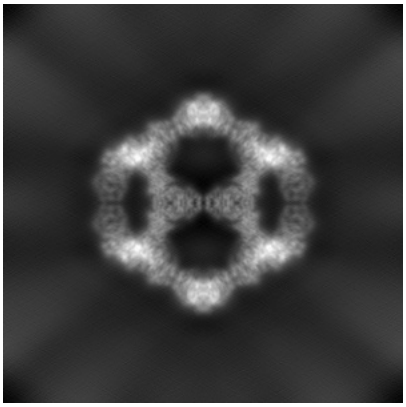

Z

The images above show the map projected in three orthogonal directions.

6.2 Central slices (i)

6.2.1 Primary map

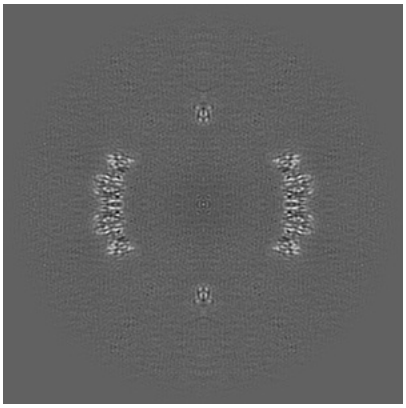

X Index: 210

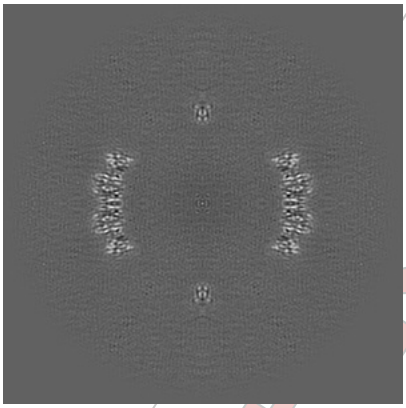

Y Index: 210

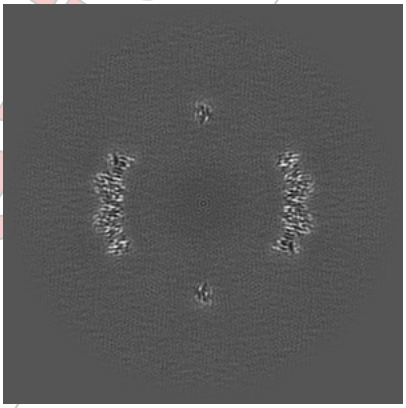

Z Index: 210

6.2.2 Raw map

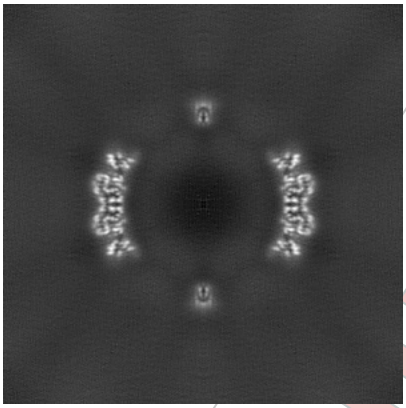

X Index: 210

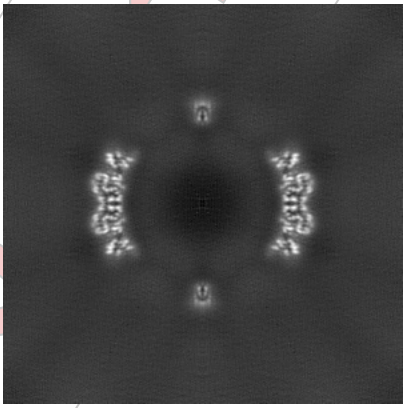

Y Index: 210

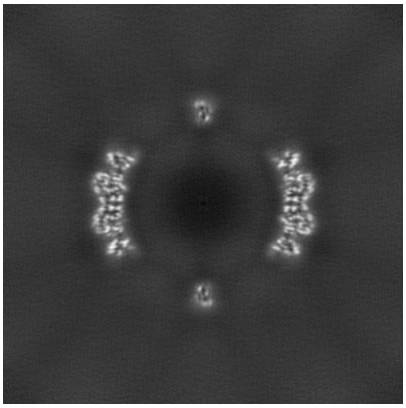

Z Index: 210

The images above show central slices of the map in three orthogonal directions.

6.3 Largest variance slices

6.3.1 Primary map

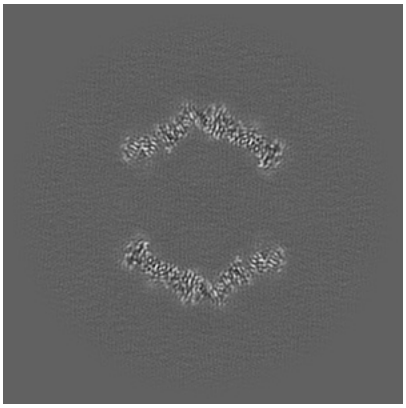

X Index: 162

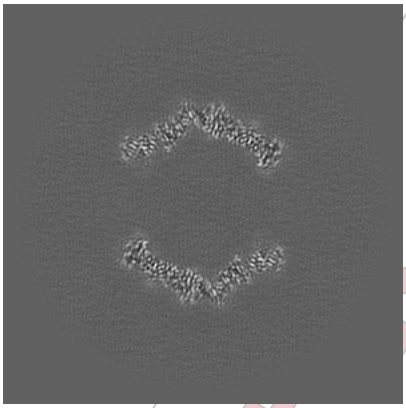

Y Index: 162

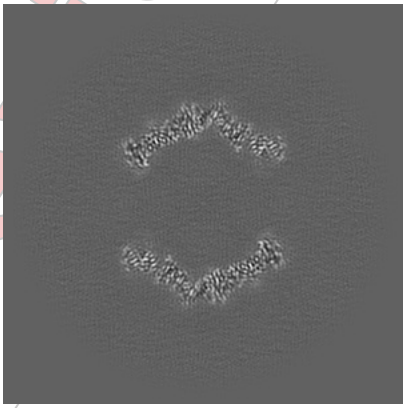

Z Index: 257

6.3.2 Raw map

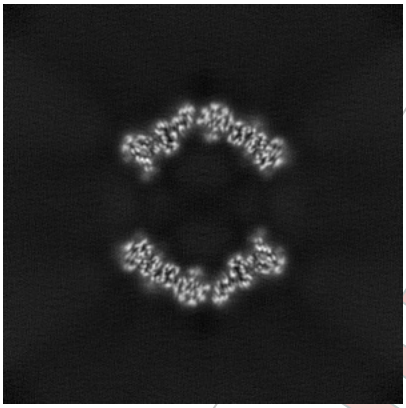

X Index: 158

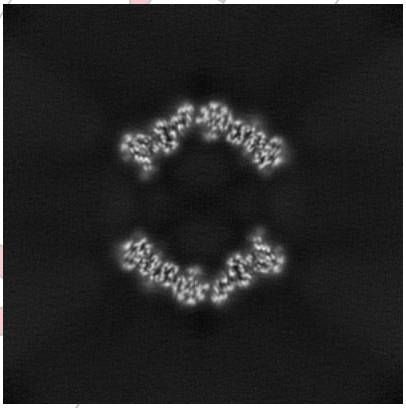

Y Index: 158

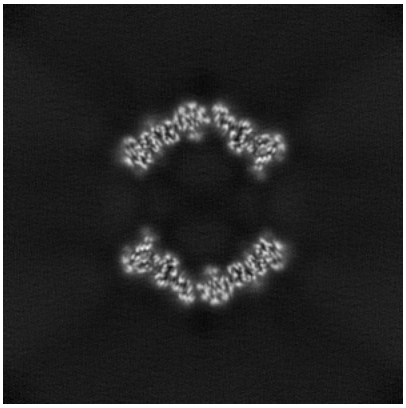

Z Index: 261

The images above show the largest variance slices of the map in three orthogonal directions.

6.4 Orthogonal surface views (i)

6.4.1 Primary map

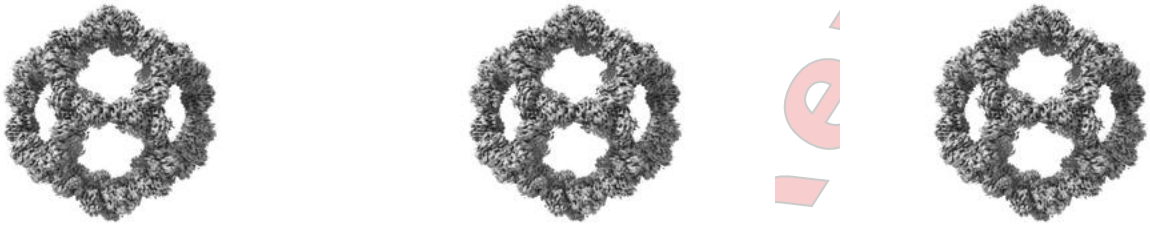

X Y Z

The images above show the 3D surface view of the map at the recommended contour level 0.9. These images, in conjunction with the slice images, may facilitate assessment of whether an appropriate contour level has been provided.

6.4.2 Raw map

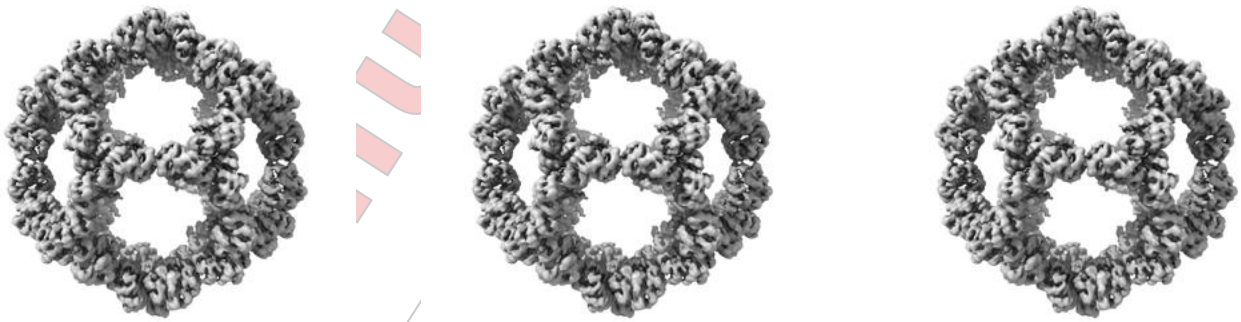

X Y Z

These images show the 3D surface of the raw map. The raw map's contour level was selected so that its surface encloses the same volume as the primary map does at its recommended contour level.

6.5 Mask visualisation (i)

This section shows the 3D surface view of the primary map at 50% transparency overlaid with the specified mask at 0% transparency

A mask typically either:

- Encompasses the whole structure
- Separates out a domain, a functional unit, a monomer or an area of interest from a larger structure

6.5.1 D_1000267547_em-mask-volume_P1.map.V3 (i)

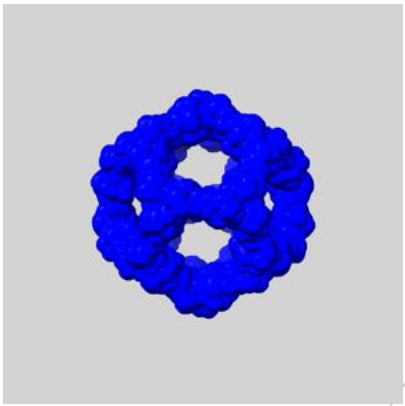

X

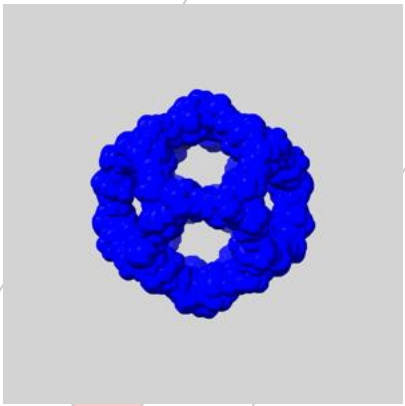

Y

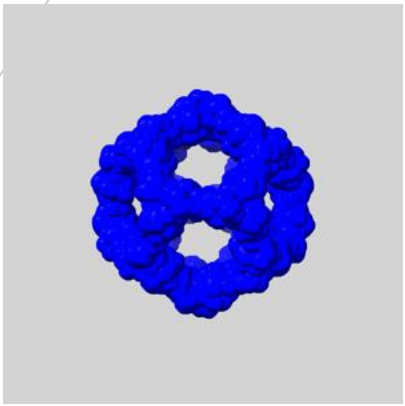

Z

7 Map analysis

This section contains the results of statistical analysis of the map.

7.1 Map-value distribution

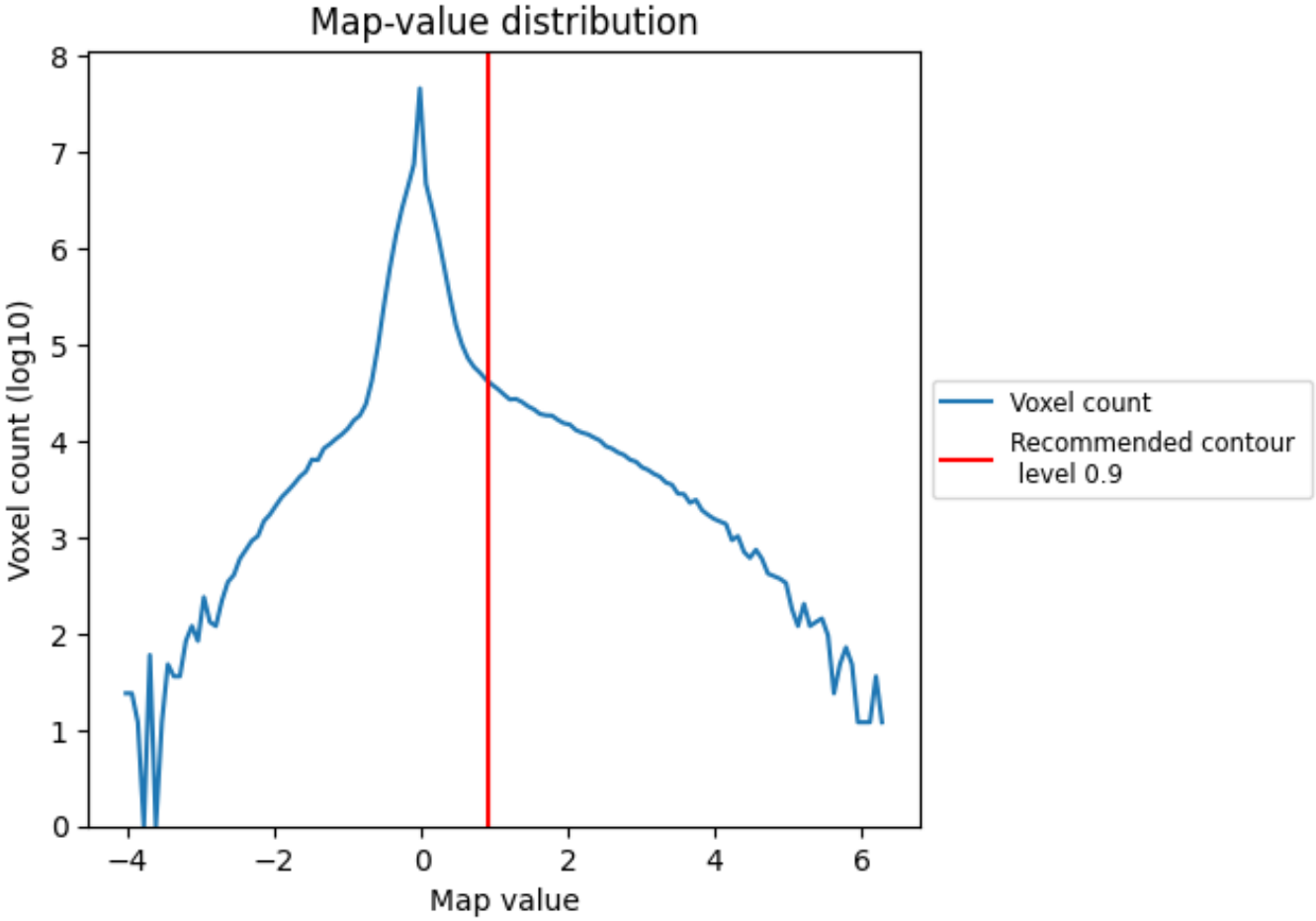

The map-value distribution is plotted in 128 intervals along the x-axis. The y-axis is logarithmic. A spike in this graph at zero usually indicates that the volume has been masked.

7.2 Volume estimate (i)

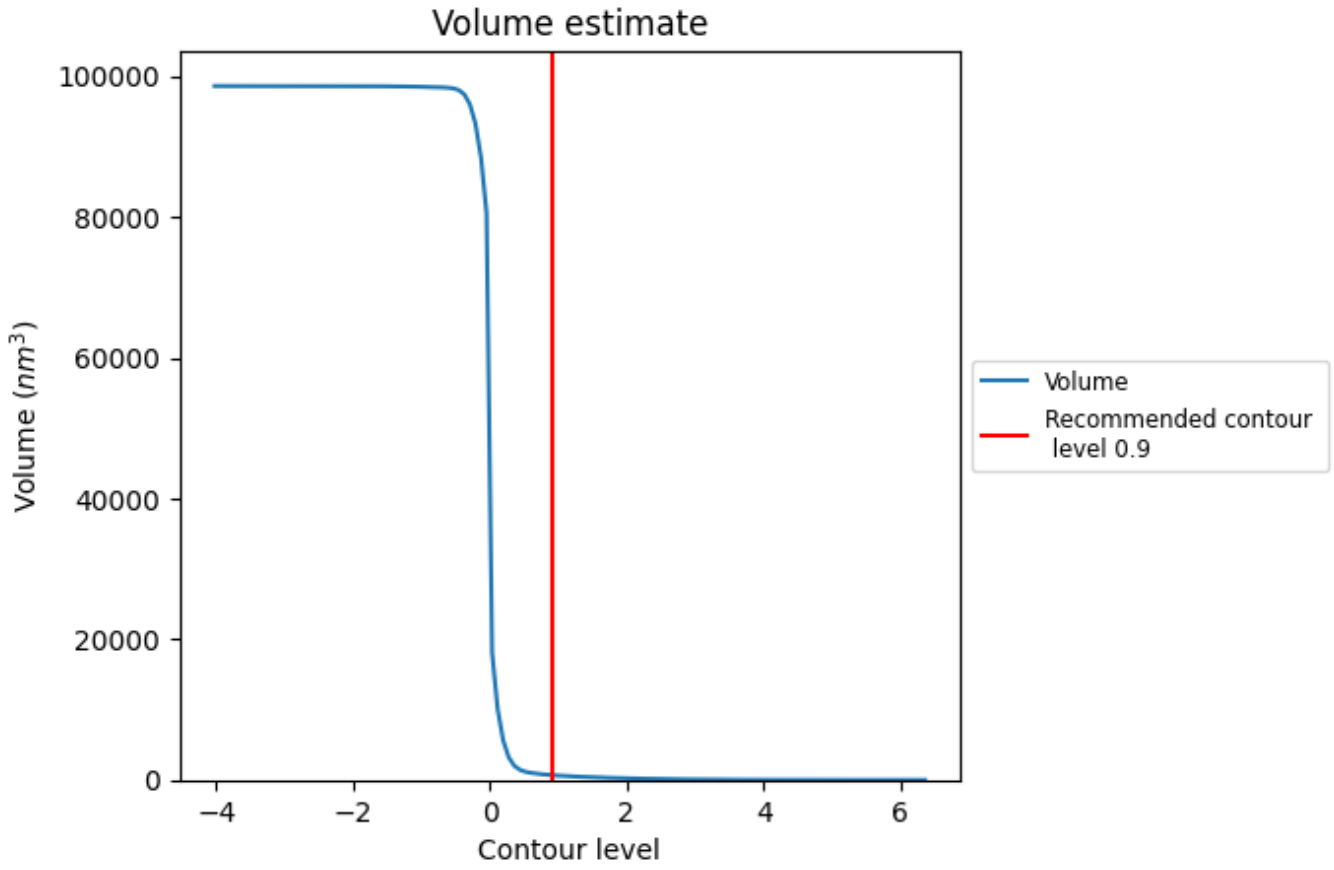

The volume at the recommended contour level is 694 nm^3; this corresponds to an approximate mass of 627 kDa.

The volume estimate graph shows how the enclosed volume varies with the contour level. The recommended contour level is shown as a vertical line and the intersection between the line and the curve gives the volume of the enclosed surface at the given level.

7.3 Rotationally averaged power spectrum (i)

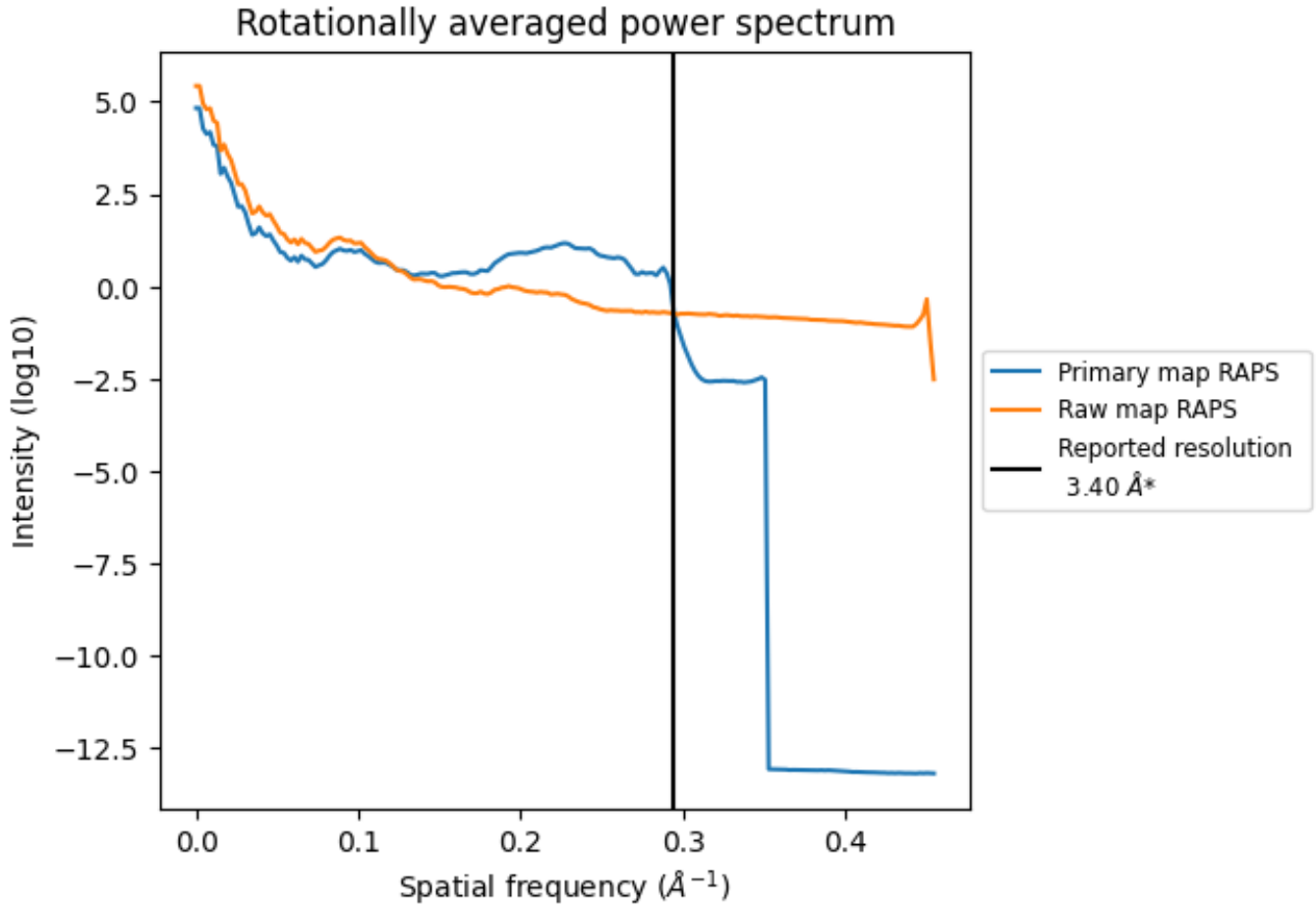

*Reported resolution corresponds to spatial frequency of 0.294 $Å^{-1}$

8 Fourier-Shell correlation

Fourier-Shell Correlation (FSC) is the most commonly used method to estimate the resolution of single-particle and subtomogram-averaged maps. The shape of the curve depends on the imposed symmetry, mask and whether or not the two 3D reconstructions used were processed from a common reference. The reported resolution is shown as a black line. A curve is displayed for the half-bit criterion in addition to lines showing the 0.143 gold standard cut-off and 0.5 cut-off.

8.1 FSC

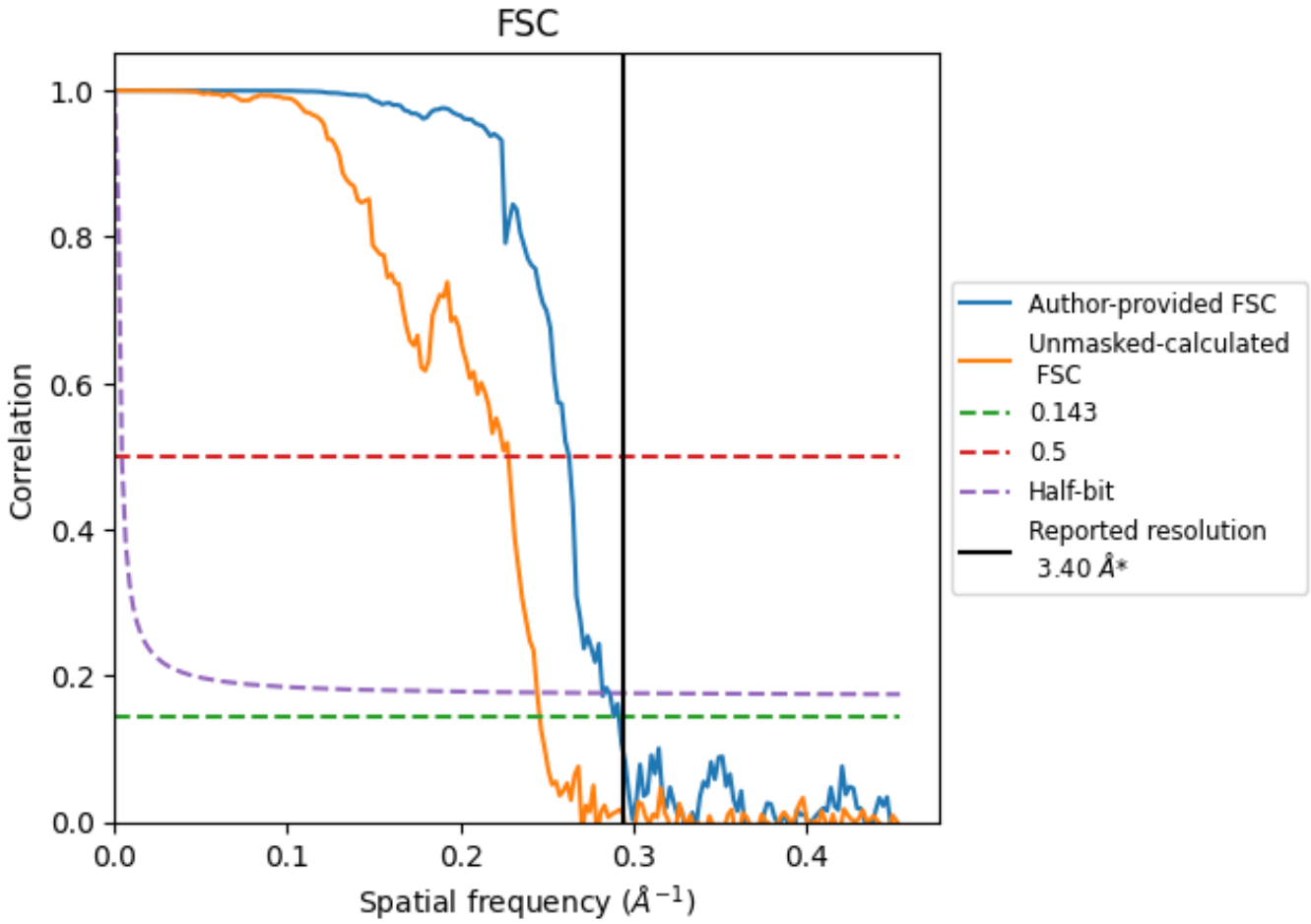

*Reported resolution corresponds to spatial frequency of 0.294 Å^{-1}

8.2 Resolution estimates (i)

Resolution estimate (Å)	Estimation criterion (FSC cut-off)		
	0.143	0.5	Half-bit
Reported by author	3.40	-	-
Author-provided FSC curve	3.43	3.80	3.54
Unmasked-calculated*	4.07	4.39	4.09

*Resolution estimate based on FSC curve calculated by comparison of deposited half-maps. The value from deposited half-maps intersecting FSC 0.143 CUT-OFF 4.07 differs from the reported value 3.4 by more than 10 %

9 Map-model fit

This section contains information regarding the fit between EMDB map EMD-27812 and PDB model 8E01. Per-residue inclusion information can be found in section 3 on page 4.

9.0.1 Map-model overlay

X Y Z

9.0.2 Map-model assembly overlay

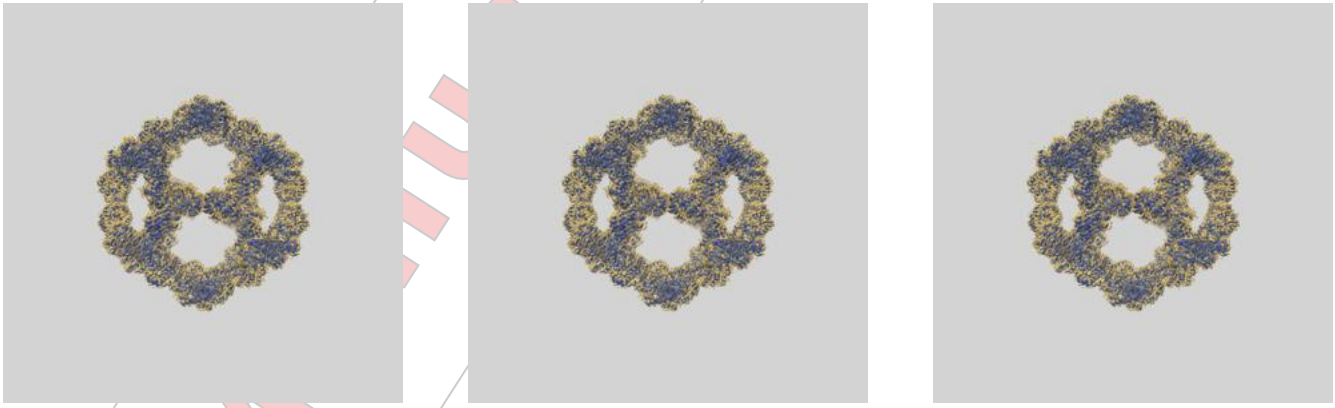

X Y Z

The images above show the 3D surface view of the map at the recommended contour level 0.9 at 50% transparency in yellow overlaid with a ribbon representation of the model coloured in blue. These images allow for the visual assessment of the quality of fit between the atomic model and the map.

9.1 Atom inclusion (i)

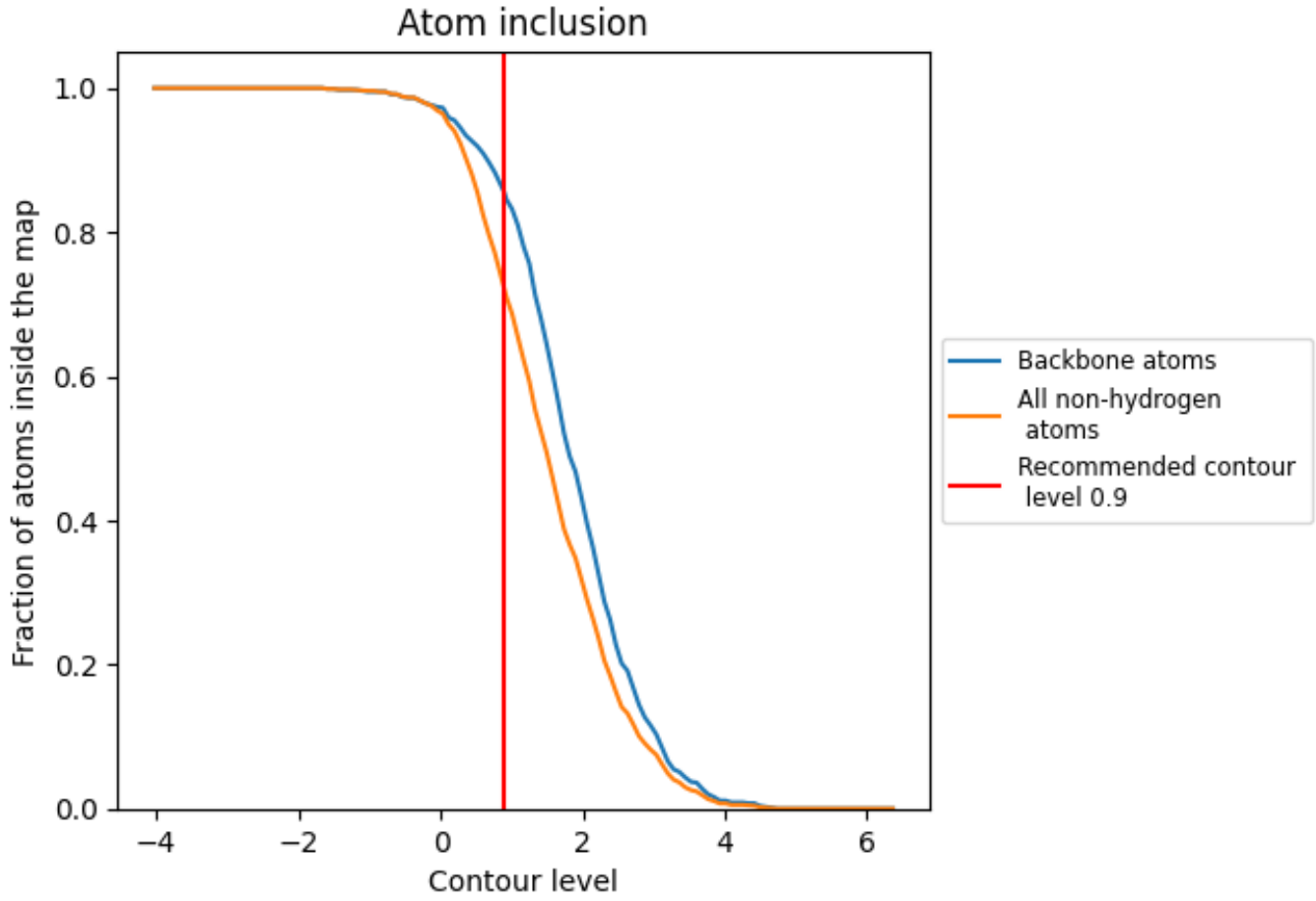

At the recommended contour level, 85% of all backbone atoms, 72% of all non-hydrogen atoms, are inside the map.